2005

Experimental Design and Analysis of Piezoelectric Synthetic Jets in Quiescent Air

Poorna Mane
Virginia Commonwealth University

School of Engineering
Virginia Commonwealth University

This is to certify that the thesis prepared by Poorna Mane entitled **EXPERIMENTAL DESIGN AND ANALYSIS OF PIEZOELECTRIC SYNTHETIC JETS IN QUIESCENT AIR** has been approved by her committee as satisfactory completion of the thesis requirement for the degree of Master of Science.

Karla Mossi, Ph.D., Committee Chair, School of Engineering

Ramana Pidaparti, Ph.D., Committee Member, School of Engineering

Robert Bryant, Ph.D., Committee Member, School of Engineering

L. Thomas Overby, Ph.D., Assistant Dean of Graduate Affairs, School of Engineering

Robert J. Mattauch, Ph.D., Dean, School of Engineering

F. Douglas Boudinot, Ph.D., Dean, School of Graduate Studies

12/07/05
Date

**EXPERIMENTAL DESIGN AND ANALYSIS OF PIEZOELECTRIC
SYNTHETIC JETS IN QUIESCENT AIR**

A thesis submitted in partial fulfillment of the requirements for the degree of Master of
Science at Virginia Commonwealth University

by

POORNA MANE
Computer Engineering, Goa University, India

Director: Dr. Karla Mossi
Assistant Professor, Mechanical Engineering

Virginia Commonwealth University
Richmond, Virginia
December, 2005

Acknowledgements

I have shared the challenging and rewarding experience of my Masters with many important people. Their support and encouragement has been invaluable in many ways.

Dr. Karla Mossi, who has been a great mentor and whom I would like to thank for her patience and encouragement. She has been an integral part in my learning and completion of this work. Thank you very much for giving me a chance and I hope you will support me throughout my PhD as well.

I would also like to thank Dr. Ramana Pidaparti and Dr. Robert Bryant who took time out of their busy schedules to be a part my committee. Your suggestions were most useful and helped me understanding the concepts better.

The people in the Department of Mechanical Engineering who have kept me sane. Susan Younce and Ann Yates, for the financial backing and support. All the fellow students who made me realize I was not alone. Specially, Nicolas whose help was invaluable in the beginning stages. The fellow students in the lab who kept the mood light and did not make all the work seem like a tedium. In particular Byron with his sarcasm and Orr, his humor. A special thank you to Justin Maddox for all his technical assistance and Ihab, who livened up the place in the latter stages. My friends and roommates who have put up with all my tantrums and nitty-gritties. Thank you very much for all your support. In particular Leena, thanks for being a great friend, colleague, roommate and not to forget a splendid cook.

My parents who have always been there with unwavering support. My brother who pushed me to keep going. I would have given up, if not for my family. A special thanks to my dog Sonu who always brings a smile to my face. BOW!!!!WOW!!!!

Table of Contents

List of Tables

List of Figures

List of Abbreviations

C_H……………Synthetic Jet Cavity Height (mm)

D_o……………..Synthetic Jet Orifice Diameter (mm)

D_D.....................Diaphragm Diameter (mm)

Y......................Velocity (m/s)

r_o………………Radius of Synthetic Jet Orifice (mm)

F_Z……………..Driving Waveform

E………………Applied Voltage (V)

f………………Frequency (Hz)

P_B……………..Passive Cavity Pressure (kPa)

Abstract

EXPERIMENTAL DESIGN AND ANALYSIS OF PIEZOELECTRIC SYNTHETIC
JETS IN QUIESCENT AIR

By Poorna Mane, B.E.

A thesis submitted in partial fulfillment of the requirements for the degree of Master of
Science at Virginia Commonwealth University.

Virginia Commonwealth University, 2005

Major Director: Karla Mossi, Ph.D.,
Assistant Professor, Mechanical Engineering

Flow control can lead to saving millions of dollars in fuel costs each year by
making an aircraft more efficient. Synthetic jets, a device for active flow control, operate
by introducing small amounts of energy locally to achieve non-local changes in the flow
field with large performance gains. These devices consist of a cavity with an oscillating
diaphragm that divides it, into active and passive sides. The active side has a small opening

where a jet is formed, whereas and the passive side does not directly participate in the fluidic jet.

Research has shown that the synthetic jet behavior is dependent on the diaphragm and the cavity design hence, the focus of this work. The performance of the synthetic jet is studied under various factors related to the diaphragm and the cavity geometry. Four diaphragms, manufactured from piezoelectric composites, were selected for this study, Bimorph, Thunder®, Lipca and RFD. The overall factors considered are the driving signals, voltage, frequency, cavity height, orifice size, and passive cavity pressure. Using the average maximum jet velocity as the response variable, these factors are individually studied for each actuator and statistical analysis tools were used to select the relevant factors in the response variable.

For all diaphragms, the driving signal was found to be the most important factor, with the sawtooth signal producing significantly higher velocities than the sine signal. Cavity dimensions also proved to be relevant factors when considering the designing of a synthetic jet actuator. The cavities with the smaller orifice produced lower velocities than those with larger orifices and the cavities with smaller volumes followed the same trend. Although there exist a relationship between cavity height and orifice size, the orifice size appears as the dominant factor.

Driving frequency of the diaphragm was the only common factor to all diaphragms studied that was not statistically significant having a small effect on jet velocity. However along with waveform, it had a combined effect on jet velocity for all actuators. With the sawtooth signal, the velocity remained constant after a particular low frequency, thus

indicating that the synthetic jet cavity could be saturated and the flow choked. No such saturation point was reached with the sine signal, for the frequencies tested. Passive cavity pressure seemed to have a positive effect on the jet velocity up to a particular pressure characteristic of the diaphragm, beyond which the pressure had an adverse effect. For Thunder® and Lipca, the passive cavity pressure that produced a peak was measured at approximately 20 and 18kPa respectively independent of the waveform utilized. For a Bimorph and RFD, this effect was not observed.

Linear models for all actuators with the factors found to be statistically significant were developed. These models should lead to further design improvements of synthetic jets.

CHAPTER 1

1. Introduction

1.1 Motivation

Methods that attempt to control the motion of fluids have been extensively explored in the past. Some of these methods can be passive or active or both (Gad-el-Hak 2000). Passive flow control is usually achieved through careful modifications to the existing system using steady state tools such as wing flaps, spoilers and vortex generators, among others. These techniques, though effective, have marginal power efficiency and are not capable of adjusting to the instantaneous flow conditions experienced during flight. This limits their implementation in operational applications.

Active flow control (AFC) methods however, are much more efficient. AFCs can adapt to the constantly changing conditions by introducing small amounts of energy locally to achieve non-local changes in the flow field with large performance gains (Amitay et al. 1998, Gad-el-Hak 2000, Kral et al. 1997, Smith & Glezer 1998). The feasibility of increasing the efficiency and simplifying fluid related systems is very appealing considering that a one percent saving in world consumption of jet fuel is worth about 1.25

million dollars a day of direct operating costs (Collis et al. 2004). Likewise, such fuel savings would lead to reduced environmental impact, although such environmental effects are difficult to quantify. McLean et al. evaluated different AFC concepts and candidate applications were considered for civil jet transports (McLean et al. 1999). The simplification of conventional high lift systems by AFC was identified as a prime candidate, possibly providing 0.3% airplane cost reduction, up to 2% weight reduction and about 3% cruise drag reduction. Also the advent of MEMS (Micro Electro Mechanical Systems) technology in the last two decades has provided a new impetus to the field of active control. The MEMS based actuators are easy to mass manufacture and they provide a unified framework for implementing flow control including actuation, power transmission, sensing and incorporation of control algorithms (Ho & Tai 1996).

In spite of all the advantages, using active flow control devices usually adds complexity in design, increases manufacturing and operation cost, which prevents their use. For this reason, many researchers have focused on designing better active flow control devices that are easy to manufacture, are small in size and require little power to operate. One of the devices that fulfill all of these qualities is called synthetic jets.

Synthetic jets consist of a cavity with an oscillating diaphragm. When the diaphragm oscillates air is pushed out an orifice forming a jet (Smith 1999). The interaction of the jets with an external flow leads to the formation of closed re-circulating flow regime near the surface. This interaction can act as a "virtual surface" and consequently is an apparent modification of the flow boundary (Amitay et al. 1997). An

array of such microfabricated devices can produce a large jet velocity if the orifices are at the correct spacing and the driving signals are in phase.

The oscillating diaphragm used in the synthetic jet cavity is usually driven using electrical or mechanical power. In the past, researchers have used compressed air or regulated blowers as a means of supplying steady or oscillating flow (Seifert et al. 1993, Seifert et al. 1996). This adds to the complexity and weight of the system. Piezoelectric disks oscillate in the same manner as a piston or a shaker when driven with an AC electric signal. Eliminating the shaker or a piston reduces the number of moving parts prone to failure. Because of these advantages, several investigators have adopted piezoelectric disks as oscillating diaphragms in synthetic jets to attempt to make the systems lighter, increase efficiency and save resources (Crook et al. 1999, Rathnasingham & Breuer 1997a,b, Smith & Glezer 1998). Piezoelectricity is the ability of certain crystals to generate a voltage in response to applied mechanical stress and the converse effect is also true. The most commonly used diaphragm consists of a Lead Zirconate Titanate (PZT) disk bonded to a metal shim using a conductive epoxy. Although these piezoelectric disks have been successful in generating high velocities capable of altering the flow fields, the devices operate at high frequencies, consequently requiring high amounts of power. Also it was found that after a time, the PZT disk would start to delaminate and/or the output of the device would drop and the resonant frequency would change. Part of the degradation of performance of the device with time may be due to a combination of small cracks appearing in the bondline and the growth of a thin oxide layer between the brass and the conductive electrode (Bryant 1996).

In the current study, piezoelectric composites are used as active diaphragms in the jet cavity. In addition to active piezoelectric layers, they are reinforced with layers of metal or other stronger materials that also increase actuator durability. These composites, besides being lightweight, have the ability to produce micro scale displacements and provide a wide bandwidth response. Such advantages make them suitable for flow control purposes as demonstrated by Mossi et al. (Mossi & Bryant 2004a & b, Mossi et al. 2005b).

The promising potential of piezoelectric synthetic jets for flow control has motivated researchers at various universities, industrial laboratories and government institutions to continue to invest time and effort into their further development. Synthetic jets have potential applications ranging from jet vectoring (Smith & Glezer 1997), mixing enhancement (Chen et al. 1999, Davis & Glezer 1999), to active control of separation and turbulence in boundary layers (Amitay et al. 1997, Amitay et al. 1998, Crook et al. 1999). Yet, the utility of these devices for controlling flows has mostly been shown in laboratory setups. Development of practical applications using this technology requires extensive research into their performance under various conditions, since performance depends on the geometry of the jet cavity, the oscillating diaphragm used, and electrical driving conditions amongst other things. There is also a lack of understanding as to how performance characteristics scale with these parameters. However promising the technology might look, significant barriers exist between the capabilities available to the technologist and the successful application. Comprehensive experiments are required to close the gap between theory, computations, and real-world applications.

Although experimental investigations are capable of providing insight into the operation of a synthetic jet, a parametric study of the flow configuration through experiments is a time consuming and expensive proposition. Design of experiments theory provides an alternate and efficient approach to accomplish the same goals. Through a series of screening experiments, the important factors are identified. These selected factors are then used in developing a regression model that quantifies the dependence of the desired response on the existing factors. Since the performance of the jet is dependant on a number of factors, such statistical tools give a direction towards the relevant areas of synthetic jet research. The screening experiments and regression models can be used in the modeling of response surfaces to optimize the performance of piezoelectric composites as synthetic jets.

1.2 Synthetic Jets

A synthetic jet is a device used to produce an oscillating jet of fluid. The jets are so called because they are synthesized from a train of vortex rings or pairs, formed from the external fluid, without net mass addition. This is one attractive feature of these devices since no hardware is required to obtain mass and flow from a separate source. The jets are formed from the working fluid of the flow system from which they are deployed. Thus linear momentum is transferred to the flow system without net mass injection across the system boundary. The interaction of synthetic jets with an external flow near the flow boundary can lead to the formation of closed recirculation flow regions and consequently

to an apparent modification of the flow boundary (Smith & Glezer 1998, Smith 1999). This attribute enables synthetic jets to significantly affect global modifications of the base flow on scales that are one to two orders of magnitude larger than the characteristics length scales of the jet themselves.

Jet flows without net mass addition can be produced by an oscillating flow having a zero mean velocity through an orifice, provided that the amplitude of oscillations is large enough to induce flow separation at the orifice. A number of different designs of synthetic jet actuators exist that share the concept of operating with zero net mass flux. In the present implementation, the periodic oscillatory motion of a piezoelectric diaphragm forms a synthetic jet normal to an orifice. Since the characteristic dimensions of the jet scale with the characteristic dimension of the orifice, it is possible to synthesize jets over a broad range of length scales. Piezoelectric diaphragms are driven using alternating fields such that jets are formed as a result of volumetric displacement within a fluid filled cavity. As the actuator oscillates it alternately draws in and blows out the ambient fluid through either a high aspect ratio slot or an axisymmetric circular orifice on the cavity. During the suction part of the cycle, the diaphragm moves away from the orifice drawing in ambient fluid to fill the increasing volume within the cavity. During the ejection cycle, the diaphragm moves towards the orifice pushing fluid out of the cavity. Some of the vortices formed at the edge of the slit or orifice will travel sufficiently far and escape re-entrainment during the suction cycle resulting in a synthetic jet with a net momentum and zero net mass flux (Smith 1999). During each cycle the net mass flux out of the cavity is zero while the linear momentum of the flow system is non zero. The jet must be capable of

introducing significant disturbances into the flow. The desired characteristics of actuators include low power consumption, high bandwidth, reliability, and low cost. The following section provides a brief discussion on the composition and mechanism of the piezoelectric diaphragms used in the current study.
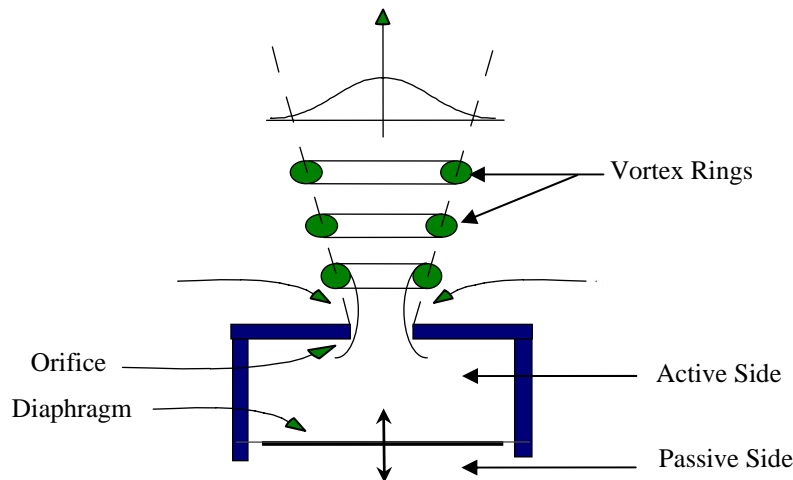
Figure 1.1 Synthetic Jet

1.3 Piezoelectric Ceramics and Composites

Piezoelectricity is the phenomenon whereby electric polarization is generated in certain acentric crystals when they are subjected to mechanical stress, that is, the direct effect. Materials showing this phenomenon must also show a geometrical strain or displacement, proportional to the applied electric field, known as the converse effect, giving them the distinction of being called active materials. Piezoelectric materials are characterized by several coefficients. The coefficients are energy ratios describing the conversion from mechanical to electrical energy or vice versa. The magnitude of the

piezoelectric coefficients depends on oxide ratios, dopants and defect structure, because of their influence on domain wall motion. These defects control the nature of the hysteresis loop in the piezoelectric ceramic. The interaction of the domains and defects leads to soft and hard piezoelectric compositions. Piezoelectrically soft materials are characterized by high piezoelectric constants and high hysteresis as a result of relatively mobile domain walls. In hard piezoelectric ceramics, the domain wall motion is inhibited, resulting in lower piezoelectric constants and reduced hysteresis. Soft piezoelectric materials are preferred for most multilayer and bimorph applications because of their high strain. For some actuator applications, that require non-hysteretic response, hard piezoelectric ceramics can be preferred.

Natural crystals such as quartz, tourmaline, and zincblende are the classical piezoelectric materials. For many years, these materials have served as transducers for converting mechanical energy into electrical energy and vice versa (Cady 1964). In general, natural crystals have rather low piezoelectric coefficients. Piezoelectric materials come in a variety of forms, ranging from rectangular patches, thin disks, and tubes to very complex shapes using injection molding (Bowen and French, 1992). Several of these active materials have been investigated for aerospace and other applications. Ceramic piezoelectric materials were developed in the second half of the 20th century and have been constantly improved since then. Lead Zirconate Titanate [Pb(Zr, Ti)O$_3$] ceramics (commonly known as PZT) are the leading materials for piezoelectric applications (Jaffe et al. 1971). However as the field becomes larger significant hysteresis is exhibited due to domain reorientation as the field becomes larger.

Among the different types of materials developed are piezoelectric polymers such as Polyvinylidene Fluoride (PVDF), electrostrictive materials, such as Lead Magnesium Niobate (PMN), shape memory alloys such as Nickel Titanium (Nitinol), and magnetostrictive materials such as Terfenol-D, among others. Piezo-polymer films (PVDF) are biocompatible, resistive to corrosion, but are highly compliant. Electrostrictive materials (PMN) have low hysteresis losses and moderate stiffness, but have poor temperature stability, and cannot operate in high voltages due to their high material dielectric. Shape memory alloys (Nitinol) are capable of very high strains, but essentially one way actuators and are limited to ultra-low bandwidth applications (< 5 Hz) due to heat transfer and entropic cooling. Finally, magnetostrictive actuators (*Terfenol-D*) have similar actuation energy density and bandwidth as piezo-ceramics, but are very heavy when the coils and flux path materials are accounted for.

All of these actuators and sensors are incorporated onto and into the host structures in many different forms depending upon the environmental and operating requirements of the overall system. Beams, truss structures, plate and shell-like structures are frequently used host structures for piezoelectric sensors and actuators for vibration and noise control applications. Several have been conceived experimentally such as vibration control for plates (Bayer et al., 1991); for beams (Bailey and Hubbard, 1985), and buckling control (Thompson and Loughlan, 1995). The actuators and sensors could either be surface bonded or embedded inside the layers in the form of lamina or fibers (Bent, 1997) of the host laminate.

Piezoelectric actuators have played a pivotal role in nanotechnology starting with their use as positioning elements in scanning tunneling microscopes in 1982 and in atomic force microscopes in 1985, and currently they are used in all nanopositioner applications. Commercial actuator applications include dot matrix printer heads, auto-tracking devices for VCR's, shutter mechanisms and auto focus motors for cameras, gas igniters, buzzers, sonar arrays and hydrophones and accelerometers among others. PZT based Electronic Modulated Suspension was introduced by Toyota in 1989 to augment shock absorber capabilities. They also play a central role in automotive airbag systems.

A piezoelectric transducer that can generate large displacement while withstanding a sizable load is essential for actuator applications (Newnham & Rushau 1991, Uchino 2000). However, the electric-field-induced displacements of those materials are much less than 1%, and in most cases, they are too small for some applications (Schwartz et al., 2000). In order to enhance the displacement, various types of actuators based on piezoelectric ceramics have been developed. These ceramics are usually of various size and shapes. When a voltage is applied across the electrodes the material changes thickness. The amplitude of the change is related to the applied voltage through a piezoelectric coefficient that, for PZT materials, is less than 600×10^{-12} m/V. One way to increase the displacement is to use a bending actuator. Basically, a bending actuator is composed of a piezoelectric plate that is bonded to an inactive substrate layer (Smits 1991). When a voltage is applied, the piezoelectric plate expands or contracts whereas the non-piezoelectric plate keeps the same geometry, causing the actuator to bend as a differential stress field is developed.

A number of transducer designs based on this principle have been developed to augment strain force, or drive level capabilities of the constituent piezoelectric materials through curvature enhancement, pre-stress augmentation or strain enhancement mechanisms. The moonie, cymbal, reduced and internally baised dome shaped oxide wafer (RAINBOW), thin layer composite unimorph ferroelectric driver and sensor (Thunder®), lightweight piezo composite actuator (LIPCA), and the radial field diaphragm (RFD) are actuator designs developed in the last 15 years. These designs provide moderate displacements in conjunction with moderate generative forces.

To investigate their performance as SJ diaphragms and to explore the relevant parameters for their performance four types of actuators are used as active diaphragms. A detailed discussion on the construction of each of these actuators, Bimorph, Thunder®, Lipca, and RFD, is given in Chapter 3.

1.4 Problem Statement

The objective of this research is to characterize synthetic jet actuators formed using piezoelectric composites as active diaphragms. For the practical implementation of any new technology, it is required that all the physics involved in the mechanism be thoroughly investigated. Since many factors may have an effect on the performance of a synthetic jet, it is the aim of this study to identify the more relevant factors from a carefully selected group. Based on these factors a model will be developed to aid in the future design optimization of a synthetic jet.

Past studies have shown that the synthetic jet is heavily dependent on the actuator device (Wlezien et al. 1998, Cattafesta et al. 2001, Schaeffler at al. 2002). Four piezoelectric diaphragms, Bimorph, Thunder[®], Lipca and RFD, are studied as possible active diaphragms in a synthetic jet cavity. Three of these diaphragms have never been used in synthetic jet research before and through this study it is attempted to show that their performance is comparable if not better than the devices used in the past. The factors involved in this study include, driving waveform, voltage, frequency, and the geometrical parameters of the cavity and the internal pressures generated in the cavity. It is intended to individually study each factor for every diaphragm, and to identify the main factors. Since the number of factors considered for this study is large, a statistical approach of fractional factorial experimental design is proposed. Through such statistical tools the significant factors will be identified and also the individual effect sizes calculated. The critical factors will be fitted in a first level linear model to generate an approximation for the desired output.

1.5 Organization of Chapters

The first chapter provides a research background on synthetic jet technology. It further gives relevant information about flow control tools and techniques, providing a detailed discussion on synthetic jet actuators. A description of the working principles involved in this technology are stated and reviewed. The latter part of the chapter details piezoelectric actuators and their potential as active diaphragms in a synthetic jet cavity.

Chapter 2 gives a brief literature review of the studies conducted in the past. A short timeline is established and the related studies discussed. The following chapter begins with a detailed description of each actuator used in the study. Using schematics, Chapter 3 also explains the various experimental setups and calibration techniques used during the course of the project. The experimental parameters and cavity parameters are shown in tables. The factors selected for the study and the analysis tools used are defined.

Results obtained through the experiments and the subsequent statistical analyses are provided in Chapter 4. This chapter has four subsections for each actuator discussing the factors individually before conducting a statistical analysis. The last section of the chapter gives a summary discussion of the factors and proposes theories for the results obtained. Finally, the last two chapters state the conclusions drawn from the study and propose future directions that this research could follow.

CHAPTER 2

2. Literature Review

The German engineer Ludwig Prandtl first introduced the world to flow control by publishing the boundary layer theory at the beginning of the 20th century. In the period leading up to and during World War II, as well as in the cold war era, flow control was extensively studied and applied, although primarily to military related flow systems. A comprehensive review and analysis was provided by Lachman and more recently by Gad-el-Hak (Lachman 1961, Gad-el-Hak et al. 1998, Gal-el-Hak 2000). All known flow control efforts preceding the pioneering work of Schubauer and Skramstad used steady state tools and mechanisms for flow management (Schubauer & Skramstad 1947). Such passive flow control techniques have marginal power efficiency, and therefore limit the implementation in operational applications. Active flow control (AFC) is a fast growing multi-disciplinary science and technology aimed at altering a naturally developing flow system into a more desired path. Active flow control using periodic excitation that exploits natural flow phenomena has the potential of overcoming the efficiency barrier.

Synthetic jets are popular flow control devices capable of causing an apparent modification to the flow boundary through periodic oscillations. Their popularity stems from their self-contained design, no fluid source, no ducting is required, only an applied voltage. The design of the micro scale synthetic jet actuator proposed by Glezer and his co-workers (Coe et al. 1994) has been adapted widely by a number of researchers. The design is very simple consisting of a diaphragm that is driven by an electric field, set within a cavity. The diaphragm is made up of a piezo disk glued to a metal shim, a Unimorph. An orifice in the lid of the device allows fluid to be drawn into, and forced out of the cavity. To obtain high velocities, the diaphragm has to be driven at its resonant frequency, which is in the kHz range.

Smith and Glezer performed a detailed experimental investigation into the synthetic jet created by these devices (Smith & Glezer 1997, 1998). It is claimed, that during the outflow cycle a vortex ring is formed at the orifice. This ring then travels away from the device under its own self-induced velocity. By the time the fluid is drawn into the cavity, the vortex ring has moved sufficiently far away so as to be relatively unaffected. Consequently, a train of vortices traveling away from the orifice is generated. In their experiments, the vortices rapidly undergo transition and lose their coherence. The resulting synthetic jet is turbulent. The experimental findings of Smith and Glezer were supported by Kral et al. who performed a two dimensional numerical study of a laminar synthetic jet (Kral et al. 1997).

Rathnasingham and Breuer drew attention away from the jet and instead focused on the physics within the cavity (Rathnasingham and Breuer 1997a). It was demonstrated,

by the use of experimental and simple numerical models, that there was significant fluid structure interaction between the resonant diaphragm and the fluid pressure in the cavity. Interest in the cavity was continued by Rizzetta et al. who solved the three-dimensional compressible Navier-Stokes equations both inside and outside of the cavity (Rizzetta et al. 1999). It was shown that significant vertical disturbances could be created in the cavity during the inflow cycle of the actuator. The cavity dimensions, such as cavity depth, also influenced the velocity profile of the jet at the orifice exit.

The effectiveness of oscillatory blowing in separation control has been established experimentally and numerically (Hasan 1998, Donovan et al. 1998, Seifert et al. 1993, Seifert & Pack 1999). Active separation control was applied successfully for the first time at Reynolds numbers, corresponding to a jetliner at takeoff conditions. Oscillatory blowing proved to be an effective and efficient tool for the control of boundary-layer separation over a wide range of chord Reynolds numbers, representative of a micro-aerial-vehicle to commercial jetliners at takeoff. Using bench-top experiments, accompanied by theoretical analysis, it was determined that the level of velocity fluctuations exiting the blowing slot was proportional to the cavity pressure fluctuations normalized by the density, for low amplitudes (velocity < 10 m/s), whereas for high amplitudes it is proportional to the square root of the normalized pressure (Seifert et al. 1999). Based on these results, Seifert et al. proposed that a possible approach to closed-loop control of separation is to sense the trailing edge pressure and use that as an input to adjust the oscillatory blowing momentum coefficient to achieve the desired aerodynamic behavior, while maintaining effective frequency as 1 at all times. Effective frequency, as defined by Seifert and Pack, is the

oscillation of the diaphragm divided by the free stream velocity multiplied by the location of the jet on a wing.

These successful attempts in separation control encouraged the investigation of the effect of synthetic jet actuator on simple two dimensional cylinder flows. Amitay et al. controlled lift and drag forces successfully by installing a pair of synthetic jet actuators side by side radially on the cylinder shell (Amitay et al. 1997 & 1998). Mallinson et al. investigated similar control on a cylinder but used a circular orifice instead of a rectangular orifice as in the previous case (Mallinson et al. 1999). Again, control over a cylinder was performed by Crook et al. also Wood et al., using a spanwise array of synthetic jet actuators to delay separation (Crook et al. 1999, Wood et al. 2000). Crook et al. constructed a device, a piezoelectric disc bonded to a brass shim, based on preliminary analysis by Rathnasingham and Breuer that modeled a thin circular plate as a piston. Results showed the model provided a good prediction of the mean value of the velocity in the developed jet though the model did not predict the peak centerline jet velocity.

The standard synthetic jet actuator cavity design proposed by Glezer et al. was modified by Bryant et al. (Bryant et al. 1999) to demonstrate the potential benefits of high displacement piezoelectric actuators (HGA's) such as Bimorph and Thunder® in synthetic jet actuation. These pre-stressed devices have the advantage of durability and being able to produce large deflections at non-resonant driving frequencies. Several studied conducted by Mossi et al. (Mossi & Bryant 2004a & b, Mossi et al. 2005b) have shown that the diaphragm used in the synthetic jet cavity has a significant effect on the jet velocity, yet its performance is highly dependant on geometrical, mechanical, and electrical parameters.

The main focus of this study is to gain complete knowledge of the physical details of the actuator device and based on the results design an efficient synthetic jet cavity capable of performing satisfactorily.

CHAPTER 3

3. Experimental Setup

The piezoelectric actuators used in this study include Bimorph, Thunder[®], Lipca and RFD. This section gives a detailed description of the construction of these piezoelectric composites. Also, the synthetic jet cavity and the various instruments used for the velocity and pressure measurements are described. It has been proven that the boundary conditions that a piezoelectric actuator is subjected to, have a significant impact on the final performance of the device. For instance Liew stated that different boundary conditions and applied voltages affect the shape control of piezo laminated composite beams (Liew et al. 2002). For this reason the clamping mechanism used becomes critical to the characterization of the synthetic jet and special consideration to its design is utilized.

3.1 Bimorph

Series Bimorphs consists of two thin ceramic sheets bonded together with their poling directions opposed and normal to the interface. When an electric field is applied to a bimorph, one of the plates expands while the other contracts. This mechanism creates a

bending mode that mimics piston like displacement. Bimorphs are capable of generating large bending displacements of several hundred micrometers on center or edge, but the response time (1 ms) and the generative force (1.0 N) are low (Dogan et al. 2001). In the current study, the Bimorph used is model T216-A4NO-573X manufactured by Piezoelectric Systems Inc. It consists of two nickel electroded PZT 5A discs with diameters of 63.5 mm and a total thickness of 0.41mm. They have a 1 kHz capacitance of 130nF and have been shown to produce displacements up to 0.3 mm at low frequencies (Mossi et al. 2005a). A schematic of the disc alignment along with the final shape is shown in Figure 3.1.
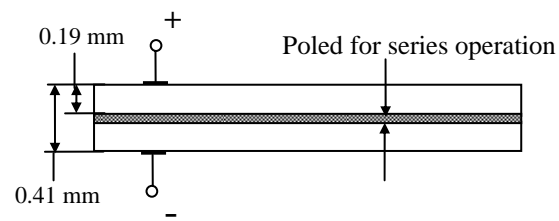
(a)
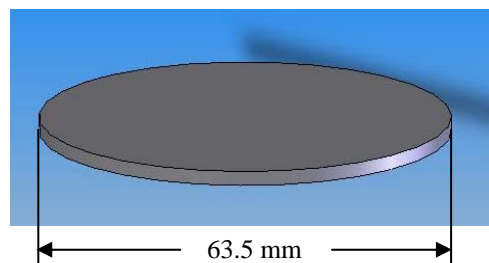
(b)

Figure 3.1 Bimorph (a) Layer Alignment, (b) Final Shape

3.2 Thunder®

Thin layer composite Unimorph ferroelectric Driver and Sensor (Thunder®) was developed at NASA Langley Research Center. It is an actuator that exploits the coefficients of thermal expansion mismatch between materials (Dausch & Wise 1998, Haertling 1994, Mossi et al. 1998, Wise 1998). The significant advantage that Thunder® actuators have over other Unimorph benders is their extremely rugged construction. This allows them to be more readily used in commercial applications, such as synthetic jets (Smith et al., 1999). The mechanical advantage of the Thunder® design is due to the increased flexibility of the device and the radial expansion created by the pairing of preselected thermally mismatched materials (Hellbaum et al. 1997). Thunder® transducers consist of an integrated sandwich of layers. The diaphragm used in the current study is made up of five layers. Prestressed metal layers make up the top and bottom and the piezoelectric layer is sandwich between them with a hot melt adhesive forming a thin bondline between the ceramic and metal layers. A schematic of the Thunder® is shown in Figure 3.2.

Thunder® actuators can be fabricated in virtually any size and thickness (Mossi et al. 1998). A circular device manufactured by Face International Inc. is used in the present study. It is composed of three main layers, with two additional being the thin bondline; a top chemically etched copper layer 0.0254 mm thick, a middle piezoelectric layer of thickness 0.254 mm, and a bottom 0.254 mm thick layer of stainless steel. The copper and ceramic layers have diameters of 63.5 mm and the steel layer, 68.58 mm leaving a circular tab along the edge of 2.54 mm. This additional tab is included in the design to facilitate

(a)

Stainless
Steel
PZT   (0.25mm)
(0.25mm)
SI
Copper   Adhesive
(0.025mm)   0.0152mm)
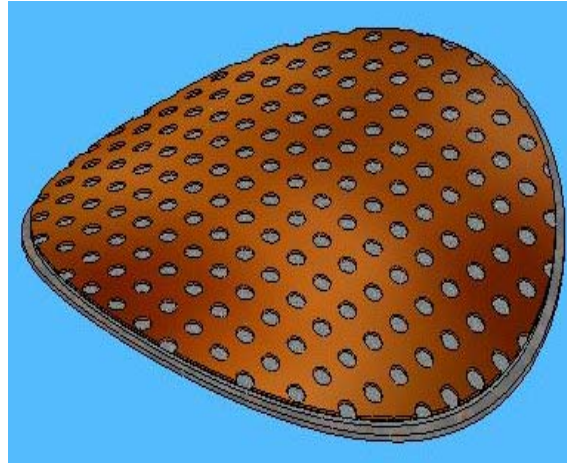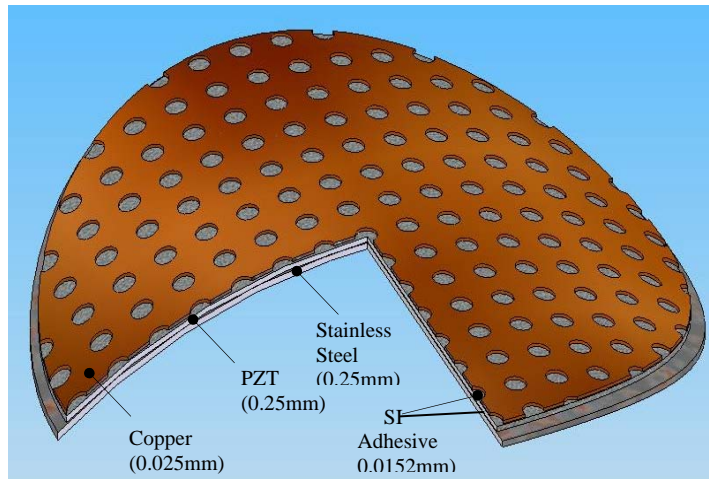
(b)

Figure 3.2 Thunder® (a) Final Shape, (b) Layer Characteristics

clamping of the device. The layers are laminated with a high temperature polyimide adhesive (Bryant 1996) through a layering high-temperature bonding process (Mossi et al. 1998). The resulting actuator is saddle shaped with a capacitance of 110nF as shown in Figure 3.2. The piezoelectric ceramic used in both these diaphragms is a soft PZT type 5A. Thunder® exhibits its highest displacement at the center of the dome, and displacement

decreases drastically towards the edge of the actuator (Mossi & Bryant 2004a). The maximum center displacement measured is approximately 0.06 mm with a sawtooth signal at 5 Hz (Mossi et al. 2005a).

3.3 Lipca

Lightweight Piezo-composite Curved Actuator (LIPCA) is a powerful actuator that can be used for adaptive structure applications. LIPCA is manufactured by co-curing layers at an elevated temperature: glass/epoxy layer, unidirectional carbon/epoxy layer, and ceramic layer (Park et al. 2001, Yoon et al. 2002). Differences in coefficient of thermal expansion (CTE) of the layers result in the LIPCA's post cure curvature. Based on the arrangement of the layers, the curvature and the displacement varies (Yoon et al. 2003a). The LIPCA shown in Figure 3.3(a) is made by Konkuk University, South Korea. It has a high CTE top layer of glass/epoxy with diameter 66.0 mm and thickness 0.09 mm, a near zero CTE unidirectional carbon/epoxy layer with 66.0 X 1.0 mm dimensions, a layer of PZT 5A ceramic 50.0 X 0.18 mm, and another glass/epoxy layer with the same dimensions in the bottom as shown by Figure 3.3(b).

The circular LIPCA is not as curved as the circular Thunder[®] but produces higher center displacement of approximately 0.075 mm with a sawtooth driving signal at 25 Hz (Mane 2005). The difference in curvature is due to the fact that the processing temperature used for the LIPCA is much lower then the Thunder[®] (Yoon et al. 2003b). The capacitance is approximately the same as the Thunder[®], 100nF.

(a)

UD
Carbon/Epoxy
(0.09mm)

PZT
(0.18mm)

Glass/Epoxy
(0.09mm)

(b)
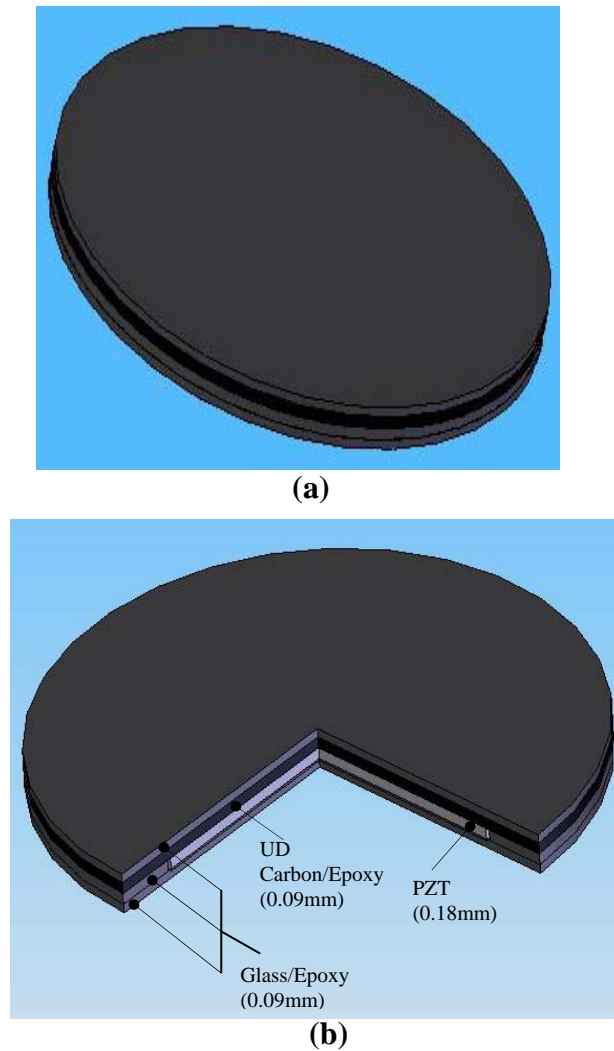
Figure 3.3 LIPCA (a) Layer Arrangement, (b) Final Shape

3.4 RFD

The Radial Field Diaphragm (RFD) was developed by NASA Langley Research Center. It is comprised of a thin circular piezoelectric ceramic disk sandwiched between two polyimide "PI" dielectric films with either copper-etched dual intercirculating spiral or circular interdigitated ring electrodes (Bryant et al 2004 – JIMSS). For the spiraled

electrode pattern, positive and negative electrodes spiral inward to the center of the disk in a serpentine manner called Inter-Circulating Electrodes (ICE). As seen in Figure 3.4 this electrode pattern induces an electric field into the piezo ceramic that extends out radially from the center of the wafer (Bryant et al. 2004). The dielectric film serves as the electrode carrier and insulator. Because of its radial electric field, the ICE-RFD exhibits out of plane movement, when electrically stimulated, and do not transmit any substantial mechanical strain beyond the boundary of the ceramic element. This behavior is distinct from all other bender type actuators. The RFD in the current study has a diameter of 63.5 mm and is based in the PZT 5A ceramic. It has a very low capacitance of approximately 4nF at 1 kHz and can produce displacements up to 0.4 mm (Mossi et al. 2005a).
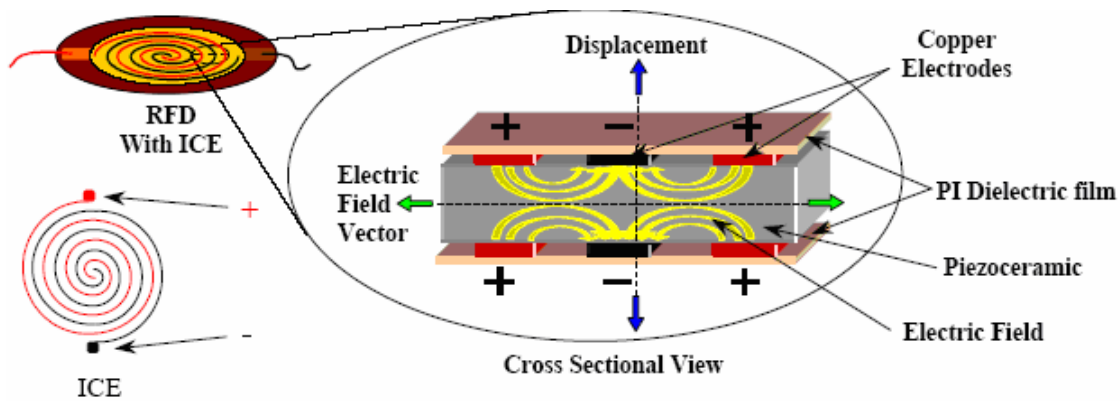
Figure 3.4 RFD & Inter-Circulating Electrodes (ICE) (Bryant et al. 2004)

3.5 Synthetic Jet Cavity

The synthetic jet cavity is constructed of two 88 mm X 88 mm Plexiglas™ pieces. The plastic pieces have a 60.5 mm circular aperture in the center. A 5 mm wide and 1 mm

deep groove is machined along the perimeter of the aperture. The actuators are placed in between the two grooves reinforced with neoprene rubber on both sides to provide both a cushion and a seal as shown in Figure 3.5(a). The plastic pieces are sealed together along with a 1.6 mm thick covering plate that provides an axisymmetric orifice in the center. Seven 4 mm screws with washers are used to clamp the cavity, while one screw hole is left empty to serve as a port for the actuator electrical leads and additional attachments to the cavity. Equal torque of 424 Nmm is applied on each screw using a torque screwdriver to ensure constant pressure along the perimeter of the actuator. Once the assembled cavity is in place, the sealed synthetic jet cavity is mounted on a height gauge as shown in Figure 3.5(b).

(a)

(b)
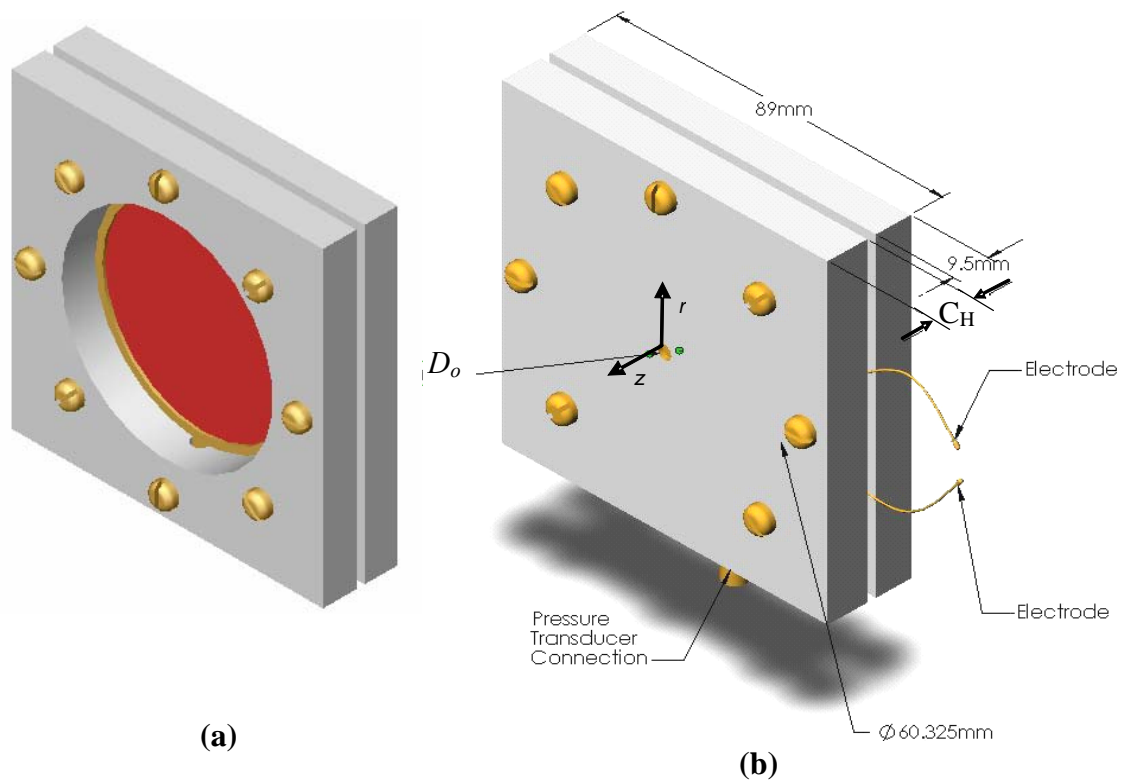
Figure 3.5 Synthetic Jet Cavity, (a) Final Assembly; (b) Clamped Actuator.

The cavity setup utilized allows variations in cavity height and orifice dimensions. The two cavities have overall dimensions of 88.0 x 88.0 x 19.1 mm and 88.0 x 88.0 x 11.0 mm, which correspond to cavity heights of 9.55 mm and 5.5 mm respectively. This cavity height, C_H, is measured from the diaphragm to the orifice exit. Two cover plates with circular orifices have approximate diameters, D_o, of 2.0 mm (small) and 3.67 mm (large) are used.

3.6 Hotwire Calibration

All velocity measurements are performed using a hotwire anemometer. It is a single cylinder sensor used for one dimensional flow measurements. It has a diameter of 4 μm and a length of 3.2 mm. With the help of the IFA 100 flow analyzer the hotwire anemometer measures the flow in terms of voltage. Using a calibration this voltage is converted to velocity.

The calibration setup consisted of a standard pipe flow, with a pitot tube and an electronic pressure transducer as the calibration standard. As fully developed flow is required for calibration, the pipe had to be sufficiently long. In order to reduce turbulence, flow straightening devices were distributed along the length of the pipe that consisted of honeycombed PVC pipe distributed in several sections was used. Various experiments were conducted with different combinations of length and number of the honeycombs until fully developed flow was achieved. Different types of nozzles and diffusers were considered in finding the desired flow condition, fully-developed flow. The nozzle used at

the mouth of the wind tunnel was a 9.53 mm male quick release fitting, mounted onto an aluminum bracket that is fixed into a 187.33 mm diameter coupler. The coupler was reduced to an 88.9 mm outside diameter pipe that was 2.52 m in length. The nozzle was situated in the wind tunnel pipe, which was fitted into the 88.9 mm diameter *PVC* pipe. Foam was used around the pipe to dampen the oscillations that the tunnel would produce during operation as they could have a significant effect on the pressure. The actual wind tunnel pipe that would become the calibration diameter was 19.05 mm diameter. This section of pipe was cut to a length of 2.65 m and measurements were taken at 2.48 m from the nozzle at the tunnel inlet. The hotwire was calibrated for use in airflows having velocities ranging from 0 to 60 m/sec. A picture of the nozzle flow coupler is shown in Figure 3.6 (a). The calibration facility along with the air supply assembly is shown in figure 3.6 (b).

A typical calibration curve is shown in Figure 3.7. A fourth order polynomial regression fit gives the coefficients required to obtain the velocity. Equation 3.1 gives the curve fit equation. Where *Y* is the velocity in m/s and *x* is the velocity in terms of voltage measured by the hotwire.

$$Y = 0.8271 + 0.0561 \cdot x - 2.4086E - 03 \cdot x^2 + 5.0757E - 5 \cdot x^3 - 3.8421E - 07$$

Equation 3.1

(a)   (b)
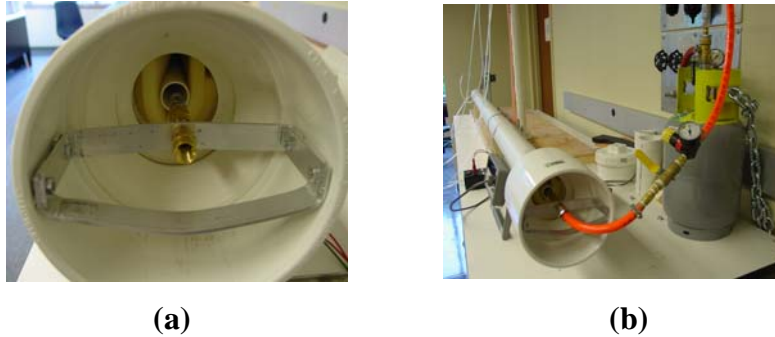
Figure 3.6 Hotwire Calibration Facility, (a) Nozzle Flow Coupler, (b) Calibration Pipe and Air Supply Assembly

The assembled actuator-cavity is mounted onto an adjustable height gauge, with the actuators surface perpendicular to the hot-wire anemometer used to measure velocity. It can be traversed through the diameter of the synthetic jet orifice as shown in Figure 3.8. The Mathcad program used for the velocity conversion is given in APPENDIX.
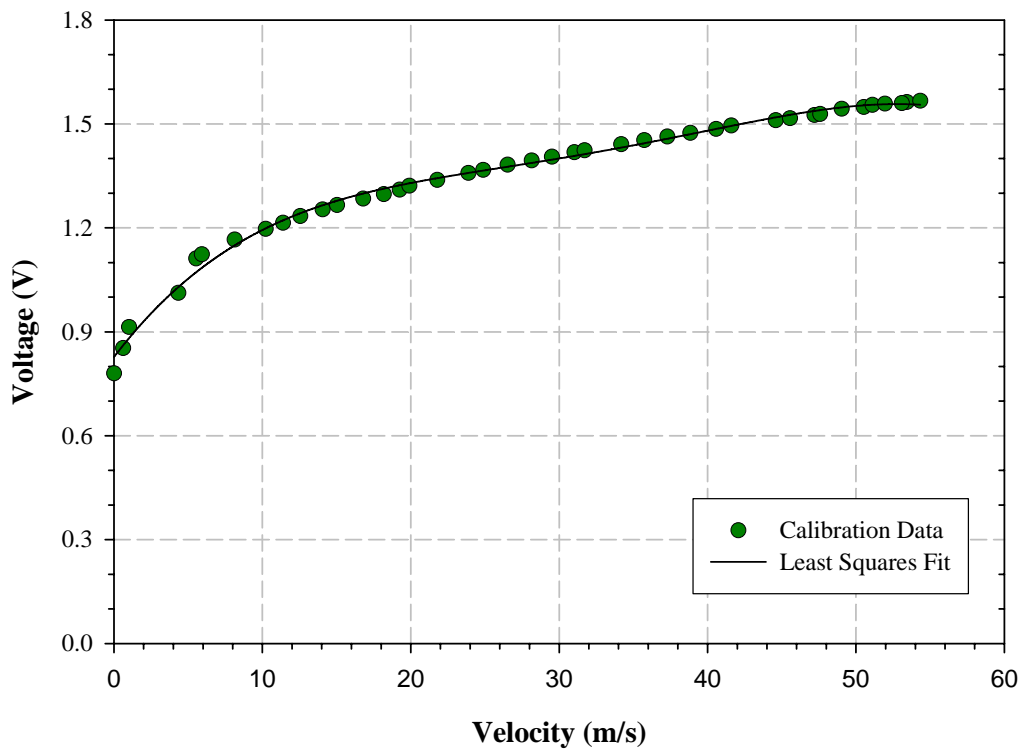
Figure 3.7 A Typical Hotwire Calibration Curve

Hotwire
Diameter 4μm

3.2 mm

$D_o = 2$ mm

(a)

Hotwire
Diameter 4μm

3.2 mm

$D_o = 3.67$ mm

(b)
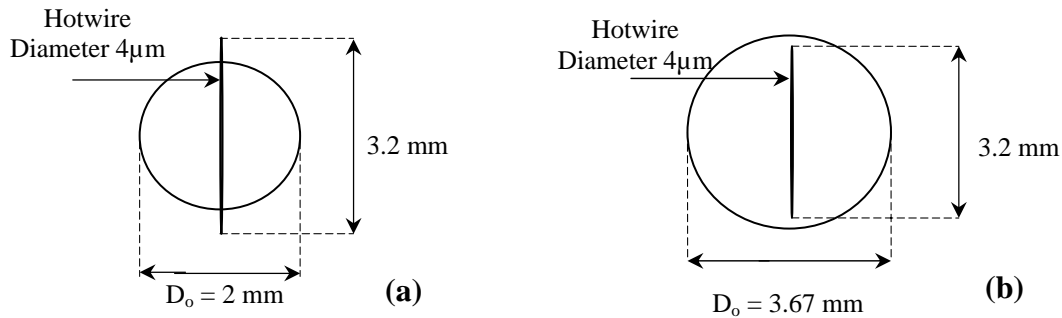
Figure 3.8 Hotwire dimensions with respect to the Synthetic Jet Orifice (a) small orifice, (b) large orifice

3.7 Instrumentation and Measurements

The driving signal is applied at high voltages and varying frequencies for each device. This signal is applied using a signal generator, a Hewlett Packard model HP33120, connected to an amplifier, TREK model PZD700. The velocity and voltage signals are monitored and recorded using an oscilloscope, LeCroy model 350L, and a National Instruments data acquisition system as shown in Figure 3.9. The amplitude and frequency of the applied signal were kept below their allowable maximums in order to prevent electrical and mechanical failure of the diaphragms. Table 3.1 gives the voltages and frequency ranges used for each actuator. Two driving signals, sine and sawtooth, are used with all experiments. In case of the RFD the square wave signal is also used.

Measurements can be divided into two sets. The first set of experiments includes velocity measurements in quiescent air with no additional attachments to the passive cavity of the synthetic jet. Velocity is measured at a fixed distance of 2 mm in the z direction for each actuator. To obtain velocity profiles along the length of the orifice, velocity is

measured at various locations along the orifice. To study the effects of frequency on the jet, the velocity is measured at the center of the orifice at the same fixed distance of 2mm in the z direction. These experiments are conducted on four synthetic jet cavity configurations. The differences in the cavities are the cavity height and the orifice diameter. The cavity configurations are shown in Table 3.2.
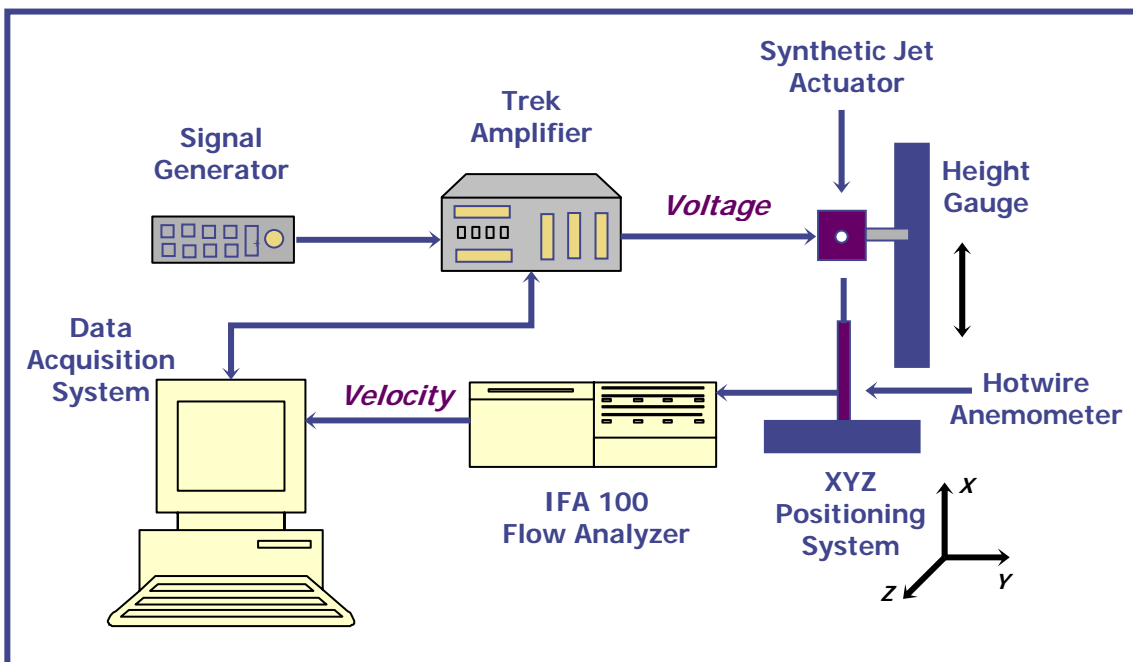
Figure 3.9 Instrument Layout

Table 3.1 Experimental Parameters

	Bimorph	THUNDER®	LIPCA	RFD
Voltage	125 Vpp 150 Vpp	250 Vpp 400 Vpp	200 Vpp 350 Vpp	800 Vpp
Frequency	5 – 100 Hz	5 – 100 Hz	5 – 100 Hz	5 – 100 Hz

Table 3.2   **Cavity**

Parameters

		C_H (mm)	
		5.50	9.55
D_o (mm)	2.00	Cavity I	Cavity II
	3.67	Cavity III	Cavity IV

In the second set of experiments, the passive cavity is pressurized. This is accomplished using compressed air from a regulated supply. A pressure regulator controls the pressure in the passive cavity to desired levels. Figure 3.10 gives a schematic of the synthetic jet cavity with the passive cavity pressurized. Again the velocities are measured and profiles mapped with different pressure levels in the passive cavity.
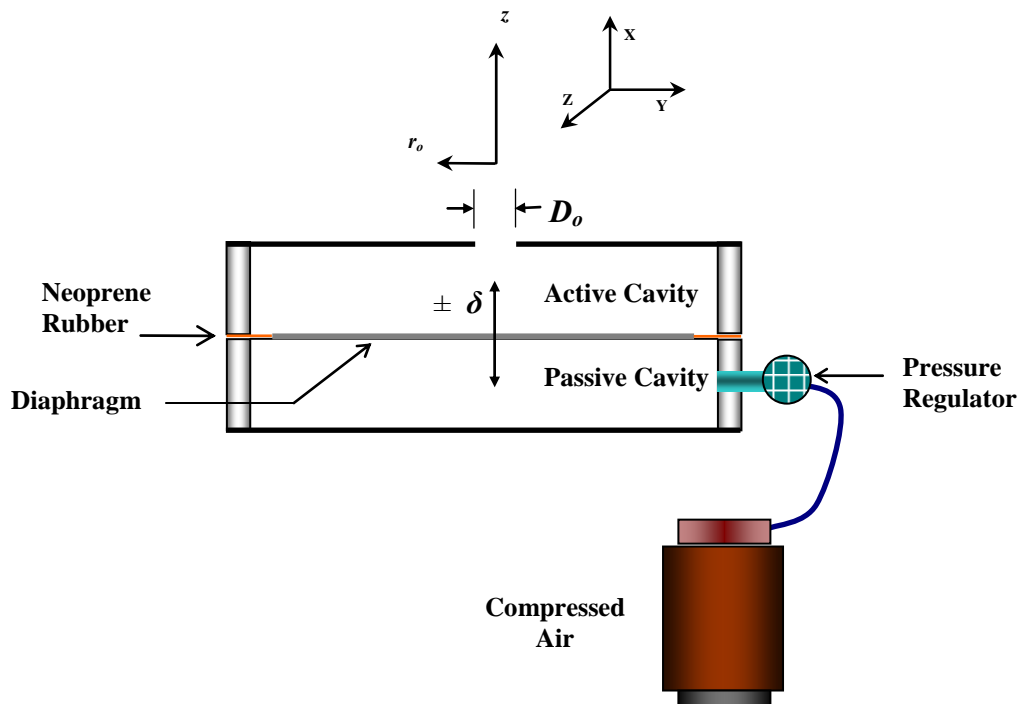
Figure 3.10 Cross sectional view of the Synthetic Jet cavity while pressurizing the Passive cavity

In case of the RFD, the differential pressure in the active cavity is also measured with respect to the pressure in the passive cavity as shown in Figure 3.11. The differential pressure in the active cavity is measured using an Endevco 8510 B-2 dynamic pressure transducer. As the pressure in the active cavity is dynamic, it cannot be measured using a regular transducer that measures average pressure. Also the pressures inside the cavity are very small and cannot be detected with a regular transducer. The dynamic pressure transducer has a range of 17.24 kPa and resolution of 0.14 kPa. A schematic of the setup is given in Figure 3.11. The active cavity pressure is measured at different voltages and frequencies, with no additional pressure added to the passive cavity. All the active and passive cavity pressure measurements throughout the project were done in the cavity IV configuration (Table 3.2).
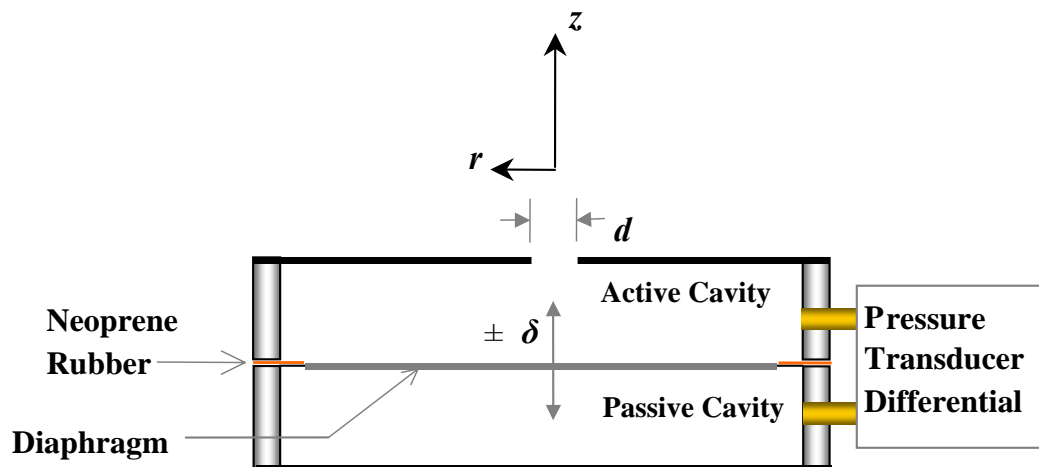
Figure 3.61 Active Cavity Pressure Measurements

CHAPTER 4

4. Results

The results presented below are divided into sections based on the factors considered for the characterization. Each factor is first discussed individually followed by a collective statistical analysis of all the factors. Such an analysis shows the significance of the factors providing a direction to future research on this topic as well as to illustrate the process of designing applications using piezoelectric actuators.

4.1 Bimorph

4.1.1 Driving Signal and Frequency Effects

Previous studies on synthetic jets have used the sine wave as the driving input signal. A sine wave as the driving input requires relatively high frequencies to match the actuators resonance frequency to enable a synthetic jet formation with significant velocity magnitude. High frequencies however, consume more power and also physically limit the oscillation amplitude of the piezoelectric diaphragm that in turn limits the amount of air

volume displaced. In this section the jets driven using a sine and a sawtooth signal are studied. A sawtooth signal provides the force required to produce large velocities at low frequencies.

A typical velocity curve formed with a sine wave is shown in Figure 4.1. Two jets are observed with the second jet smaller in magnitude. The first jet (larger jet) follows the leading edge of the input signal and the second jet (smaller jet) follows the trailing edge. The larger jet is believed to occur during the expulsion cycle, while the smaller jet is believed to occur during the ingestion cycle. Previous studied on the synthetic jet flow fields by Glezer et al. have indicated that during the ingestion cycle the flow reenters the cavity from the sides of the orifice. Thus the second jet may be due to the nonparallel direction of the flow, relative to the hotwire, entering the cavity. At lower frequencies, only one jet is formed indicating that at lower frequencies the flow during ingestion cycle is nearly parallel to the hotwire anemometer and hence cannot be detected.

In the case of the sawtooth signal a single velocity jet is formed. As shown in Figure 4.2, the jet follows the leading edge of the input signal, with series of smaller jets immediately following the first jet. These jets may be caused by vibrations of the clamped actuator. The jets formed using sawtooth driving signals are larger in magnitude as compared to the ones formed with a sine wave.

The amplitude of the driving signal has an effect on the maximum jet velocity as seen in Figure 4.3 for cavity IV. An increase in the input voltage produces greater velocities. This effect is seen in all the cavities and frequencies for both the studied driving signals.
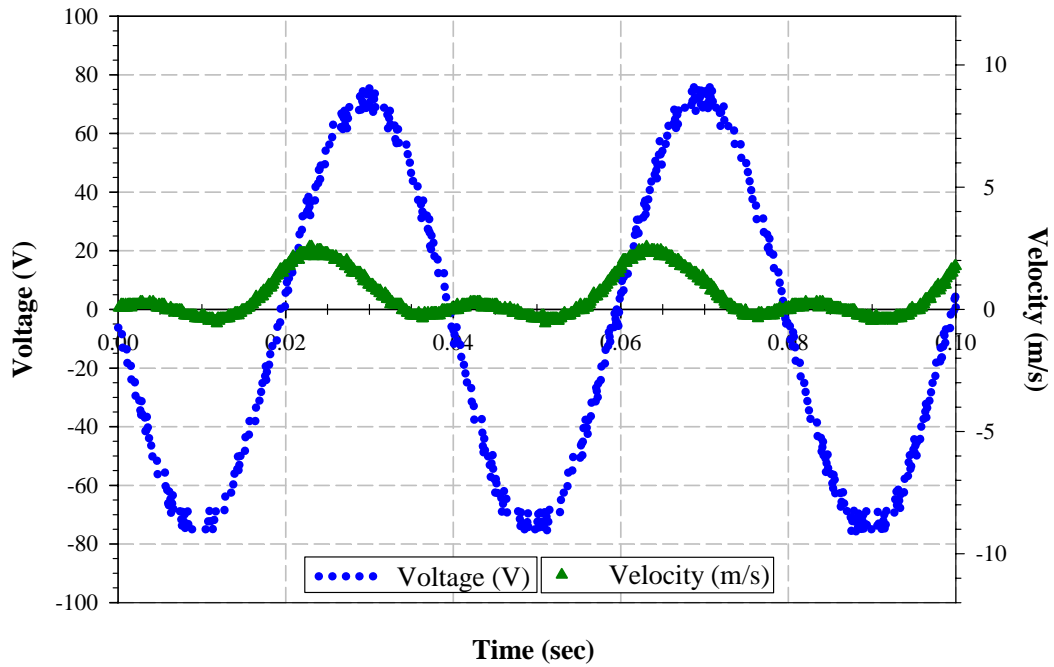
Figure 4.1 Typical Velocity Curve with Sine Driving Voltage with Cavity IV for a Bimorph Diaphragm at 100 Hz and 150Vpp
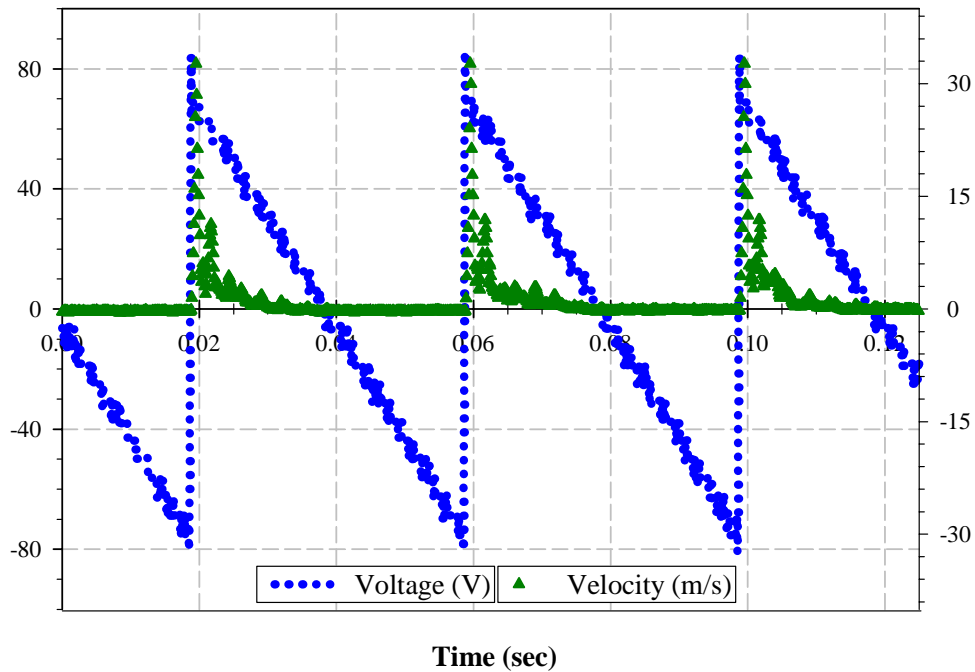
Figure 4.2 Typical Velocity Curve with Sawtooth Driving Voltage with Cavity IV for a Bimorph Diaphragm at 25 Hz and 150 Vpp
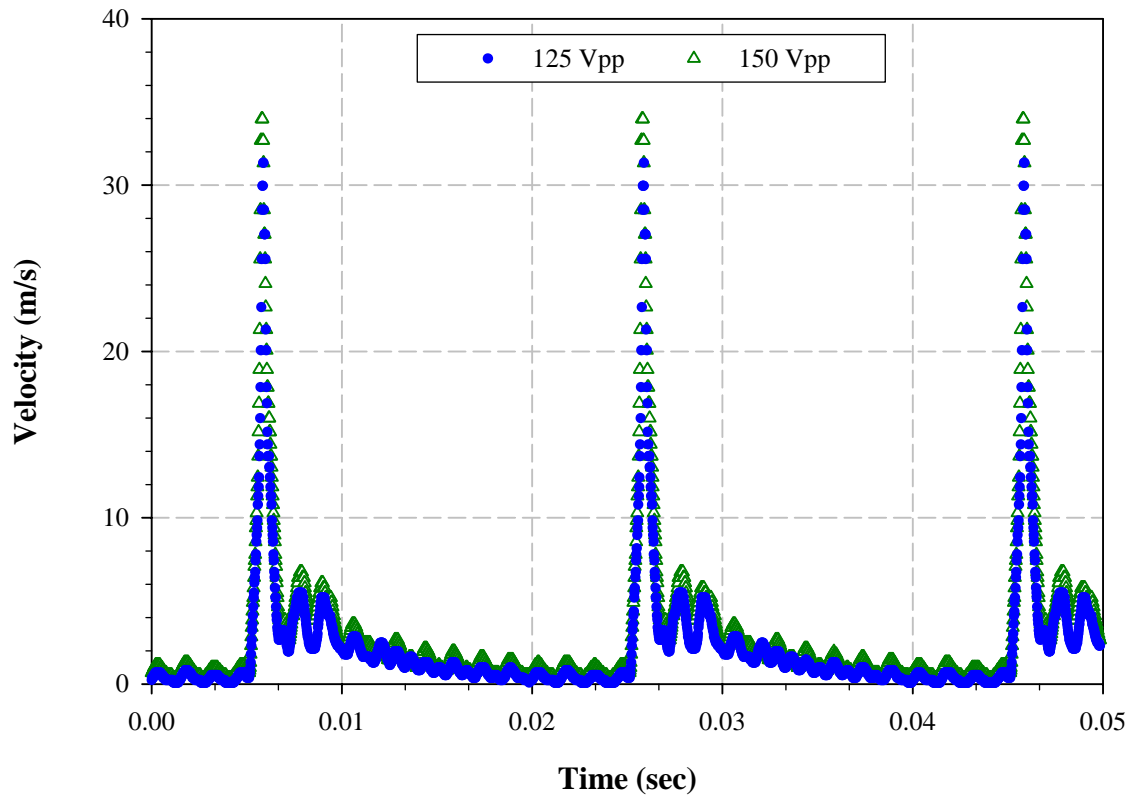
Figure 4.3 Effect of Voltage on Velocity Magnitude with Cavity IV for a Bimorph Diaphragm at 50 Hz using a Sawtooth Signal

To test the effects of frequency on velocity, the Bimorph is operated at various frequencies up to 100 Hz. As seen in Figure 4.4 with a sine wave input signal the velocity increases as frequency increases. In case of a sawtooth input, the velocity remains constant after approximately 10 Hz. This behavior is observed at all voltages and for all the cavities tested. Further discussion on these effects is given in the discussion and summary section at the end of this chapter.
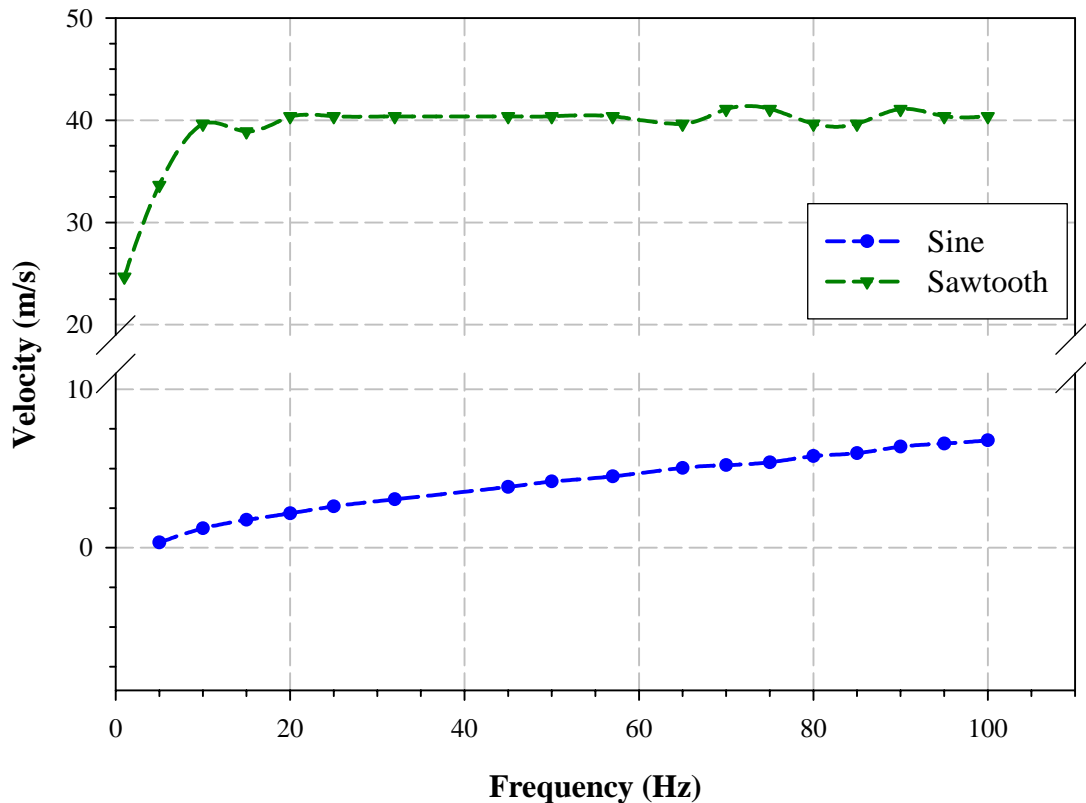
Figure 4.4 Frequency Effects on Bimorph Diaphragm Peak Velocities for Cavity IV at 150 Vpp

4.1.2 Cavity Height Effects

In order to test the effects of changes in cavity height the profiles obtained from the four cavities were compared. Since cavity III and cavity IV have the same orifice diameter but different cavity heights their profile comparison will show the effects of changes in cavity height or cavity volume on the velocity magnitudes.

Profiles for cavity III and cavity IV are shown in Figure 4.5. In the case of a sine driving signal, a difference of approximately 30% is observed between the maximum velocities of the two cavities with the smaller height/volume cavity producing the higher

velocity. Similarly, cavity I and cavity II are also compared as they have the same orifice

diameter, a difference of 33% is observed.
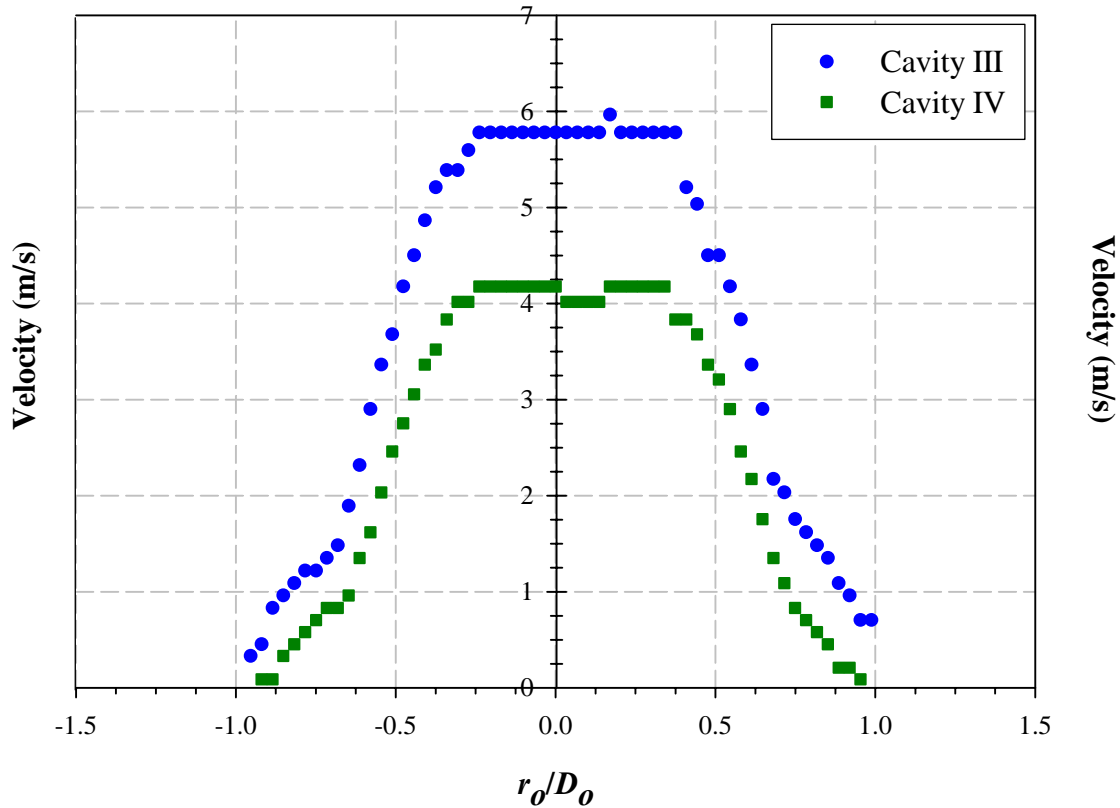
Figure 4.5 Cavity Height Effects using a Sine Driving Signal for a Bimorph
Diaphragm at 50Hz and 150 Vpp

With a sawtooth driving signal the differences in velocities are smaller as shown in

Figure 4.6. A comparison of cavity I and II profiles at 50Hz shows a difference of 25% and

between cavity III and IV of only 13%. Similar to the sine signal, the cavity with the

smaller volume produces higher velocities. The cavity I and II comparison is shown in

Figure 4.6. The large difference between cavities I and II could be due to the relatively

larger orifice of cavities III and IV.
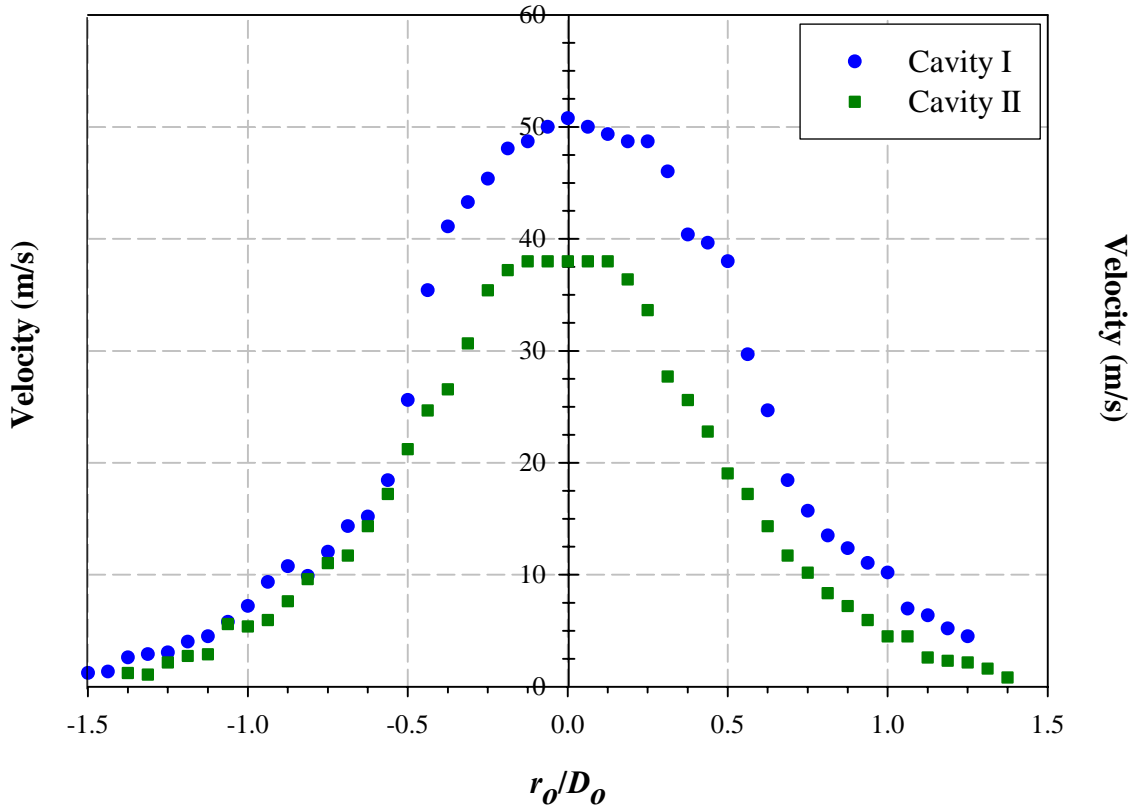
Figure 4.6 Cavity Height Effects using a Sawtooth Driving Signal for a Bimorph Diaphragm at 50Hz and 150 Vpp

4.1.3 Orifice Effects

Next the effects of orifice size on jet velocity are studied. Figure 4.7 shows the sine wave driven profiles for cavities I and III that have the same cavity height (smaller C_H) but different orifice diameters. It is observed that the smaller orifice diameter (smaller D_o), cavity I, produces 63% higher velocities than cavity III, larger D_o. This result is expected since to maintain a constant mass flow rate, the velocity through the smaller orifice has to be higher than the larger orifice. Similar trends are observed in the comparison between cavities II and IV with differences of 61%.
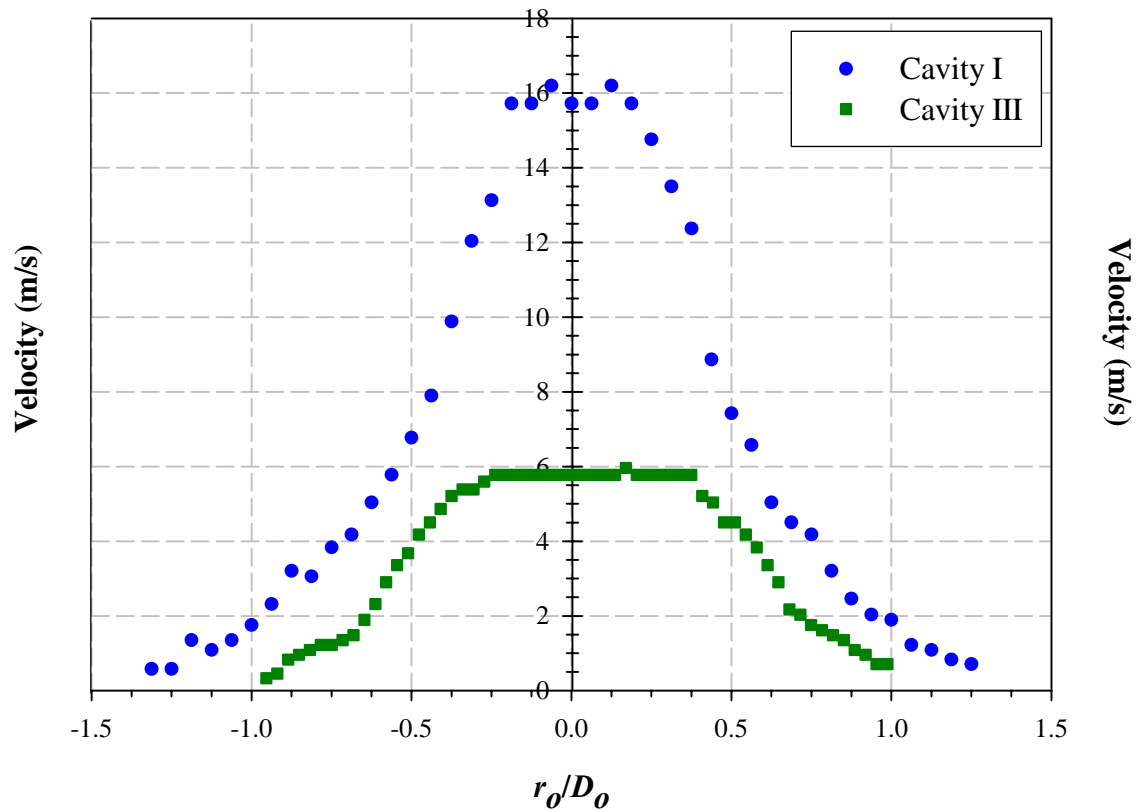
Figure 4.7 Orifice Size Effects using a Sine Driving Signal for a Bimorph Diaphragm at 50Hz and 150 Vpp

In case of the sawtooth driven profiles, the differences in velocities are much smaller as shown in Figure 4.8 for cavities I and III. Differences between cavity I and III peak velocities are 17% and between cavity II and IV are only 4%. These results indicate that the synthetic jet velocity is dependent on the type of driving signal used.
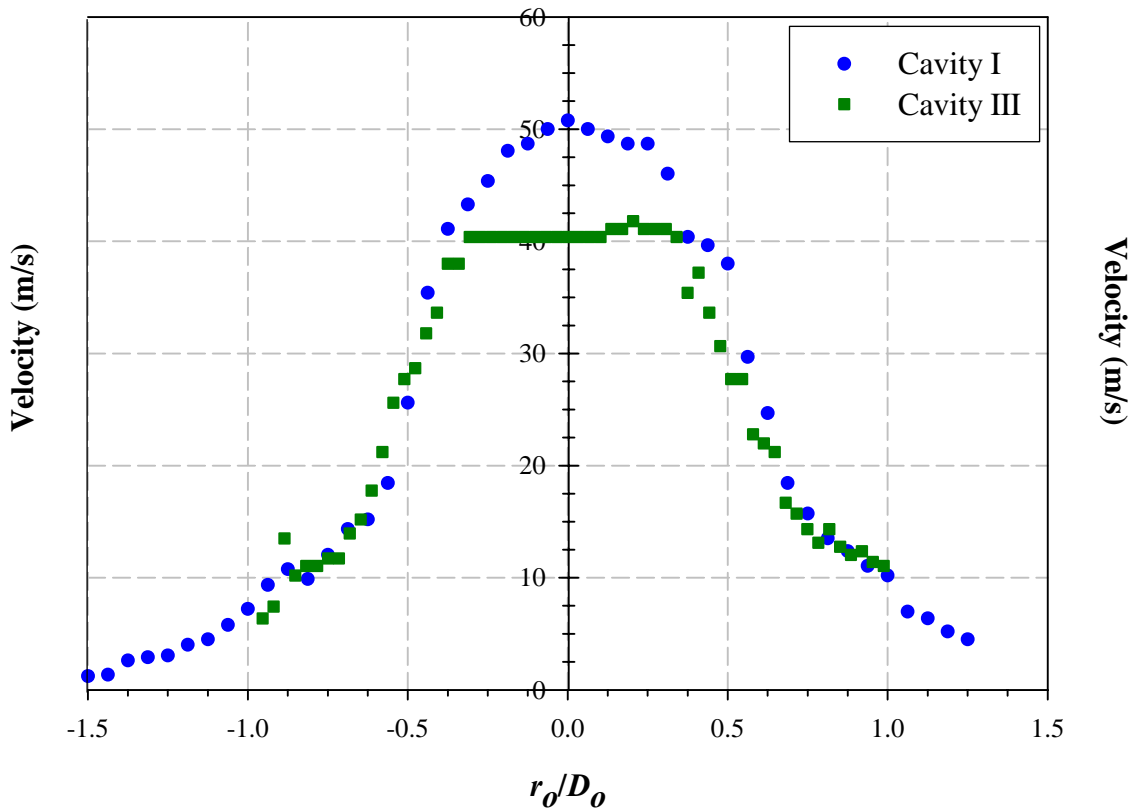
Figure 4.8 Orifice Size Effects using a Sawtooth Driving Signal for a Bimorph Diaphragm at 50 Hz and 150Vpp

4.1.4 Passive Cavity Pressure Effects

To investigate the effects of pressure on the synthetic jet velocity the passive jet cavity is pressurized. Measuring the jet at various passive cavity pressures and frequencies showed that the peak jet velocity decreases as the passive pressure increases. The jet velocity decrease with increasing passive cavity pressure is shown in Figure 4.9 for a range of frequencies. While the graph shown is for a sine driving signal, similar results are seen for sawtooth driven synthetic jets.
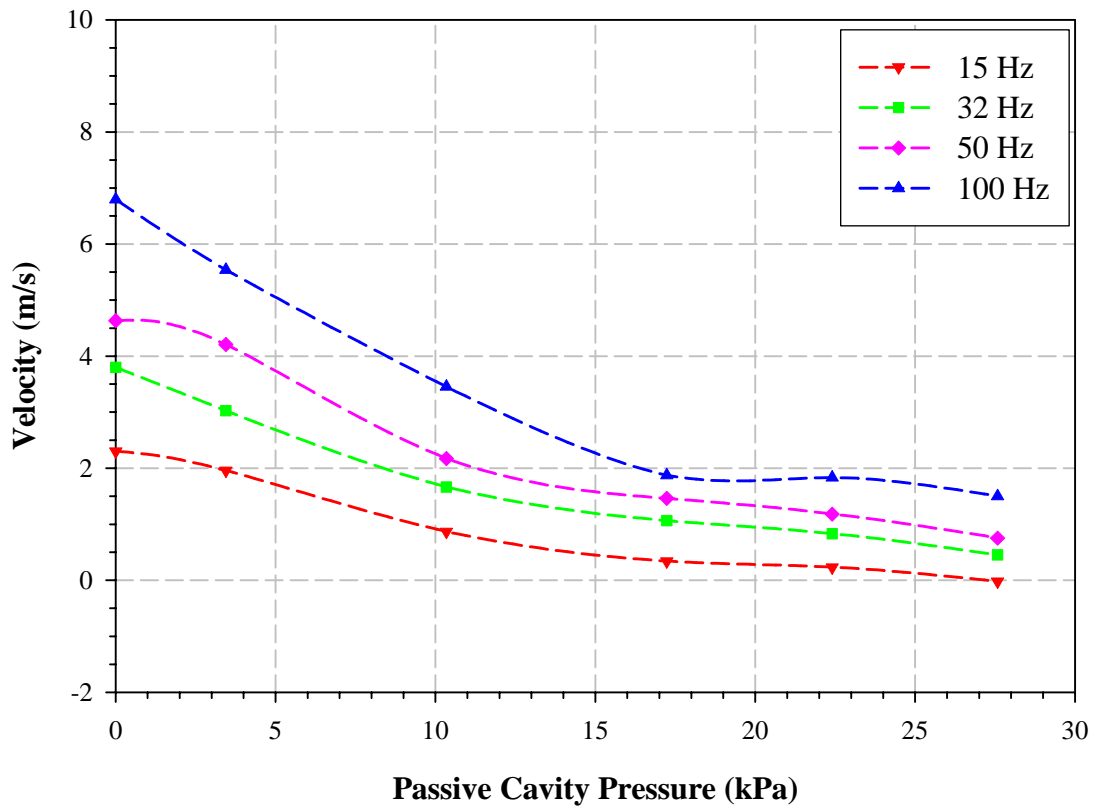
Figure 4.9 Passive Cavity Pressure Effects on Synthetic Jet Velocity for a Bimorph Diaphragm Maximum Velocity at 150 Vpp using a Sine Driving Signal

4.1.5 Statistical Factor Analysis

In an experiment, one or more variables or factors are deliberately changed in order to observe the effect the changes have on one or more response variables. Experimental data are used to derive an empirical (approximation) model linking the outputs and inputs. These empirical models generally contain first and second-order terms. Screening designs are used to identify the few significant factors from a list of many potential ones. In short, screening designs are economical experimental plans that focus on determining the relative

significance of many main effects. This can be achieved using factorial designs (Montgomery 2005).

The basic purpose of a factorial design is to economically investigate cause-and-effect relationships of significance in a given experimental setting. By a factorial design, each complete trial or replication of the experiment for all possible combinations of the levels of the factors are investigated. The effect of a factor is defined to be the change in response produced by a change in the level of the factor. This is called a main effect as it refers to the primary factors or interest in the experiment. For some experiments, it is seen that the difference in response between the levels of one factor is not the same at all levels of the other factors. When this occurs, there is an interaction between the factors. As the number of factors in a 2^k factorial design increases, the number of runs required for a complete replicate of the design rapidly outgrows the resources of most experimenters. If the experimenter can reasonably assume that certain high-order interactions are negligible, information on the main effects and low-order interactions may be obtained by running only a fraction of the complete factorial experiment. Since we are able to choose fractions of a full design, the whole experimental research process is made more economical and efficient. These fractional factorial designs are among the most widely used types of designs for product and process design and for process improvement.

Screening experiments are usually performed in the early stages of a project when many of the factors initially considered may have little or no effect on the response. The factors identified as important are then investigated more thoroughly in subsequent experiments. It is common to begin with several discrete or continuous input factors that

can be controlled, that is, varied when desired by the experimenter and one or more measured output response variables which always are assumed to be continuous. In the current study, five factors were considered for each actuator, driving waveform, voltage, frequency, cavity height, and orifice size. The peak velocity of the jet is used as the response variable. A two level design is chosen due to the large number of factors involved. In a two factor experimental design each factor has two levels. These levels "low" and "high" are denoted by "–" and "+" respectively.

The factor distribution showing the levels and the types of each factor is given in Table 4.1. A full factorial design requires $2^5 = 32$ runs without center points or repetitions. Instead, a fractional factorial design, 2^{5-1}, was utilized requiring a total of 16 observations. The factors, shown in Table 4.1, have a resolution V which indicates that no main effects are confounded with any 2-factor interactions or 3-factor interactions; main effects are confounded with four-factor interactions. All the runs and their characteristics are shown in Table 4.2 such that the influence of each factor can be assessed individually.

Table 4.1 Factor Distribution for a Bimorph Device

Factors	Symbols	Low Level (-1)	High Level (+1)	Units	Types
Driving Waveform	F_z	Sawtooth (-1)	Sine (+1)	None	Discrete
Applied Voltage	E	125 (-1)	150 (+1)	V_{pp}	Continuous
Frequency	f	25 (-1)	50 (+1)	Hz	Continuous
Orifice Size	D_o	2 (-1)	3.67 (+1)	mm	Continuous
Cavity Height	C_H	5.5 (-1)	9.5 (+1)	mm	Continuous

Table 4.2 Experimental Design

Run No.	Factors (X_i)					Response$_j$
j	F_z	E	f	D_o	C_H	Y_j
1	-1	-1	-1	-1	1	y_1
2	1	-1	-1	-1	-1	y_2
3	-1	1	-1	-1	-1	y_3
4	1	1	-1	-1	1	y_4
5	-1	-1	1	-1	-1	y_5
6	1	-1	1	-1	1	y_6
7	-1	1	1	-1	1	y_7
8	1	1	1	-1	-1	y_8
9	-1	-1	-1	1	-1	y_9
10	1	-1	-1	1	1	y_{10}
11	-1	1	-1	1	1	y_{11}
12	1	1	-1	1	-1	y_{12}
13	-1	-1	1	1	1	y_{13}
14	1	-1	1	1	-1	y_{14}
15	-1	1	1	1	-1	y_{15}
16	1	1	1	1	1	y_{16}

The most common empirical models fit to the experimental data take either a linear form or a quadratic form. In the present study only linear models are considered. A linear model will contain the main effect terms and interaction effect terms. The model is of the form shown in Equation 4.1.

$$Y = \mu + \sum_{i=0}^{n} \beta_i \cdot X_i + \sum_{\substack{i=0 \\ k=0}}^{n} \beta_{ik} \cdot X_i X_k + \sum_{\substack{i=0 \\ k=0 \\ z=0}}^{n} \beta_{ikz} \cdot X_i X_k X_z + \cdots + \varepsilon$$

Equation 4.1

$i = 1,2,...,n$

$k = 1,2,...,n$

$z = 1,2,...,n$

n is the number of factors

Here, *Y* is the response for given levels of the main effects X_i and the X_iX_k term is included to account for a possible interaction effect between X_i and X_k. Depending on the number of factors considered, the interaction term could contain more than two factors. The constant μ represents the sample mean of the response; β's are parameters whose values are determined represent the coefficients for the considered factors and ε is the experimental error. Statistical results are used to assess the validity and influence of the particular effect on the response.

From the entries in Table 4.2 all effects such as main effects, first-order interaction effects, etc can be calculated. To compute the main effect estimate of a factor, the average response at all runs at the 'high' setting are subtracted from the average response of all runs set at 'low' for that particular factor. This estimate is shown in Equation 4.2.

$$\Delta x_i = \frac{2}{n}\left[\sum_{j=1}^{n} y_j^+ - \sum_{j=1}^{n} y_j^-\right]$$

Equation 4.2

i = 1,2,...,n

k = 1,2,...,n

Δx_i is the effect estimate, y_j^+ are all the responses with a high effect level for the corresponding effect; y_j^- are all the responses with a low effect level for the corresponding

effect and *n* is the total number of runs. Similar the interactions effects can also be estimated.

A regression analysis of the factors is shown in Table 4.3. The first part of the table shows a summary output of the regression. The *R*-square value is the relative predictive power of a model. The model shown has an *R*-square value of 0.9702 and an adjusted *R*-square of 0.9627 indicating that 97% of the data can be predicted using the model. The adjusted *R*-square value is a better estimate of the model as it accounts for the size of the model as well. This is unlike the *R*-square value, which increases as the number of factors increase even though they might not have an effect on the experiment.

Following the summary is the Analysis of Variances (ANOVA). The ANOVA is sometimes called the *F*-test, and it helps determine the validity of the experimental design by testing the difference between two or more groups. When the *F*-value is larger than the *Significance F*-value, the experiment design is considered to be valid, indicating that at least one of factors have an effect on the response variable. The *F*-value shown in Table 4.3 is computed from the mean square values, and *Significance F*-value is selected from the *F*-distribution tables based on the size of the sample, the number of factors, and the significance level selected which is 95% in this case. As the *F*-value is larger than the *Significance F*-value as seen in Table 4.3, the experiment design is considered to be valid and further analysis of the design can continue.

The ANOVA only shows that the experimental design as a whole is valid but all the factors considered in the design may not be relevant. The analysis following the

ANOVA helps in determining the importance of all factors. The factors are analyzed on the basis of the corresponding *p-value* generated in the table. The *p-value* or calculated probability is the estimated probability of rejecting the null hypothesis of a study question when that hypothesis is true. If the *p-value* is less than the chosen significance level then the null hypothesis is rejected. The choice of significance level at which the hypothesis is rejected is arbitrary. In the current study, the null hypothesis is that none of the factors considered in the study are significant enough such that they may affect the jet velocity. The alternate hypothesis is that one or more factors are significant and to identify these factors the corresponding *p-values* are considered. Conventionally for this analysis the 5% (less than 1 in 20 chance of being wrong) levels or the 95% confidence internal mark has be chosen such that the *p-value* has to be less than 0.05 (Devore 2004).

The *p*-values for F_z, D_o and C_H are found to be below the 0.05 mark at 2.58E-10, 0.0018 and 0.0030 respectively. For the fractional factorial design of Table 4.1 the other two factors, E and f, did not appear to be significant. This does not indicate that these factors can be ignored completely. Interaction with main effects may be present but as the focus is only on linear models any additional effects are ignored in this study.

From these results, a model is obtained as shown in Equation 4.3 such that Y is the velocity in m/s. This equation shows that F_z, D_o and C_H, the main effects can be linearly related to each other.

$$Y = 23.08 - 16.05 \cdot F_z - 3.47 \cdot D_0 - 3.13 \cdot C_H$$

Equation 4.3

4.3 Initial Regression Analysis for a Bimorph Device

SUMMARY OUTPUT

Regression Statistics

Multiple R	0.98498
R Square	0.97019
Adjusted R Square	0.96274
Standard Error	3.38352
Obs.	16

ANOVA

	df	SS	MS	F	Sig. F
Regression	3	4471.342	1490.447	130.1901	2.03E-09
Residual	12	137.3788	11.44824		
Total	15	4608.72			

	Coeffs.	Standard Error	t Stat	P-value	Lower 95%	Upper 95%	Lower 95.0%	Upper 95.0%
Intercept	23.08	0.84588	27.28516	3.62E-12	21.23698	24.92302	21.23698	24.92302
F_z	-16.05038	0.84588	-18.97474	2.58E-10	-17.8934	-14.20736	-17.89339	-14.20736
D_o	-3.46688	0.84588	-4.09854	0.00148	-5.30989	-1.62386	-5.30989	-1.62386
C_H	-3.1345	0.84588	-3.7056	0.00301	-4.97752	-1.29148	-4.97752	-1.29148

In the next section of the statistical analysis an additional factor, passive cavity pressure (P_B), is added to the experimental design. For this factor the low level (-1) is set at 0 pressure and the high level (+1) is set at 17.24 kPa or 2.5 psi. This modified fractional

factorial design has 24 runs with 6 factors and the same response variable of maximum

velocity is used. The complete experimental design is shown in Table 4.4.

Table 4.3 Complete Experimental Design

Run No.	Factors (X_i)						Response$_j$
j	F_z	E	f	D_o	C_H	P_B	Y_j
1	-1	-1	-1	-1	1	-1	y_1
2	1	-1	-1	-1	-1	-1	y_2
3	-1	1	-1	-1	-1	-1	y_3
4	1	1	-1	-1	1	-1	y_4
5	-1	-1	1	-1	-1	-1	y_5
6	1	-1	1	-1	1	-1	y_6
7	-1	1	1	-1	1	-1	y_7
8	1	1	1	-1	-1	-1	y_8
9	-1	-1	-1	1	-1	-1	y_9
10	1	-1	-1	1	1	-1	y_{10}
11	-1	1	-1	1	1	-1	y_{11}
12	1	1	-1	1	-1	-1	y_{12}
13	-1	-1	1	1	1	-1	y_{13}
14	1	-1	1	1	-1	-1	y_{14}
15	-1	1	1	1	-1	-1	y_{15}
16	1	1	1	1	1	-1	y_{16}
17	-1	-1	-1	1	1	-1	y_{17}
18	1	-1	-1	1	1	1	y_{18}
19	-1	1	-1	1	1	1	y_{19}
20	1	1	-1	1	1	-1	y_{20}
21	-1	-1	1	1	1	1	y_{21}
22	1	-1	1	1	1	-1	y_{22}
23	-1	1	1	1	1	-1	y_{23}
24	1	1	1	1	1	1	y_{24}

The table now contains all the experiments performed using the Bimorph device

during the course of this study. The regression analysis shown in Table 4.5 gives all the

important effects through the *p-values*. The model has an *R*-square value of 0.9264 and an

adjusted *R*-square value of 0.9109. The most recently added factor P_B is also found to be

significant. Thus four factors, F_z, D_o, C_H and P_B, are seen to have main effects with *p-values* of 2.02E-11, 0.0105, 0.0194 and 0.0053 respectively. Using Equation 4.2, the average effect sizes for the selected factors are estimated as -28.499 for F_Z,-10.430 for D_o, -9.931 for C_H and -14.443 for P_B. For the remaining factors the effect sizes were 2.614 for E and 1.094 for f. Plots of all the effects showing the average responses are shown in Figure 4.10. The main effects, F_Z, D_o, C_H and P_B, have a large slope as seen in the plots and the remaining factors have a very small slope indicating that they do not have a significant effect on the jet velocity.

Using the coefficients determined in the regression a model is obtained as shown by Equation 4.4. $Y^{'}$ is the velocity of the jet in m/s. Using this equation the jet velocity can be predicted for any set of conditions considered in the study.

$$Y' = 18.53 - 14.25 \cdot F_z - 3.29 \cdot D_0 - 2.96 \cdot C_H - 4.72 \cdot P_B$$

Equation 4.4

Table 4.4 Final Regression Analysis for a Bimorph Device

SUMMARY								

Regression Statistics	
Multiple R	0.96249
R Square	0.92638
Adjusted R Square	0.91088
Standard Error	5.0128
Obs.	24

ANOVA

	df	SS	MS	F	Sig. F
Regression	4	6007.821	1501.955	59.7718	1.69E-10
Residual	19	477.435	25.12816		
Total	23	6485.256			

	Coeffs.	Standard Error	t Stat	P-value	Lower 95%	Upper 95%	Lower 95.0%	Upper 95.0%
Intercept	18.5336	1.64082	11.2953	7.15E-10	15.09932	21.96788	15.09932	21.96788
F_z	-14.2495	1.02323	-13.9259	2.02E-11	-16.3911	-12.1078	-16.3911	-12.1078
D_o	-3.2947	1.160238	-2.83968	0.01048	-5.72311	-0.86629	-5.72311	-0.86629
C_H	-2.96233	1.16024	-2.55321	0.019427	-5.39073	-0.53392	-5.39073	-0.53392
P_B	-4.71858	1.49786	-3.15021	0.00527	-7.85363	-1.58352	-7.85363	-1.58352
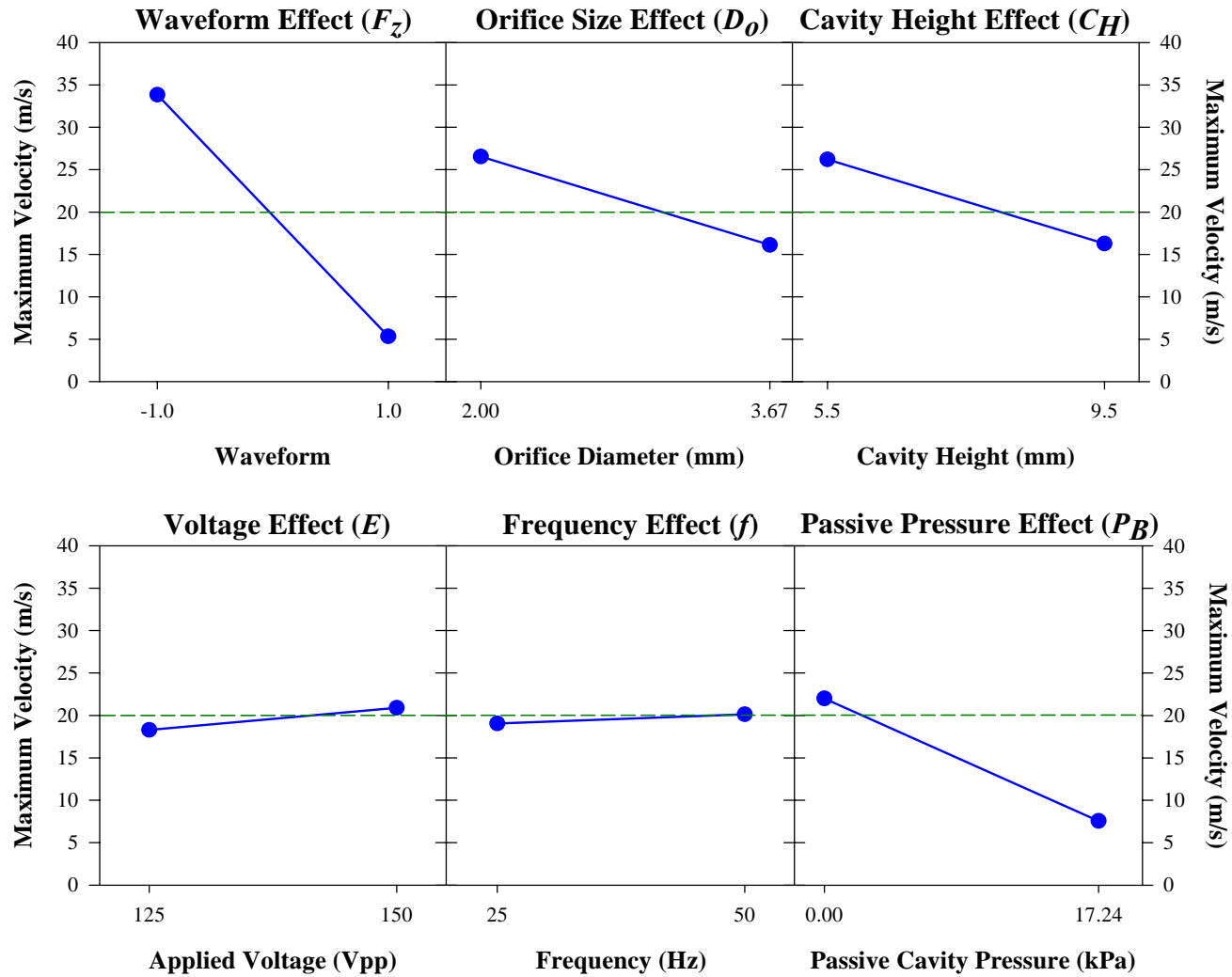
Figure 4.10 Average Factor Effects for a Bimorph Device

4.2 Thunder®

4.2.1 Driving Signal and Frequency Effects

The Thunder® device is also operated using a sine and a sawtooth driving signal. The synthetic jet velocity curves are similar in shape to the Bimorph but smaller in magnitude for both driving signals. A typical velocity curve formed with a sine driving signal is shown in Figure 4.11. The voltage and velocity curves are out of phase with the velocity peak at an offset from the voltage peak and two peaks of different magnitudes are present. The larger peak follows the trailing edge of the voltage, and the smaller peak follows the leading edge. The larger jet is assumed to be during the expulsion phase of the synthetic jet cycle, and the smaller jet during the ingestion phase. At low frequencies the second jet is very small in magnitude and in some cases it may also be absent depending on the applied voltage. Similar behavior was observed with a Bimorph device.

With a sawtooth driving signal a single jet is formed as shown in Figure 4.12. A single peak is seen with the velocity following the leading edge of the input signal. Immediately following the peak, oscillations are observed in the jet. Due to the stiffness nature of the Thunder® device, the impulse provided by the sawtooth signal causes it to oscillate. Since the magnitudes of oscillations are small compared to the jet velocity, these oscillating velocities are not taken into account. Overall, the magnitude of the jet formed by a sawtooth signal is larger than the jet formed with a sine driving signal.
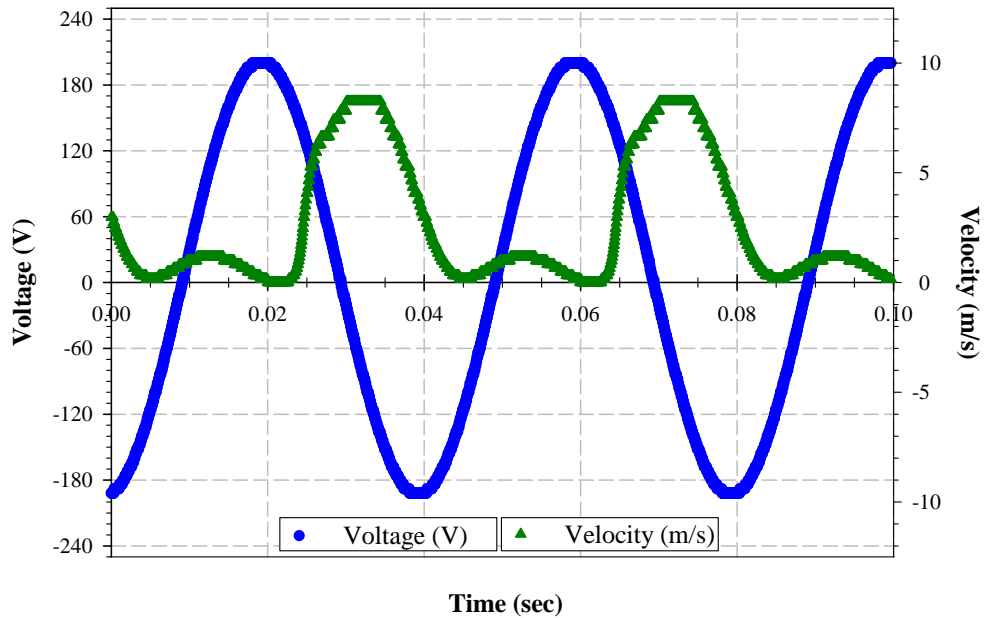
Figure 4.11 Typical Velocity Curve with Sine Driving Voltage with Cavity IV for a Thunder® Diaphragm at 25 Hz and 400 Vpp
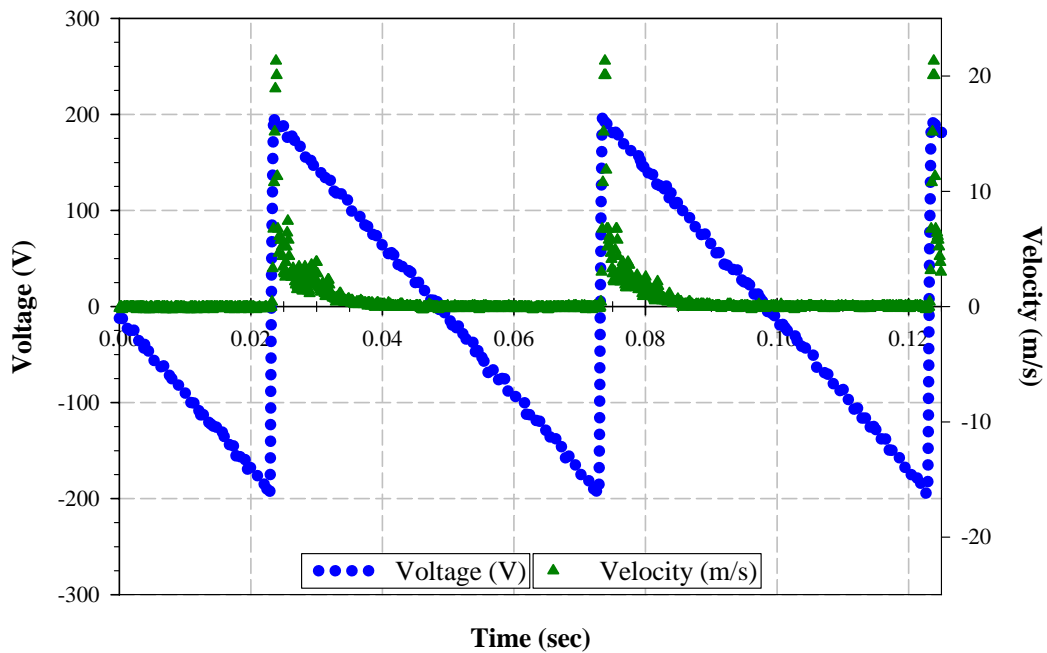
Figure 4.12 Typical Velocity Curve with Sawtooth Driving Voltage with Cavity IV for a Thunder® Diaphragm at 25 Hz and 400 Vpp

The magnitude of the synthetic jet is also dependent on the magnitude of the applied voltage for both driving signals. At higher voltages the shape of the velocity curve does not change but the magnitude of velocity increases as shown in Figure 4.13 using a sine driving signal. Similar changes in synthetic jet velocity are observed with a sawtooth driven Thunder®.
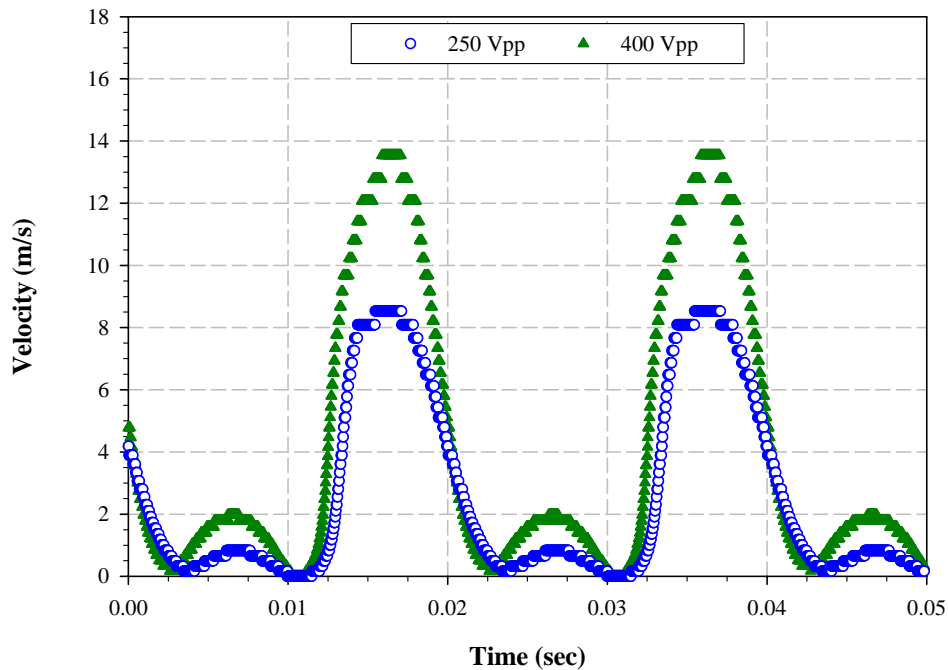
**Figure 4.13 Effects of Voltage on Velocity Magnitude with Cavity IV for a Thunder®
Diaphragm at 50 Hz with a Sine Signal**

The effects of frequency on the synthetic jet velocity are tested for both applied waveforms. With a sine wave driving signal the velocity is very small at low frequencies but it increases as the frequency increases. The velocity may stabilize at higher frequencies beyond the range tested here. A different behavior is seen in case of a sawtooth driven Thunder®. In this case the velocity increases up to approximately 10 Hz and then stays constant as the frequency increases. This behavior is shown in Figure 4.14 for both the

driving signals. Further discussion in this behavior is given in the last section of this chapter.
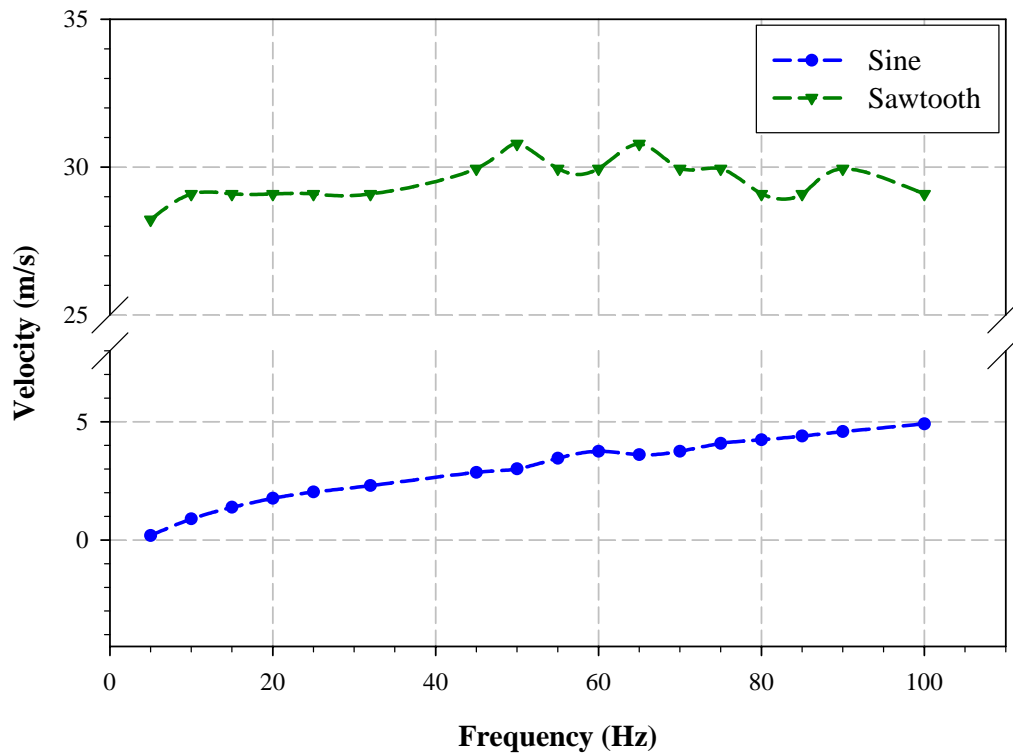
Figure 4.14 Frequency Effects on Thunder® Diaphragm Peak Velocities for Cavity IV at 400 Vpp

4.2.2 Cavity Height Effects

To test the effects of changes in cavity height and volume on the jet velocity, cavities having different heights but the same orifice size are tested. Since cavity I and cavity II have the same orifice size, their profiles are compared using both sine and sawtooth driving signals. The profiles for cavity I and II with a sine wave signal are shown in Figure 4.15.

The cavity with the smaller height, cavity I, produces velocities approximately 9% higher than the larger cavity. Similarly, cavity III and cavity IV are also compared as they have the same orifice. Differences between these profiles are higher approximately 27%. These differences could be due to the cavity III and IV combination of cavity height and large orifice, and thus the flow rate has to be higher to maintain a constant mass flow through the orifice. The cavity III and IV profiles are shown in Figure 4.16.
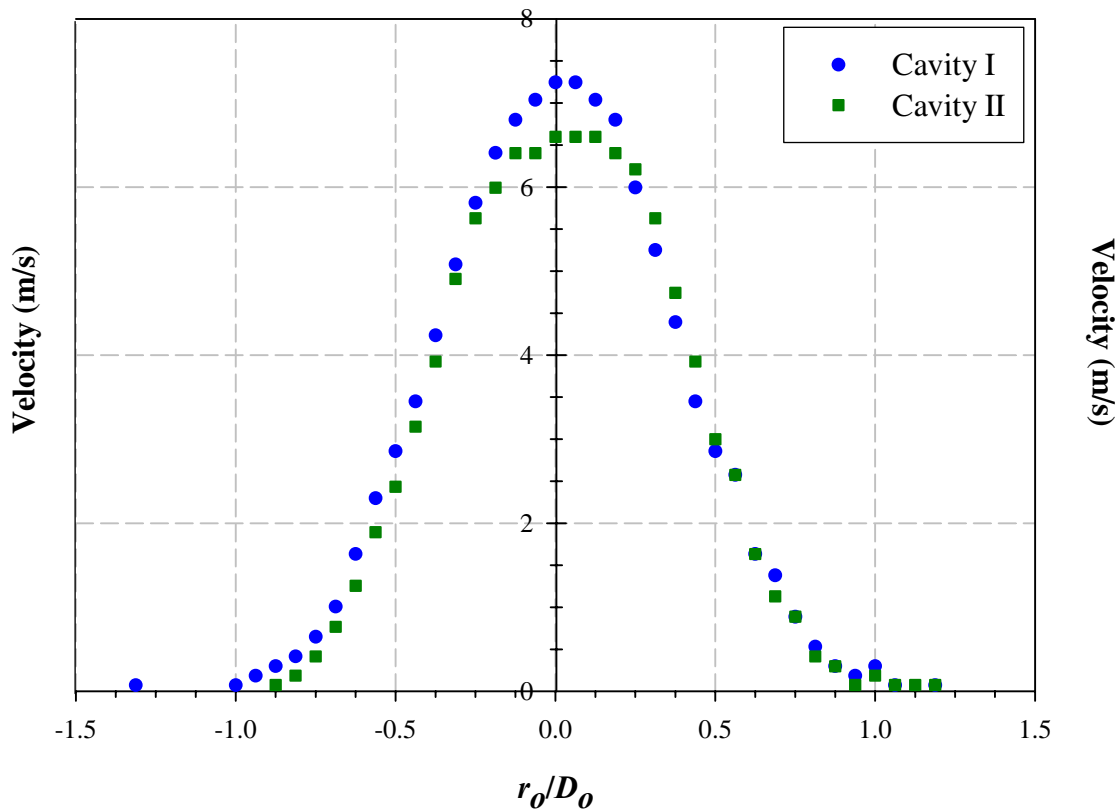
**Figure 4.15 Cavity Height Effects shown using Cavities I and II for a Thunder®
Diaphragm at 32 Hz and 400 Vpp with a Sine Driving Signal**

To see the effect of cavity height on jet velocity with a sawtooth driving signal, cavities I and II, and cavities III and IV, are compared. Figure 4.17 shows the cavity I and

II comparison. Cavity I produces approximately 20% higher velocity than cavity II and cavity III produces approximately 22% higher velocity than cavity IV. The differences in maximum velocities are higher with a sawtooth signal than a sinusoidal signal regardless of the orifice size. In general, regardless of the driving signal used the smaller cavity produces higher velocities. A possible reason for the smaller cavity producing more mass flow rate, hence velocity, might be that there are no areas in the cavity where vortices or pressure gradients can develop.
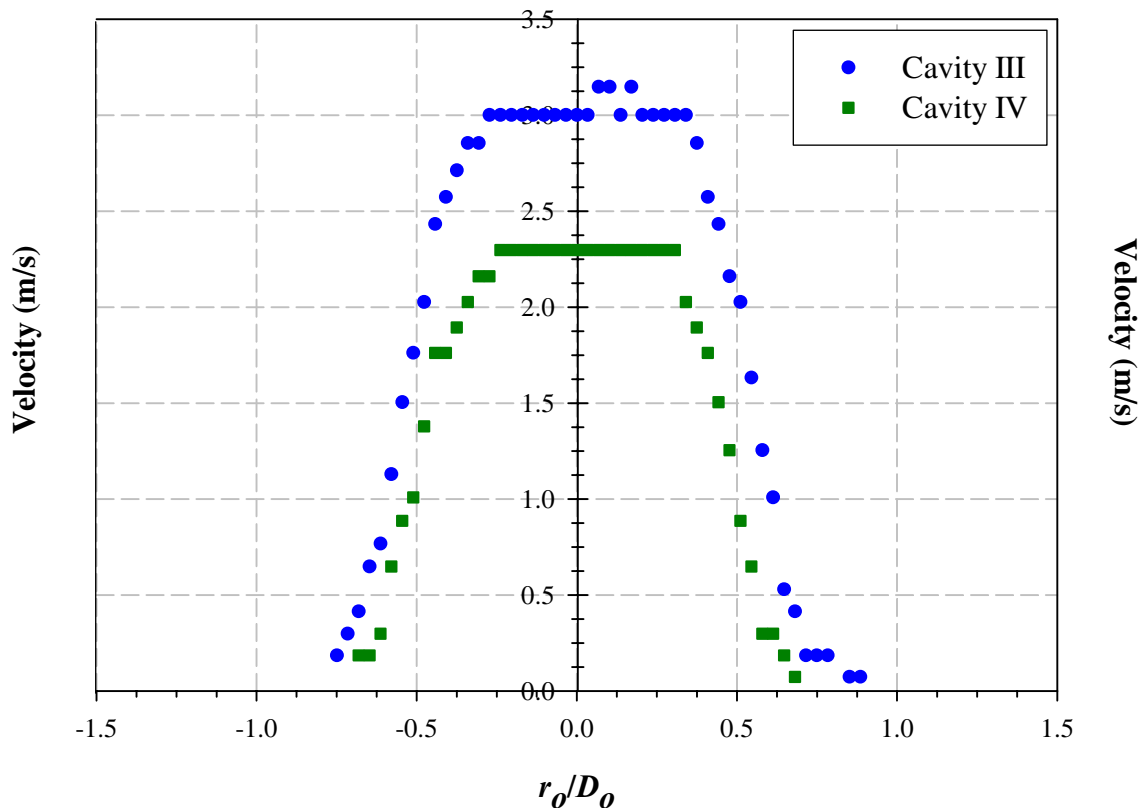
Figure 4.16 Cavity Height Effects shown using Cavities III and IV for a Thunder[®] Diaphragm at 32 Hz and 400 Vpp with a Sine Driving Signal

4.2.3 Orifice Effects

The previous section showed that the orifice size may have some effect on the jet velocity. To further investigate this effect, cavities with the same volume but different orifice sizes are studied using two combinations, with the same volume: cavities I and III and cavities II and IV. The profiles for cavities I and III with a sine driving signal are shown in Figure 4.18. Differences of over 56% are seen in the maximum velocities of the two cavities. Analogous to the Bimorph device, the smaller orifice produces higher velocities. Similar differences of approximately 65% are seen in between cavities II and IV.
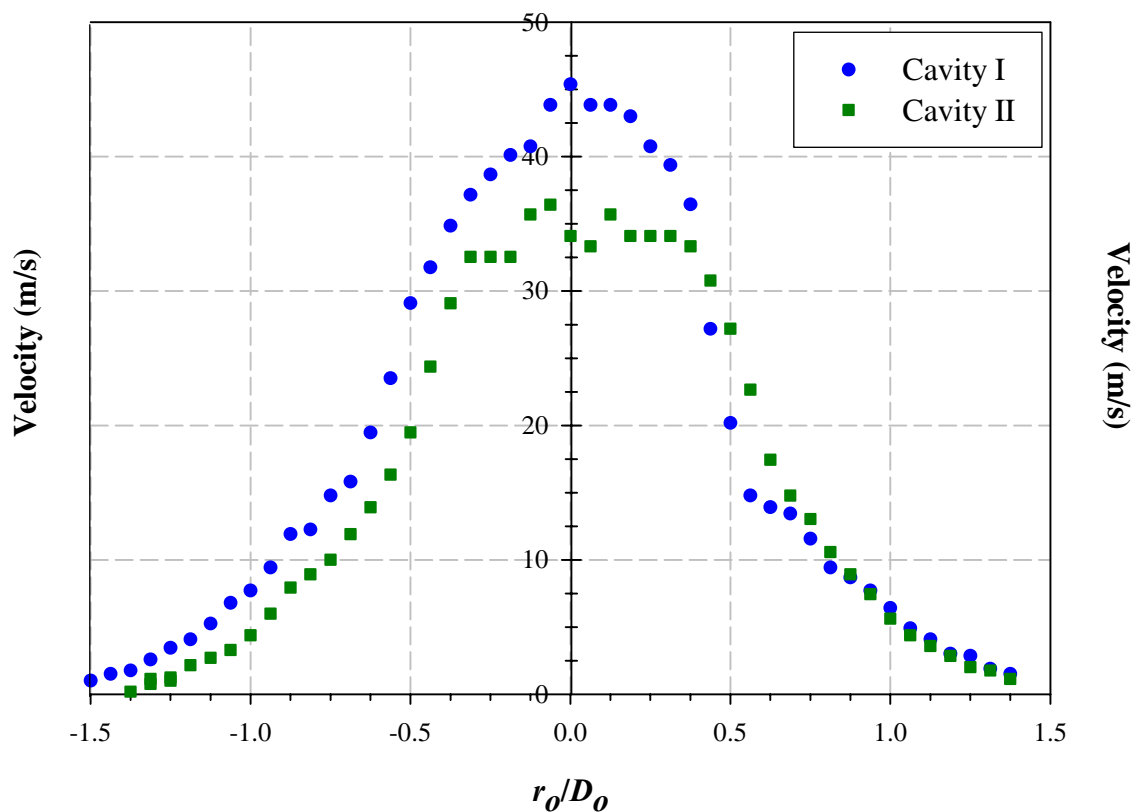
Figure 4.17 Cavity Height Effects using a Sawtooth Driving Signal for a Thunder® Diaphragm at 32 Hz and 400 Vpp

Smaller differences in velocities are seen with sawtooth driven synthetic jets as shown in Figure 4.19. A comparison of cavity I and III profiles shows a difference of 10% at 32 Hz at higher frequencies such as at 50 Hz, however the differences in the cavity I and III profiles is approximately 22%. These differences are still not as large as those seen with the sine driving signal. Similar results are seen while comparing cavities II and IV. At lower frequencies, the differences are lower approximately 13%, and increase at higher frequencies to approximately 23%. Similar to the sine driven jets the smaller orifice cavities form jets with larger velocities.
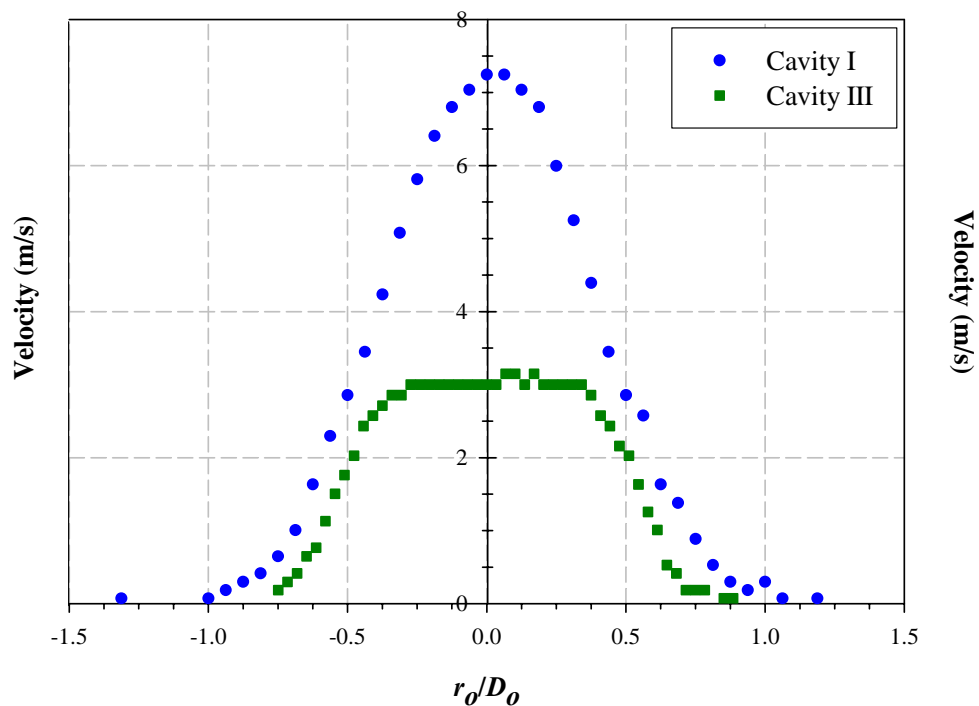
Figure 4.18 Orifice Size Effects using a Sine Driving Signal for a Thunder[®] Diaphragm at 32 Hz and 400 Vpp
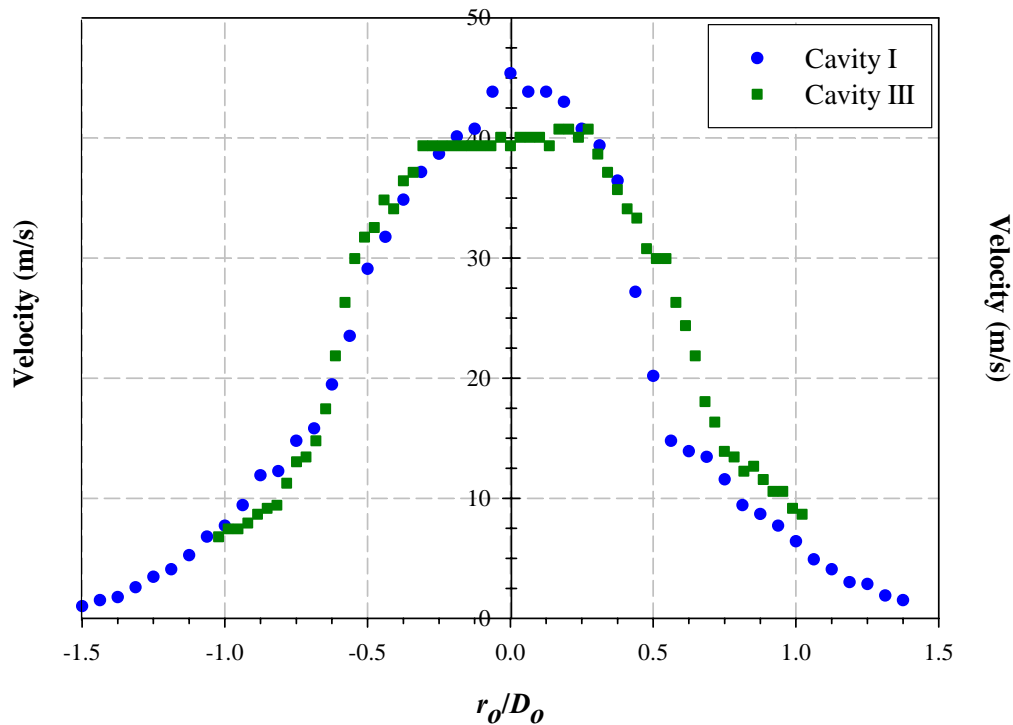
Figure 4.19 Orifice Size Effects using a Sawtooth Driving Signal for a Thunder[®] Diaphragm at 32 Hz and 400 Vpp

4.2.4 Passive Cavity Pressure Effects

The passive cavity of the Thunder[®] based synthetic jet is pressurized at various levels up to 55 kPa to investigate the effects on synthetic jet velocity produced by the diaphragm, as shown in Figure 4.20, for a sawtooth driven jet. Results show that the velocity increases, reaches a peak, and then drops below the initial level as the passive pressure is increased. The peak is reached at approximately 20 kPa thus any increase in pressure above this level causes the jet velocity to drop. When the signal used is sinusoidal, a similar trend is observed with the velocity reaching a maximum at the same pressure as in the sawtooth of approximately 20 kPa as shown in Figure 4.21. This characteristic of the
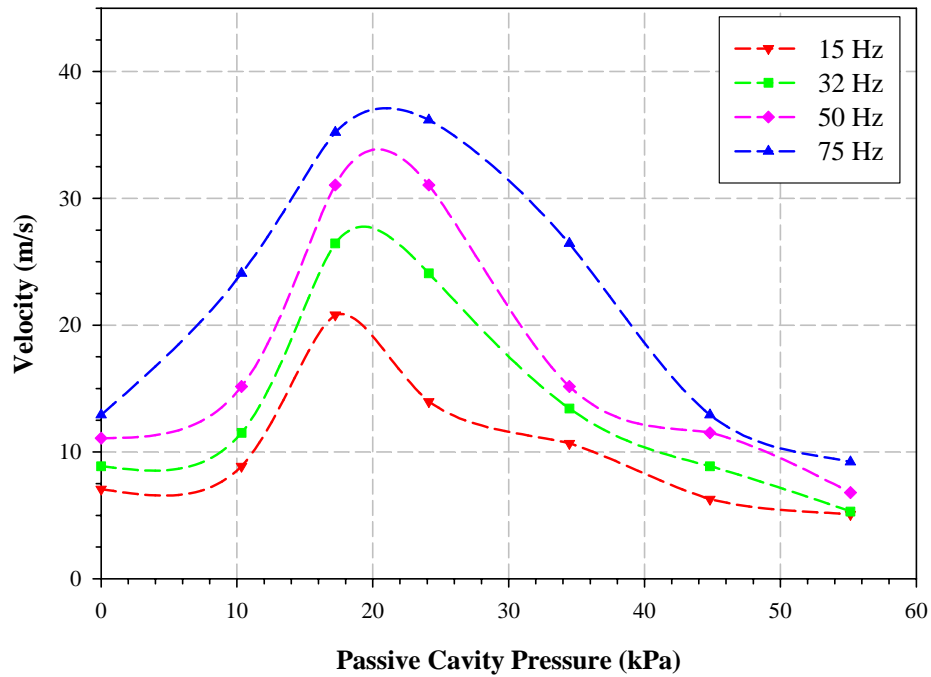
Figure 4.20 Passive Cavity Pressure Effects on Synthetic Jet Velocity for a Thunder[®] Diaphragm at 400 Vpp using a Sawtooth Driving Signal
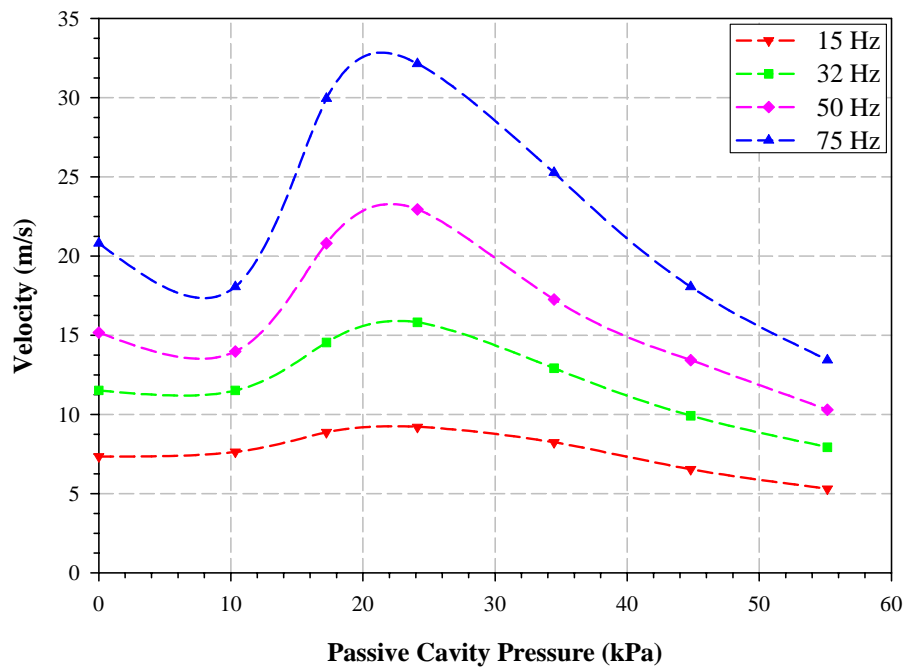
Figure 4.21 Passive Cavity Pressure Effects on Synthetic Jet Velocity for a Thunder[®] Diaphragm at 400 Vpp using a Sine Driving Signal

Thunder® device may be useful in the design of a pressure jet. This behavior of the jet is observed at all frequencies and voltages as shown in Figures 4.20 and 4.21 for a few selected frequencies at 400 Vpp.

4.2.5 Statistical Factor Analysis

A similar process used for the Bimorph is repeated for the Thunder® with the same factors. The analysis begins with a resolution V two level fractional factorial design, 2^{5-1}, requiring a total of 16 runs. A few of the factor levels used in case of the Thunder® are different from the Bimorph as shown in the factor distribution of Table 4.6, however, the response variable, maximum jet velocity, is the same.

The 2^{5-1} fractional factorial experimental design is the same as Table 4.2 used for the Bimorph. All the 16 runs with different level combinations for each factor are listed. A regression analysis with 95% confidence interval is shown in Table 4.7. The regression had an R-square value of 0.9394 and an adjusted R-square value of 0.9173. Only one factor, frequency f, was eliminated as its p-value, 0.8070, was found to be above the critical value of 0.05 for a 95% confidence interval analysis. This meant that the remaining four factors, F_Z, E, D_o and C_H, having p-value, 9.4954E-08, 0.0370, 0.0180 and 0.0207 respectively had main effects. Frequency was not a main effect, but it could have an interaction effect which cannot be neglected.

Table 4.5 Factor Distribution for a Thunder$^{\circledR}$ Device

Factors	Symbols	Low Level (-1)	High Level (+1)	Units	Types
Driving Waveform	F_z	Sawtooth (-1)	Sine (+1)	None	Discrete
Applied Voltage	E	250 (-1)	400 (+1)	V$_{pp}$	Continuous
Frequency	f	25 (-1)	50 (+1)	Hz	Continuous
Orifice Size	D_o	2 (-1)	3.67 (+1)	mm	Continuous
Cavity Height	C_H	5.5 (-1)	9.5 (+1)	mm	Continuous

Using the coefficient values calculated in the regression a linear model fit is obtained shown by Equation 4.5 where Y is the velocity in m/s.

$$Y = 18.287 - 13.9164 \cdot F_z + 2.6968 \cdot E - 3.1563 \cdot D_o - 3.0694 \cdot C_H$$

Equation 4.5

Table 4.6 Initial Regression Analysis for a Thunder® Device

SUMMARY								
Regression Statistics								
Multiple R	0.96921							
R Square	0.93936							
Adjusted R Square	0.91732							
Standard Error	4.54818							
Obs.	16							
ANOVA								
	df	SS	MS	F	Sig. F			
Regression	4	3525.13489	881.28372	42.60305	1.245E-06			
Residual	11	227.54521	20.68593					
Total	15	3752.68010						
	Coeffs.	Standard Error	t Stat	P-value	Lower 95%	Upper 95%	Lower 95.0%	Upper 95.0%
Intercept	18.28700	1.13704	16.08292	5.460E-09	15.78438	20.78962	15.78438	20.78962
F_z	-13.91638	1.13704	-12.23908	9.495E-08	-16.41899	-11.41376	-16.41899	-11.41376
E	2.69675	1.13704	2.37172	0.03704	0.19413	5.19937	0.19413	5.19937
D_o	-3.15625	1.13704	-2.77584	0.01804	-5.65887	-0.65363	-5.65887	-0.65363
C_H	-3.06938	1.13704	-2.69943	0.02068	-5.57199	-0.56676	-5.57199	-0.56676

In the next part of the statistical analysis an additional factor, passive cavity pressure (P_B), is added to the experimental design. For this factor the low level (-1) is set at 0 and the high level (+1) is set at 17.24 kPa or 2.5 psi. This experimental design is now a two level modified fractional factorial design with 6 factors and 24 runs. The response variable remains the same which is the maximum velocity. The complete design is shown in Table 4.4.

A regression analysis is then conducted on this design as shown in Table 4.8. Here again f was eliminated as a main effect as its *p-value*, 0.3543, was found to be above the critical limit of 0.05. Four factors, F_Z, E, D_o and C_H, had their *p-values* below 0.05 which is

the necessary condition for a 95% confidence interval. The pressure factor, P_B, has a *p-value* of 0.1725 which is not acceptable. However, eliminating this factor has a direct effect on the other factors, thus pressure cannot be eliminated from the regression but it is not considered as a main effect. The regression had an *R* square value of 0.8461 and an adjusted *R* square value of 0.8034. The *p-values* for the main factors are 0.0096 for F_Z, 0.0194 for *E,* 0.0426 for D_o and 0.0480 for C_H.

The coefficients calculated in the regression are used in the model Equation 4.6 where Y' is the peak velocity in m/s. As pressure cannot be eliminated it is included in the model as a main effect. Using this equation the velocity of the jet can be approximated.

$$Y' = 26.3293 - 11.521 \cdot F_z + 0.0438 \cdot E - 3.7865 \cdot D_o - 1.5374 \cdot C_H + 2.1264 \cdot P_B$$

Equation 4.6

Using Equation 4.2, the average effect sizes for the selected factors are estimated as -23.0419 for F_Z, 6.5619 for *E*, -6.5318 for D_o, -6.4015 for C_H and 0.3268 for P_B. The only factor not included *f*, the average effect size is 2.4403. Plots of all the effects showing the average responses are shown in Figure 4.22. The main effects, F_Z, E, D_o and C_H graphs shown have large slopes indicating that they have a significant effect on the synthetic jet velocity. P_B, has the smallest slope as seen in Figure 4.22 even lower than *f*. Even then it cannot be removed from the design maybe because P_B, constitutes a distributed load across the surface of the device and it cannot be considered a factor by itself but in combination with other factors. The current study does not consider any factor combinations and is only aimed toward developing a first level linear model including the main effects.

Table 4.7 Final Regression Analysis for a Thunder® Device

SUMMARY								
Regression Statistics								
Multiple R	0.91986							
R Square	0.84614							
Adjusted R Square	0.80341							
Standard Error	6.26057							
Obs.	24							

ANOVA						
	df	SS	MS	F	Sig. F	
Regression	5	3879.96284	775.99257	19.79838	9.531E-07	
Residual	18	705.50541	39.19475			
Total	23	4585.46826				

	Coeffs.	Standard Error	t Stat	P-value	Lower 95%	Upper 95%	Lower 95.0%	Upper 95.0%
Intercept	26.32927	9.08776	2.89722	0.00960	7.23659	45.42195	7.23659	45.42195
F_z	-11.52096	1.27793	-9.01530	4.294E-08	-14.20580	-8.83612	-14.20580	-8.83612
E	0.04375	0.01704	2.56739	0.01938	0.00795	0.07954	0.00795	0.07954
D_o	-3.78646	1.73538	-2.18192	0.04261	-7.43236	-0.14057	-7.43236	-0.14057
C_H	-1.53741	0.72452	-2.12197	0.04798	-3.05957	-0.01525	-3.05957	-0.01525
P_B	2.12639	1.49656	1.42085	0.17245	-1.01778	5.27055	-1.01778	5.27055
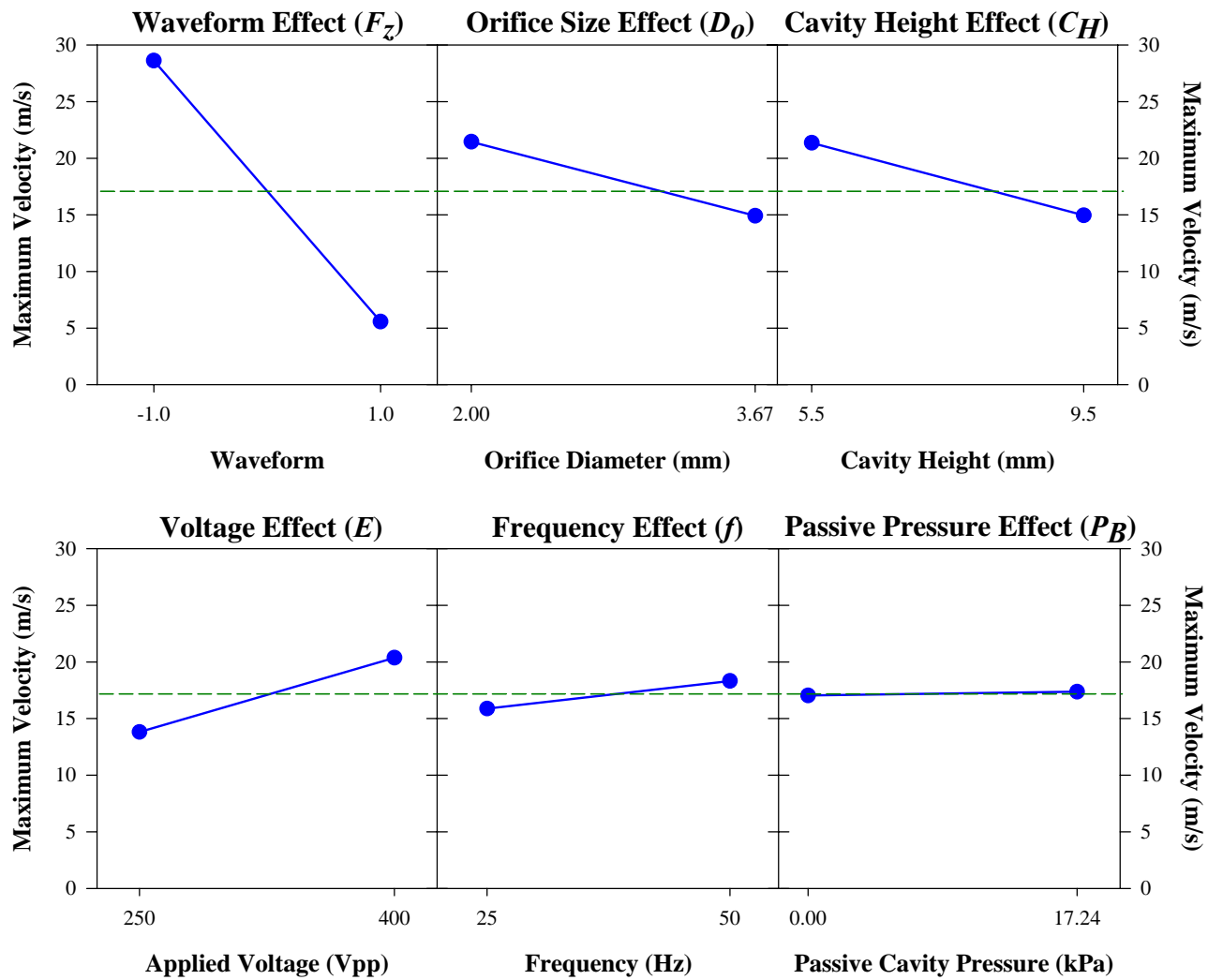
Figure 4.22 Average Factor Effects for a Thunder® Device

4.3 Lipca

The factors considered for the Bimorph and Thunder® were also studied for the Lipca. In the following sections each factor is discussed individually followed by a statistical analysis of all the factors collectively. All the analysis leads to an empirical equation which can be used to optimize the synthetic jet velocity in m/s.

4.3.1 Driving Signal and Frequency Effects

The sine and sawtooth signals are used to drive the synthetic jet actuator similar to the Bimorph and Thunder® actuators. A typical velocity curve with a sine signal has two peaks for different magnitudes. The larger peak is thought to be during the expulsion part of the jet cycle and the smaller peak the ingestion part. Similar behavior was observed for the other two actuators. The larger peak follows the leading part of the signal and the smaller peak the trailing part as seen in Figure 4.23. At low frequencies, the second peak becomes smaller similar to the behavior of the other actuators.

The magnitude of the velocity produced by a sawtooth signal was greater than with a sine signal. This could be due to the extra impulse present in the signal as opposed to the gradual rise and fall of a sine wave. This is illustrated by the velocity curve with a sawtooth signal, that has a single peak as shown in Figure 4.24. The peak follows the leading edge of the signal and drops immediately after. The graph also shows oscillations immediately following the big velocity peak similar to the behavior of the Thunder®.
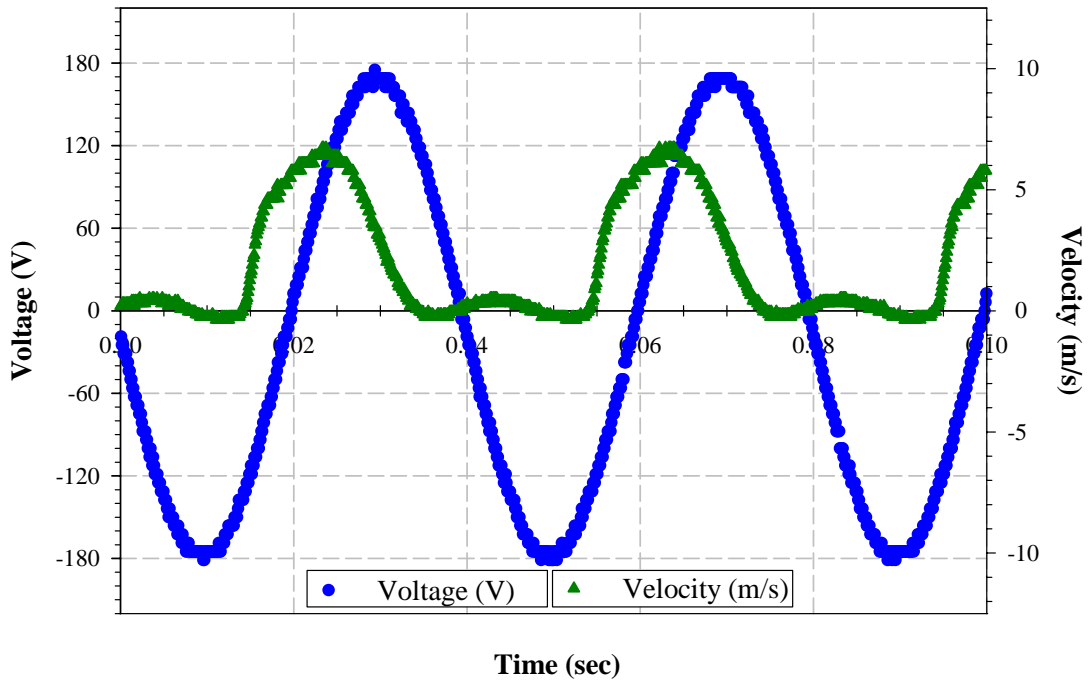
Figure 4.23 Typical Velocity Curve with Sine Driving Voltage with Cavity I for a Lipca Diaphragm at 25 Hz and 350 Vpp
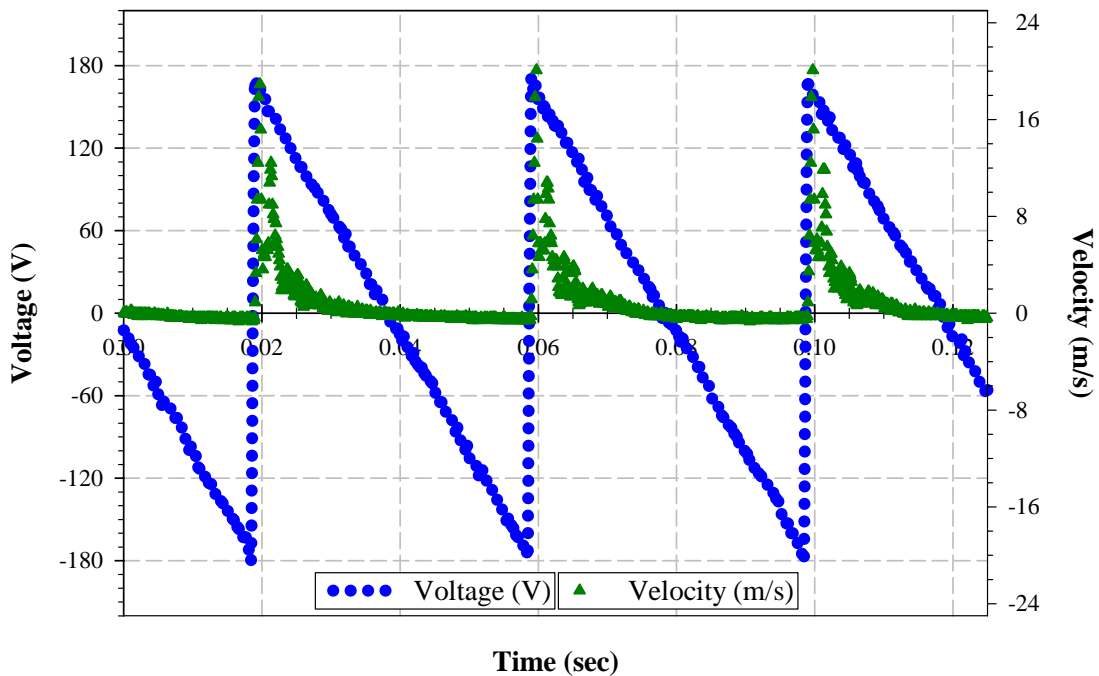
Figure 4.24 Typical Velocity Curve with Sawtooth Driving Voltage with Cavity IV for a Lipca Diaphragm at 25 Hz and 350 Vpp

As seen in the previous two actuators, the velocity was also dependent on the magnitude of the input signal. At higher voltages the velocity was higher, as seen in Figure 4.25, with a sawtooth driving signal for 200 Vpp and 350 Vpp at 25 Hz. Similar behavior was observed with sine driven synthetic jets regardless of the frequency used.
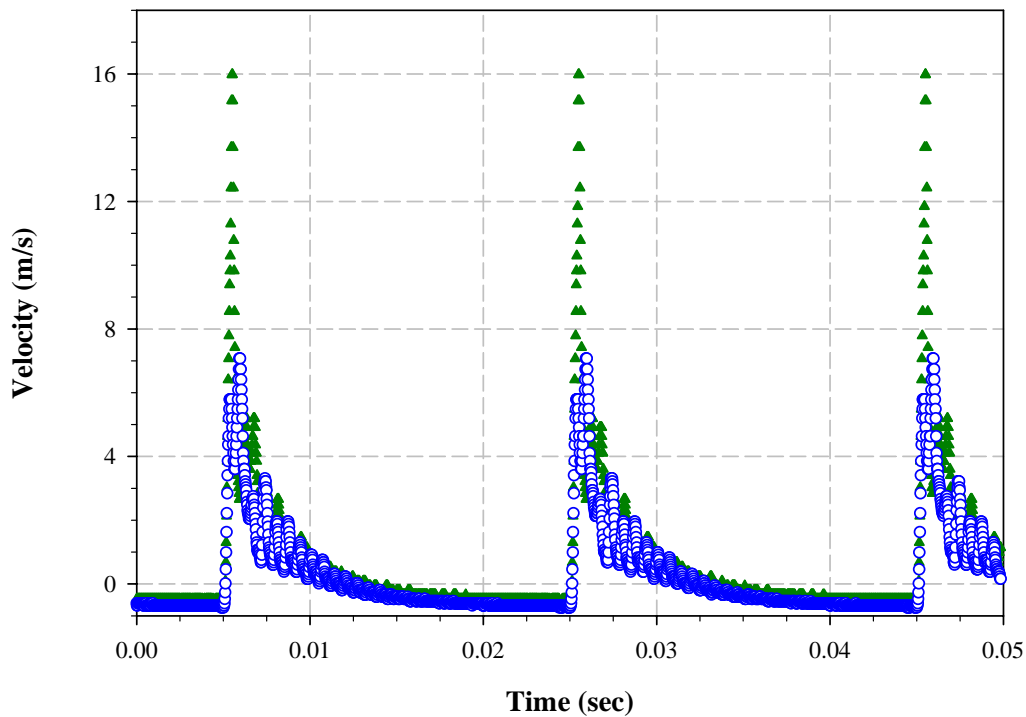
Figure 4.25 Effect of Voltage on Velocity Magnitude with Cavity IV for a Lipca Diaphragm at 25 Hz with a Sawtooth Signal

Next the effects of frequency on the synthetic jet velocity are studied using both the driving signals. With the sine wave the velocity produced increases as the frequency increases. The sawtooth signal causes a very different effect on the jet with the velocity stabilizing at approximately 10 Hz as shown in Figure 4.26.
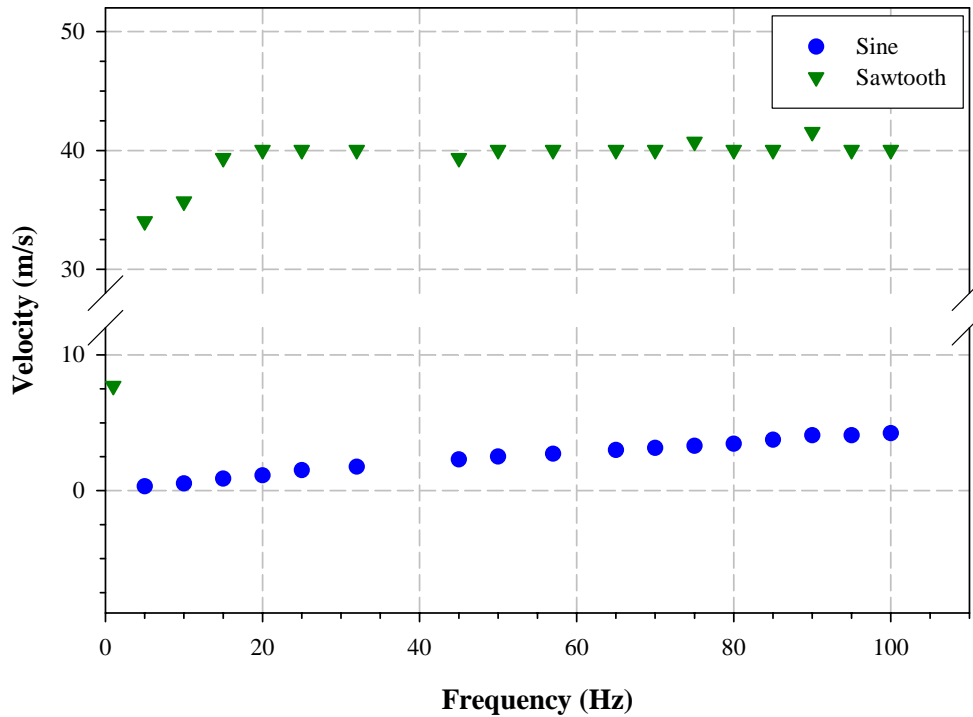
Figure 4.26 Frequency Effects on Lipca Diaphragm Peak Velocities for Cavity IV at 350 Vpp

This trend has been observed in all three actuators studied so far. It is hypnotized that in case of the sawtooth signal the active cavity is saturated at a low frequency (10 Hz in this case) such that the velocity cannot increase any further. However, with sine, as the rise and fall is gradual, the saturation frequency is reached in the frequency range tested. It is predicted that at higher frequencies, then tested in the current study, a constant will be reached at which the active synthetic jet cavity will be saturated. A graph showing the effects with the two signals is shown in Figure 4.26. This characteristic was seen at all voltages and with all cavity sizes and orifice diameters.

4.3.2 Cavity Height Effects

Cavity height effects are studied using velocity profiles measured at the orifice of the synthetic jet. Comparing the velocity profiles of cavities with different heights but same diameters such as cavity I and cavity II and also cavity III and cavity IV help in identifying these effects. The comparison between cavity I and II profiles using a sine driving signal is shown in Figure 4.27. Differences on velocities at frequencies of 50 and 32 Hz for cavities I and II, are in the range of 20 – 30%. Differences on velocity at frequencies of 50 Hz and 32 Hz for cavities III and IV are in the range of 37 – 40%. Cavities III and IV have higher difference than cavities I and II. This could be due to the differences in orifice diameter and an interaction on these factors D_o, C_H may be possible.
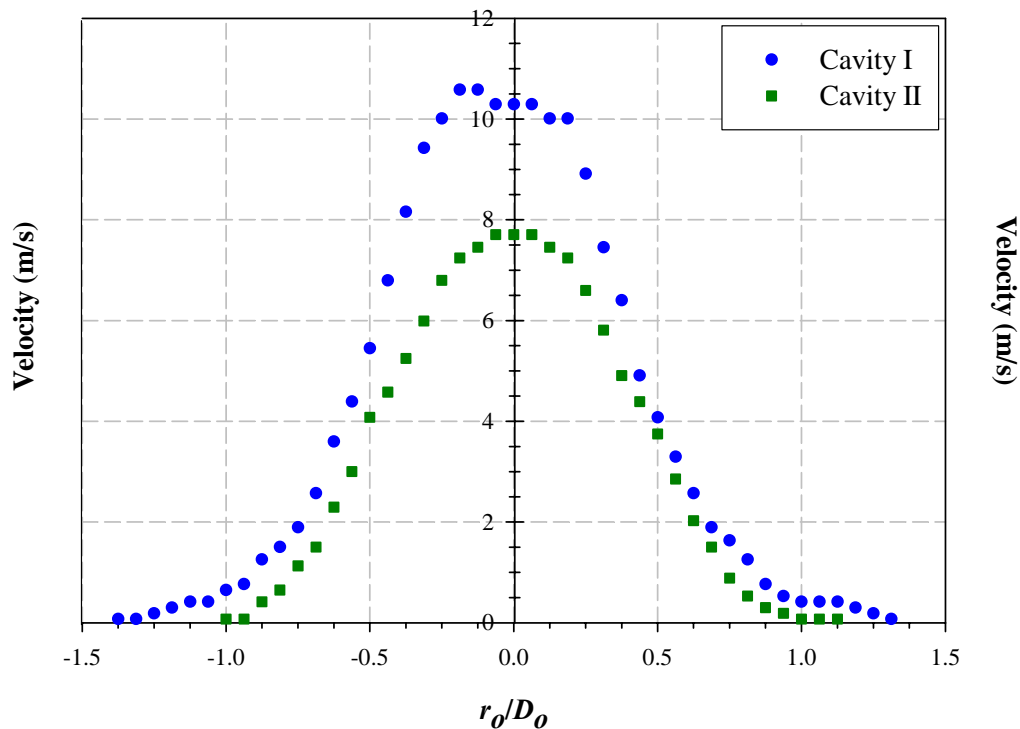
Figure 4.27 Cavity Height Effects using a Sine Driving Signal for a Lipca Diaphragm at 50 Hz and 350 Vpp

When the synthetic jet is driven with a sawtooth signal, the differences are much smaller. Cavity I and II comparison shows differences of only 9% at 32 Hz and 16% at 50 Hz. The cavity I and II comparison at 50 Hz is shown in Figure 4.28. Cavity I with a smaller height produces higher velocity than cavity II. The differences comparing cavities III and IV are higher at approximately 28% at 32 Hz and 20% at 50 Hz. Here again the larger differences in velocity are seen in cavities with larger orifice diameters.
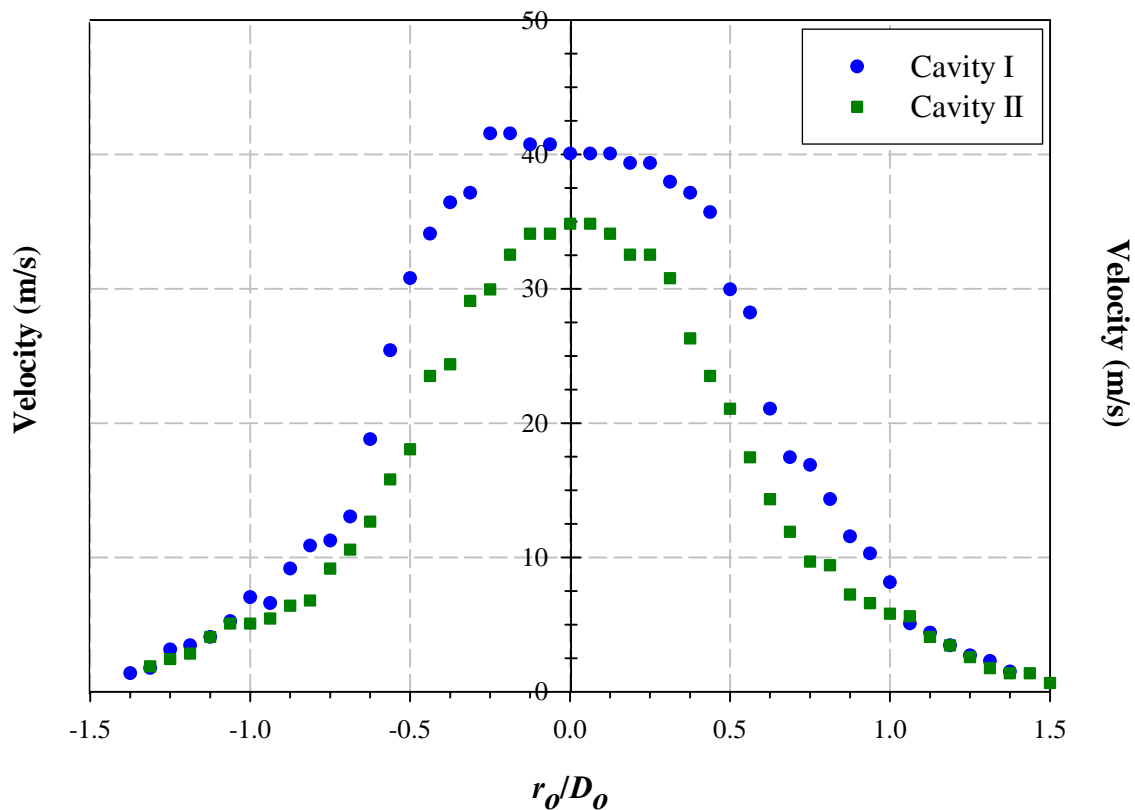
Figure 4.28 Cavity Height Effects using a Sawtooth Driving Signal for a Lipca Diaphragm at 50 Hz and 350 Vpp

4.3.3 Orifice Effects

In the previous section it was seen that orifice size had some effect on the jet velocity. Comparing cavities I and III and also cavities II and IV help in studying these differences in detail as they have the same cavity heights but different orifice diameters. The differences with a sine driving signal between cavities I and III at 32 Hz are shown in Figure 4.29. Large differences of approximately 58% are seen at 32 Hz and of 61% at 50Hz. Similarly comparing II and IV also shows high differences of 67% at 32 Hz and 66% at 50 Hz. These differences are significant and could lead to the conclusion that orifice is an important factor.
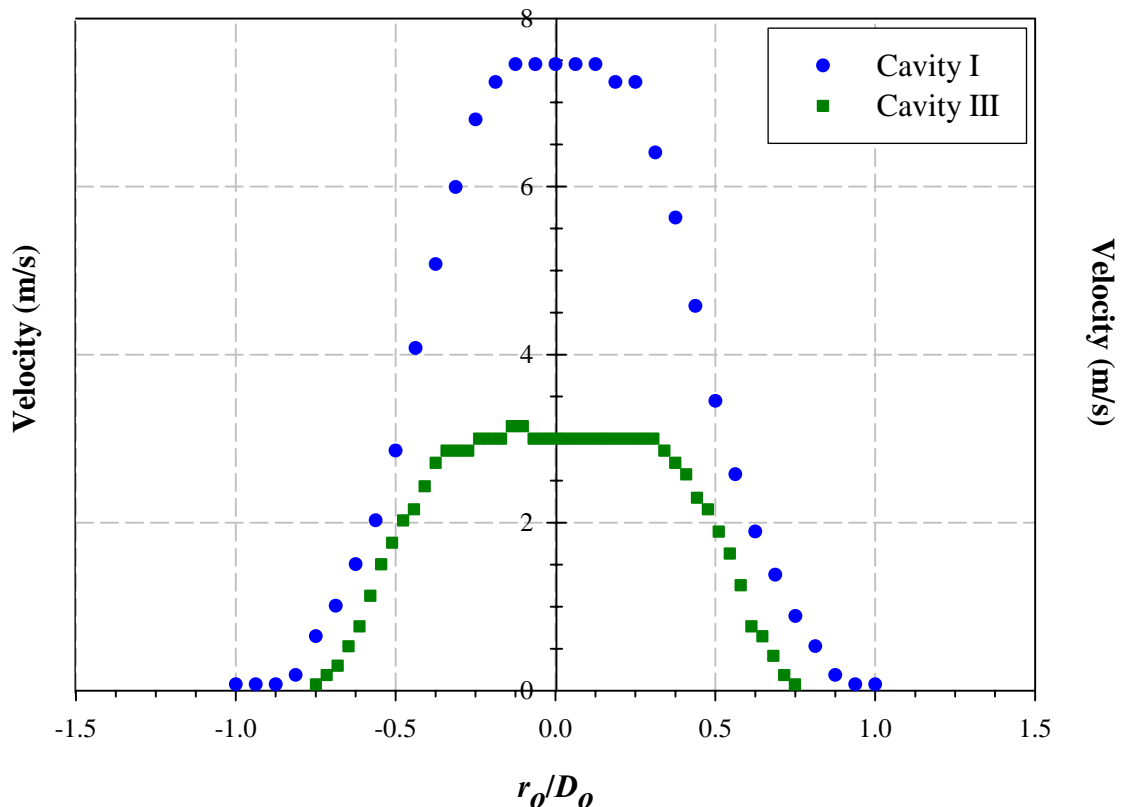
Figure 4.29 Orifice Size Effects using a Sine Driving Signal for a Lipca Diaphragm at 32 Hz and 350 Vpp

The results are opposite with a sawtooth driving signal. As seen in Figure 4.30 the profiles for cavities I and III at 32 Hz were almost identical with minimal differences at 50 Hz (not shown), only 2% differences were observed. Cavities II and IV however, show higher variations, 21% at 32Hz and 6% at 50Hz. Thus, with a sine wave large differences are measured and with a sawtooth signal small differences.
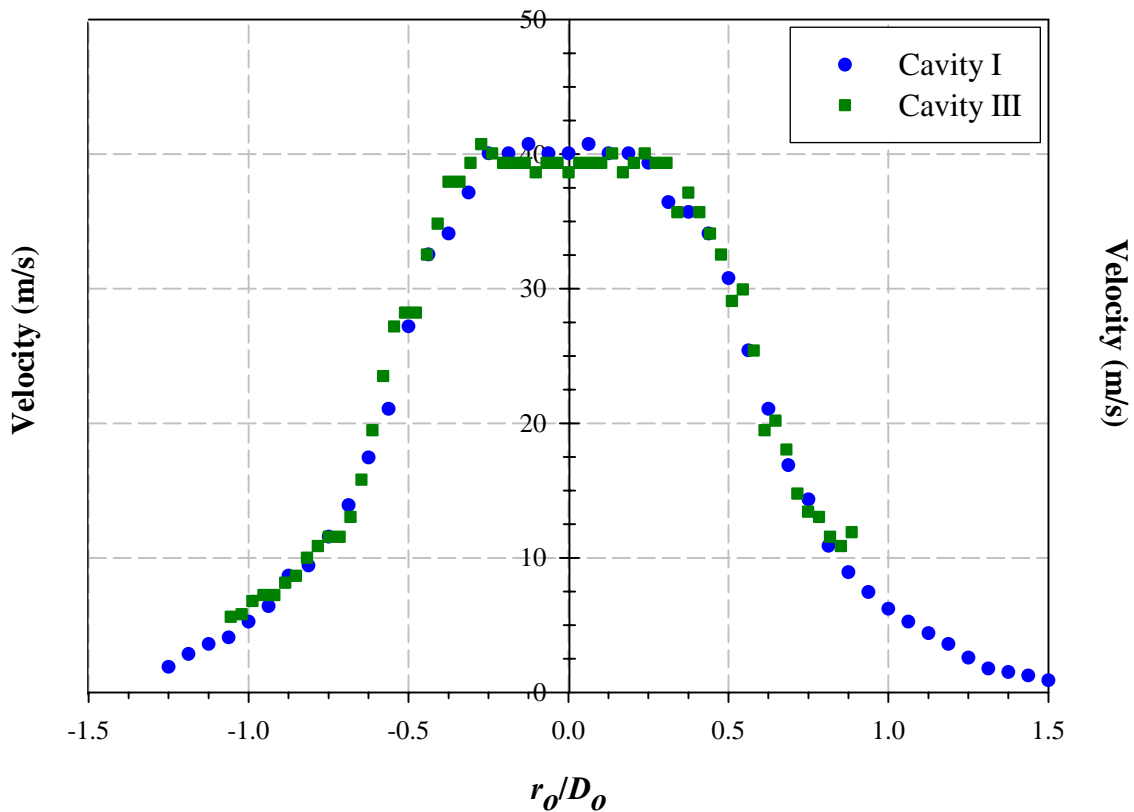
Figure 4.30 Orifice Size Effects using a Sawtooth Driving Signal for a Lipca Diaphragm at 32Hz and 350 Vpp

4.3.4 Pressure Effects

The passive cavity of the synthetic jet actuator was pressurized at various levels until the jet velocity dropped to zero. As the pressure was increased the velocity of the jet also increased until it reached a peak at a certain pressure and then falls as the pressure is further increased. The velocity peak was seen at approximately 17 kPa with both the driving signals, and at approximately 55 kPa the velocity returned to its initial level. This behavior is shown in Figure 4.31 with a sine driving signal. Similar behavior was seen with a sawtooth driving signal, with the velocity peaking at approximately the same passive cavity pressure of 17 kPa.
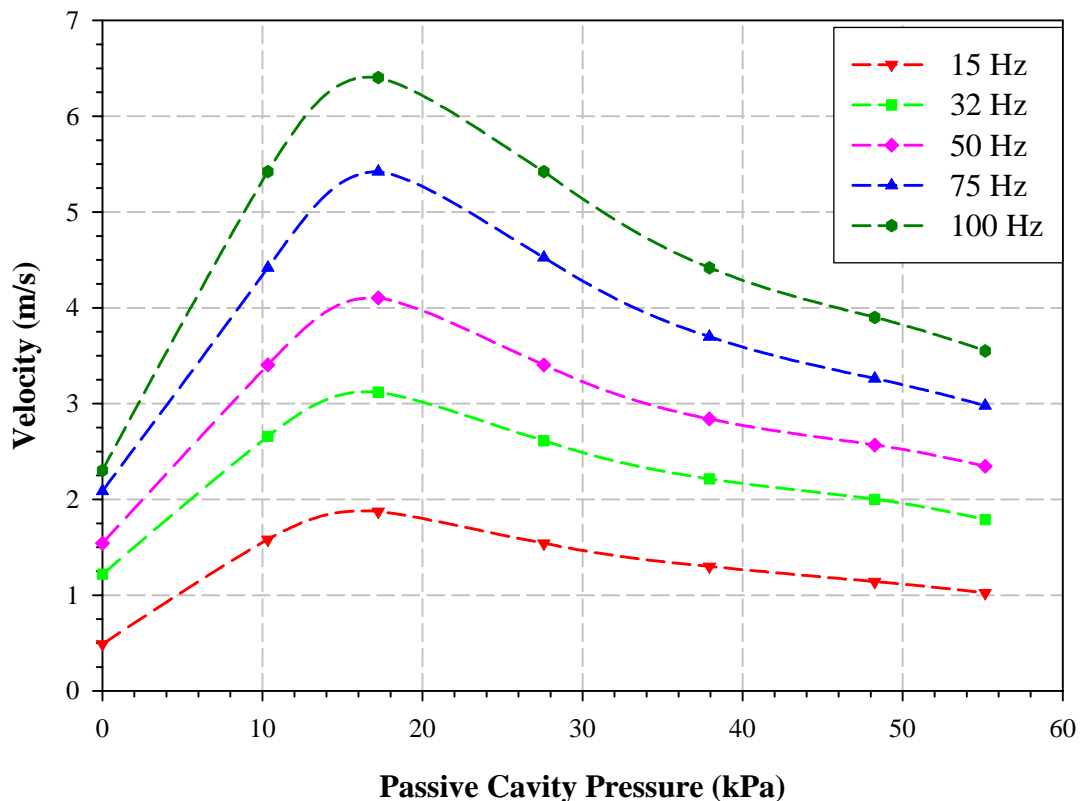
Figure 4.31 Passive Cavity Pressure Effects on Synthetic Jet Velocity for a Lipca Diaphragm at 350 Vpp

4.3.5 Statistical Factor Analysis

In this section all the factors discussed above are related with an empirical equation using statistical tools such as factorial experimental designs and regression analysis. The procedure used in case of the Bimorph and Thunder® devices was repeated for the Lipca as well. Since a full factorial design is not practical a two level fractional factorial design, 2^{5-1}, requiring 16 runs or experiments is used.

Table 4.8 Factor Distribution for a Lipca Device

Factors	Symbols	Low Level (-1)	High Level (+1)	Units	Types
Driving Waveform	F_z	Sawtooth (-1)	Sine (+1)	None	Discrete
Applied Voltage	E	250 (-1)	350 (+1)	V_{pp}	Continuous
Frequency	f	25 (-1)	50 (+1)	Hz	Continuous
Orifice Size	D_o	2 (-1)	3.67 (+1)	mm	Continuous
Cavity Height	C_H	5.5 (-1)	9.5 (+1)	mm	Continuous

Table 4.9 gives the factor distribution along with the levels used for each factor. The levels for each factor are chosen based on the characteristics of the actuator. Except for the driving waveform factor, all the factors are continuous. Maximum jet velocity is the response variable.

Using these factors an experimental design similar to the one used for the previous two actuators is constructed. A 95% confidence interval regression analysis on this design

shown in Table 4.10 helps in identifying the main effects. Since frequency, f, has a *p-value* of 0.4832 which is above 0.05 it is not considered as one of the main effects. The other four factors have valid *p-values* thus they are considered as main effects. The *p-values* of the selected factors were 8.2368E-08 for F_Z, 0.0254 for E, 0.0259 for D_o and 0.0147 for C_H. The regression had an R square value of 0.9411 and an adjusted R square value of 0.9196.

Using the coefficients obtained from the regression analysis a model fit is possible as given by Equation 4.7. The factors included in the equation are considered as main effects with Y as the velocity of the jet in m/s.

$$Y = 17.6170 - 13.4064 \cdot F_z + 2.7906 \cdot E - 2.7803 \cdot D_o - 3.1216 \cdot C_H$$

Equation 4.7

Table 4.9 Initial Regression Analysis for a Lipca Device

SUMMARY								
Regression Statistics								
Multiple R	0.97008							
R Square	0.94106							
Adjusted R Square	0.91963							
Standard Error	4.32153							
Obs.	16							

ANOVA								
	df	*SS*	*MS*	*F*	*Sig. F*			
Regression	4	3279.90553	819.97638	43.90633	1.067E-06			
Residual	11	205.43142	18.67558					
Total	15	3485.33694						

	Coeffs.	*Standard Error*	*t Stat*	*P-value*	*Lower 95%*	*Upper 95%*	*Lower 95.0%*	*Upper 95.0%*
Intercept	17.61694	1.08038	16.30622	4.718E-09	15.23903	19.99484	15.23903	19.99484
F_z	-13.40644	1.08038	-12.40899	8.237E-08	-15.78434	-11.02853	-15.78434	-11.02853
E	2.79056	1.08038	2.58294	0.02546	0.41266	5.16847	0.41266	5.16847
D_o	-2.78031	1.08038	-2.57345	0.02589	-5.15822	-0.40241	-5.15822	-0.40241
C_H	-3.12156	1.08038	-2.88932	0.01472	-5.49947	-0.74366	-5.49947	-0.74366

Based on this initial analysis the last factor of passive cavity pressure, P_B, is added to the experimental design increasing the number of runs or experiments to 24. The low level (-1) is set to 0 Pa and the high level (+1) is set at 27.58 kPa or 4.0 psi. The modified fractional factorial design is shown in Table 4.4. The table now contains all the factors and represents all the experiments conducted during the course of this project using the Lipca actuator.

A regression on the complete design leads to the elimination of f and P_B from the factors as their *p-values*, 0.8757 and 0.2816, are out of the critical limit of 0.05 for a 95% confidence interval. The final regression table containing the remaining factors, F_Z, E, D_o and C_H, as the main effects is shown in Table 4.11. The *p-values* for F_Z, E, D_o and C_H are 5.4827E-09, 0.01329, 0.0231 and 0.0131 respectively. The regression had an R square value of 0.8681 and an adjusted R square value of 0.8404 indicating that 87% of the data can be predicted using the model. The main effect average sizes calculated using Equation 4.2 are -23.4788 for F_Z, 6.4268 for E, -8.1390 for D_o and -8.6509 for C_H. The average effects for the eliminated factors are 0.3812 for f and -2.0898 for P_B. These two factors are eliminated as main effects, but could be coupled to the main effects. Figure 4.32 shows the average response size graphs for each factor. f and P_B have very small slopes and the main effect graphs have larger slopes with F_Z having the highest slope in the negative direction indicating that the sawtooth signal gives higher velocities.

Table 4.10 Final Regression Analysis for a Lipca Device

SUMMARY								
Regression Statistics								
Multiple R	0.93173							
R Square	0.86812							
Adjusted R Square	0.84035							
Standard Error	5.76574							
Obs.	24							

ANOVA								
	df	SS	MS	F	Sig. F			
Regression	4	4157.67688	1039.41922	31.26661	4.053E-08			
Residual	19	631.63122	33.24375					
Total	23	4789.30810						

	Coeffs.	Standard Error	t Stat	P-value	Lower 95%	Upper 95%	Lower 95.0%	Upper 95.0%
Intercept	17.20990	1.28926	13.34868	4.202E-11	14.51145	19.90835	14.51145	19.90835
F_z	-11.73942	1.17693	-9.97464	5.483E-09	-14.20275	-9.27608	-14.20275	-9.27608
E	3.21342	1.17693	2.73035	0.01329	0.75008	5.67675	0.75008	5.67675
D_o	-3.18735	1.28926	-2.47224	0.02305	-5.88580	-0.48890	-5.88580	-0.48890
C_H	-3.52860	1.28926	-2.73692	0.01310	-6.22705	-0.83015	-6.22705	-0.83015

The final model fit equation is given below by Equation 4.8 where Y' is the velocity in m/s. Using this equation an approximate velocity can be calculated for a set of conditions.

$$Y' = 17.210 - 11.739 \cdot F_z + 3.2134 \cdot E - 3.1874 \cdot D_o - 3.5286 \cdot C_H$$

Equation 4.8
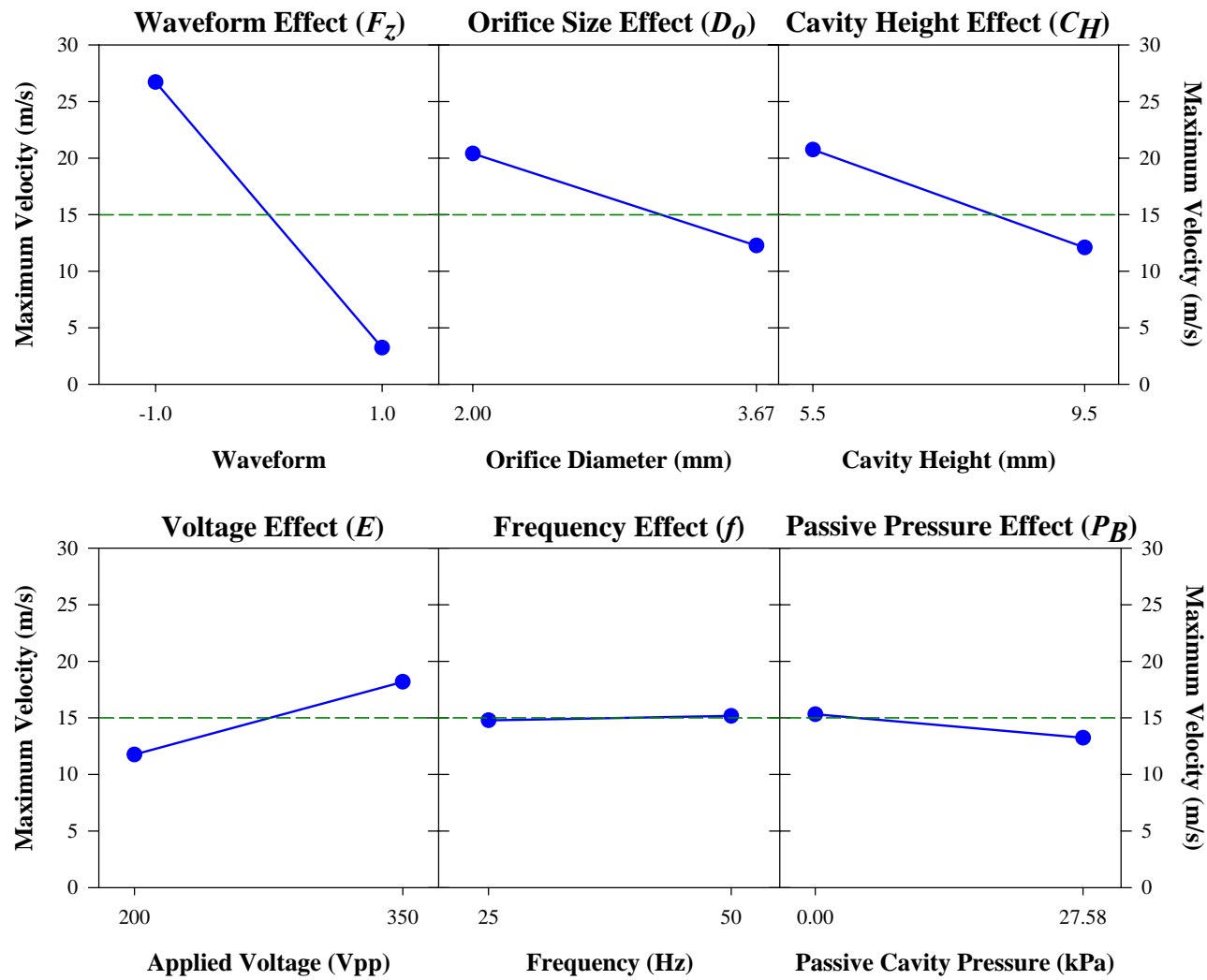
Figure 4.32 Average Factor Effects for a Lipca Device

4.4 RFD

This actuator is very different from the others in its construction. The following sections discuss all the experiments that were conducted on these actuators with the aim to better understand them.

4.4.1 Waveform Effects

For this actuator three driving signals, sine, sawtooth and square were used. Each signal produces a velocity curve with a different shape and magnitude. The sine driving velocity curve at 50 Hz in cavity IV is shown in Figure 4.33. As seen in the previous three actuators, two velocity peaks are observed with the larger peak following the leading edge of the driving signal and the smaller peak following the trailing edge. The larger peak is formed during the expulsion part of the synthetic jet cycle, and the smaller peak is formed during the ingestion part of the cycle.

Similar to the other actuators with a sawtooth signal, a single velocity peak is formed during the expulsion cycle. As seen in Figure 4.34 the jet follows the leading edge of the input signal. Immediately following the peak oscillations are observed in the velocity curves that are present at all voltages and frequencies.
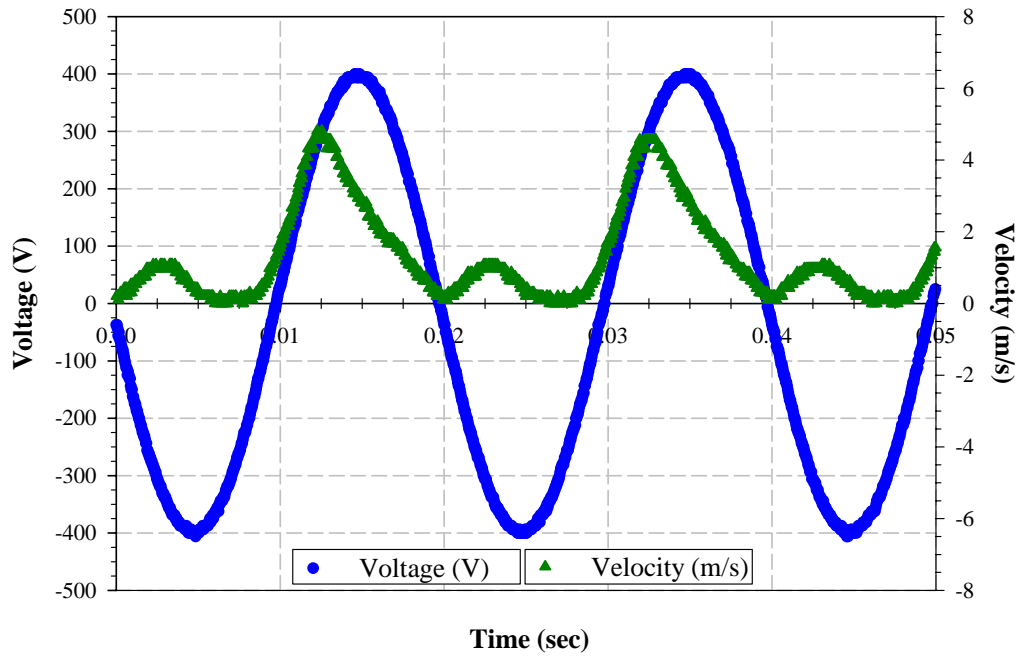
Figure 4.33 Typical Velocity Curve with a Sine Driving Signal with Cavity IV for a RFD Diaphragm at 50 Hz and 800 Vpp
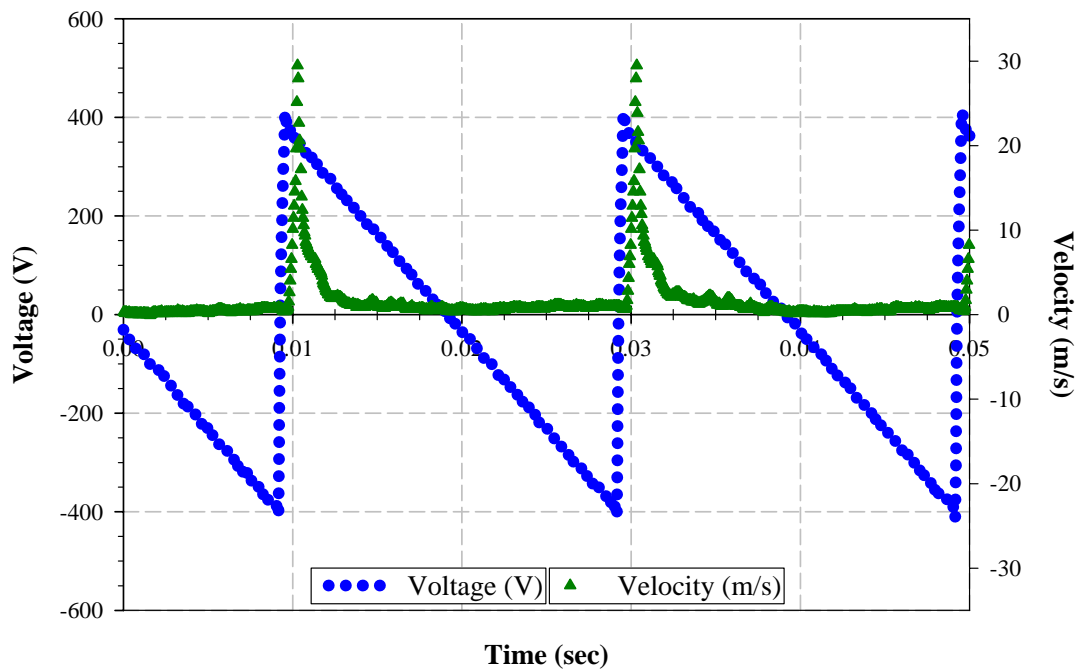
Figure 4.34 Typical Velocity Curve with a Sawtooth Driving Signal with Cavity IV for a RFD Diaphragm at 50 Hz and 800 Vpp

Based on the results with the sine and sawtooth signals, it can be concluded that the synthetic jet flow was affected by the driving signal used. To verify the effects another waveform, square wave was tried. By studying the behavior of the velocity jets formed using these different waveforms, the movement of the flow into and out of the cavity can be assessed. Thus, a square wave signal is studied as it provides a stronger force compared to the sine and it has two impulses versus one with a sawtooth signal. As seen in Figure 4.35, with a square driving, signal two peaks of different magnitudes are formed. The first peak follows the leading edge and the second peak follows the trailing edge of the driving signal. The double peaks are due to the double impulse provided by the square wave signal. The larger peak formed during the expulsion cycle follows the leading edge of the driving signal and the smaller peak during the ingestion cycle follows the trailing edge.

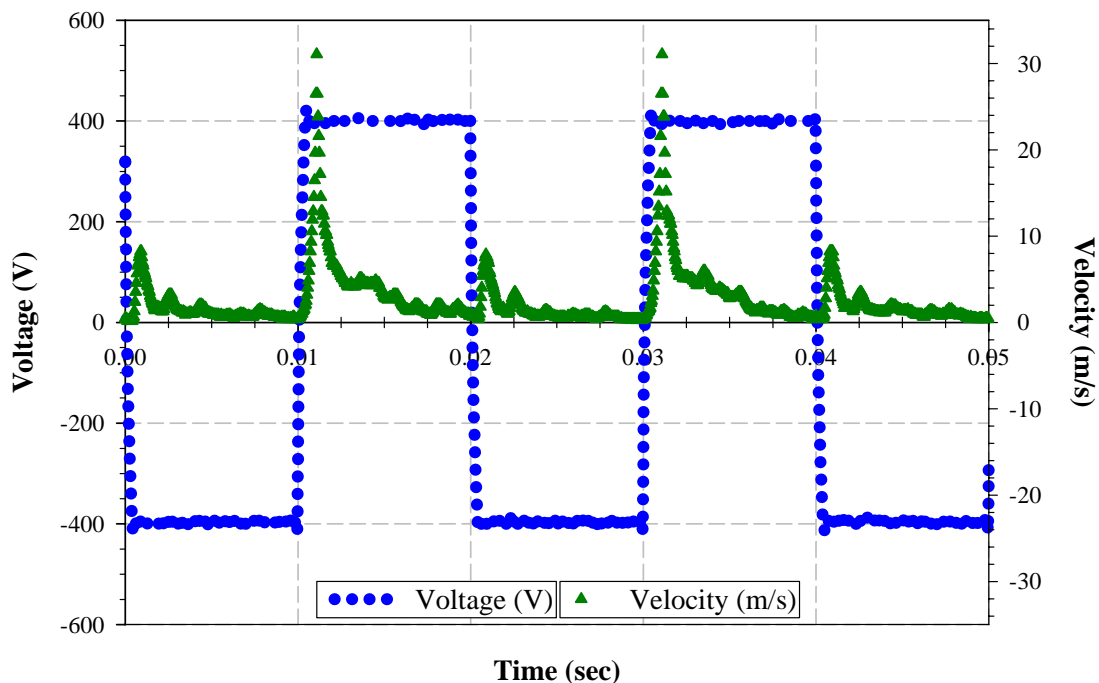**Figure 4.35 Typical Velocity Curve with a Square Driving Signal with Cavity IV for a RFD Diaphragm at 50 Hz and 800 Vpp**

The sawtooth and square signals provide a sudden impulse that causes the diaphragm to oscillate, and also produce larger velocity than a sine wave. The magnitude of the jet produced with a square signal was similar to the sawtooth jet and much larger than the sine jet.

4.4.2 Frequency Effect

To study the effects of frequency on velocity the jet is run at various frequencies from 1 – 90 Hz. Figure 4.31 shows the graphs for each driving signal at 800 Vpp. With a sine and a sawtooth signal the behavior of the RFD was similar to the previous three actuators. In case of the sine driving signal, the velocity increases as the frequency is increased. With a sawtooth signal, the velocity increases up to approximately 10Hz and then remains constant. This behavior is shown in Figure 4.36 at 800 Vpp. This figure also shows the square signal output, which is similar to the sawtooth signal, the peak velocity increased up to approximately 10 Hz and then remained constant. The frequency range tested with a square signal was smaller then the range used for the other two signals as the actuator tends to fail at high frequencies. This could be due to the dielectric break down of the adhesive.
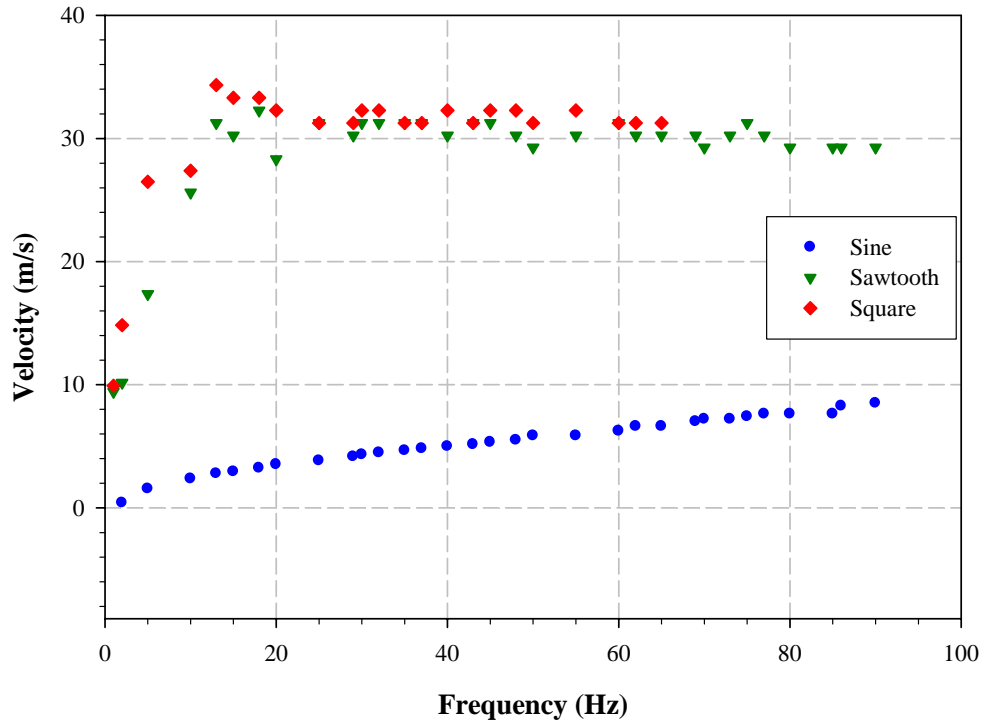
Figure 4.36 Frequency Effects on RFD Diaphragm Peak Velocities with Cavity IV at 800 Vpp

4.4.3 Active Cavity Pressure

As the diaphragm oscillates, pressure changes are expected in the active cavity. As these pressures are very small in magnitude they are difficult to measure with standard pressure transducers. This section contains a brief discussion on the dynamic pressure measurements in the synthetic jet active cavity. The differential pressure in the active cavity was measured with respect to the passive cavity pressure.

The graph in Figure 4.37 shows the velocity and active cavity pressure curves at 50 Hz with a sawtooth signal. The transducer has a resolution of 0.14 kPa and the pressures in the cavity are in the range of -0.6 to +0.6 kPa. Thus the pressure signal was noisy;

however, it appears to follow the velocity and the leading edge of the voltage curve. The pressure peaks the same time as the velocity indicating that there may be a relationship between the velocity produced by the synthetic jet and the pressure in the active cavity. With a sine signal the pressures are below the minimum range of the pressure transducer, thus it could not be measured.
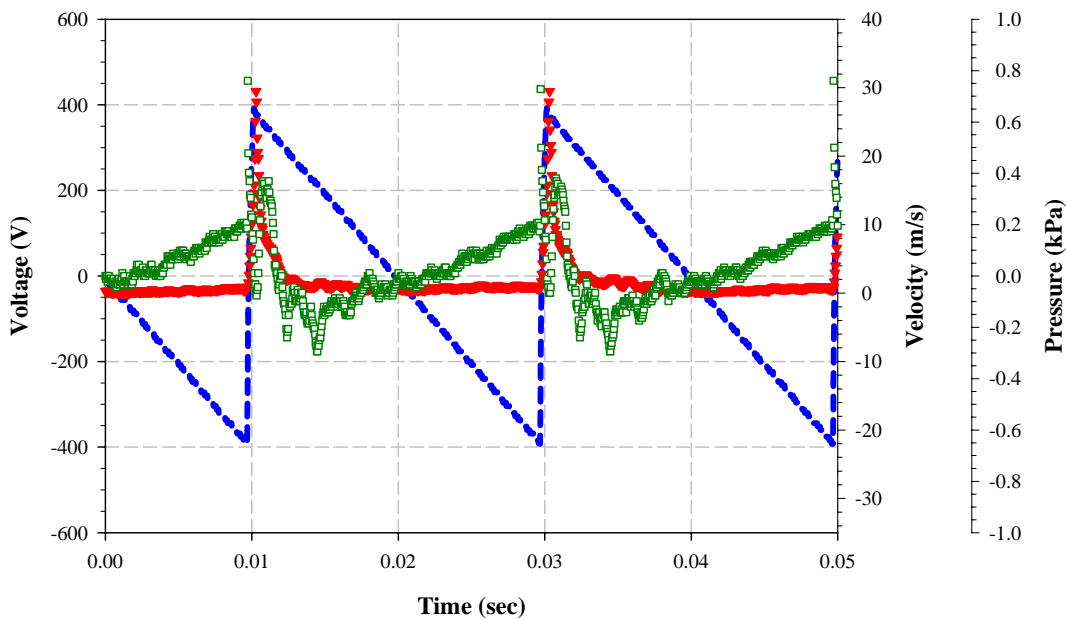
Figure 4.37 Active Cavity Pressure with Velocity and Voltage with a Sawtooth Driving Signal in Cavity IV for a RFD Diaphragm at 50 Hz and 800 Vpp

Next, the effects of frequency on active cavity pressure were tested as shown in Figure 4.38. It is expected that the pressure follows the same trend as the velocity. In case of a sinusoidal waveform the pressures are so low that a clear result is not obtainable although a slight increase in pressure was noticed as the frequency increased. With a sawtooth and square wave, the pressures are higher and were measured successfully. In these cases, the pressure increases until approximately 40 Hz, and then remains constant.

This behavior was similar to the velocity, with the velocity stabilizing at a lower frequency than with added pressure. This indicates that there is a coupling between jet velocity and active cavity pressure.
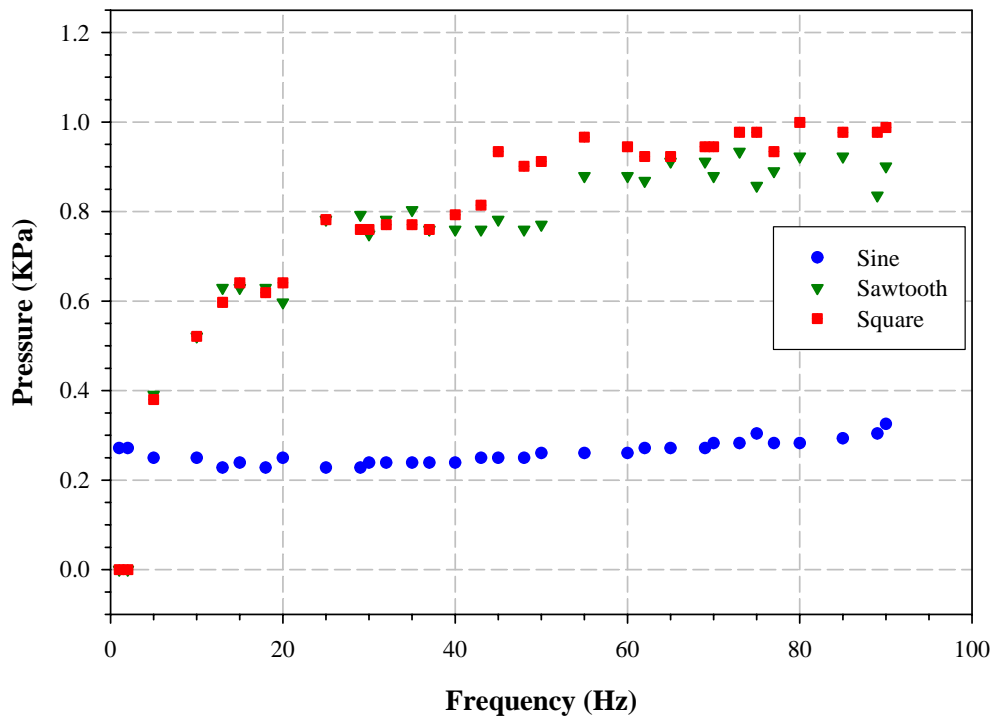
Figure 4.38 Frequency Effects on Active Cavity Pressure for Cavity IV with a RFD Diaphragm at 800 Vpp

4.4.4 Velocity Profiles

Similar to the other three actuators velocity profiles are mapped at the orifice diameter. The profile is shaped like a Gaussian curve with the velocity maximum at the center of the orifice and minimum at the edges as seen in the previous three actuators. With a square signal as well profiles having a similar shape are measured as shown in Figure

4.39 at 50Hz. The only difference in profiles with the three signals was magnitude with the square signal producing the highest velocities and the sine signal producing the lowest velocities. A profile with sine driving signal is shown in Figure 4.40 at 32 Hz.
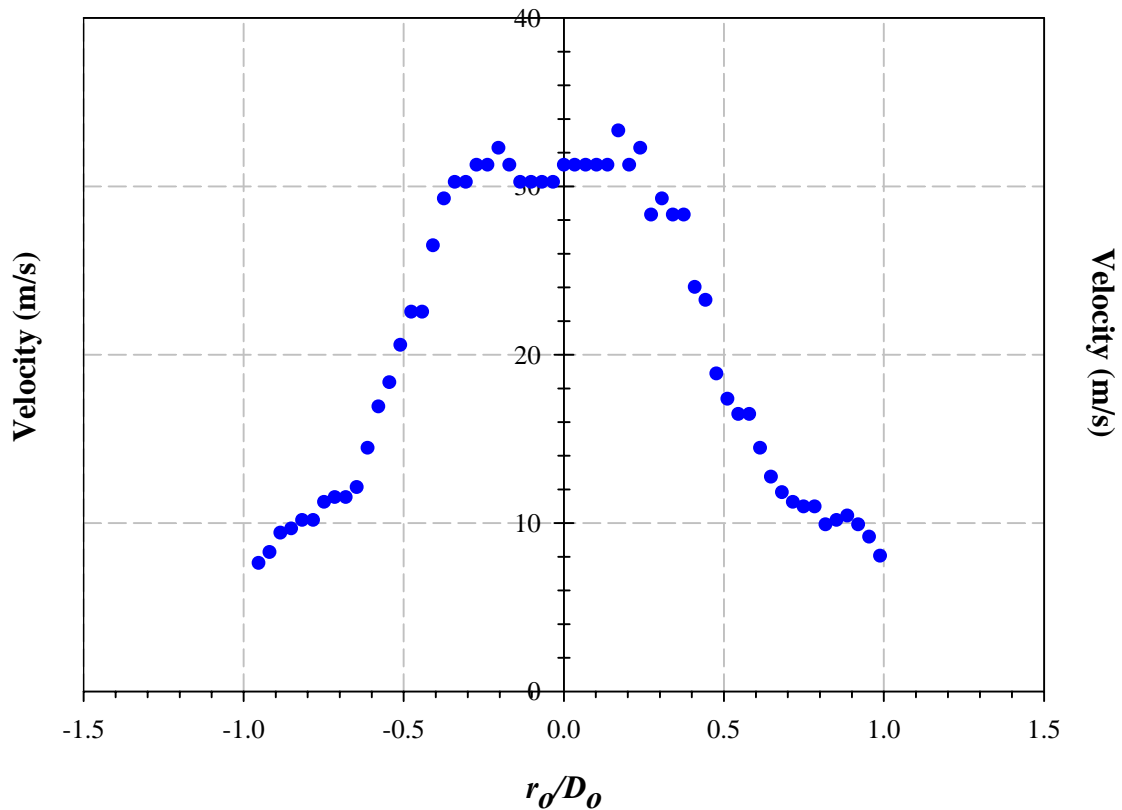
Figure 4.39 Velocity Profile with Cavity IV using a Square Driving Signal for a RFD Diaphragm at 50 Hz and 800 Vpp
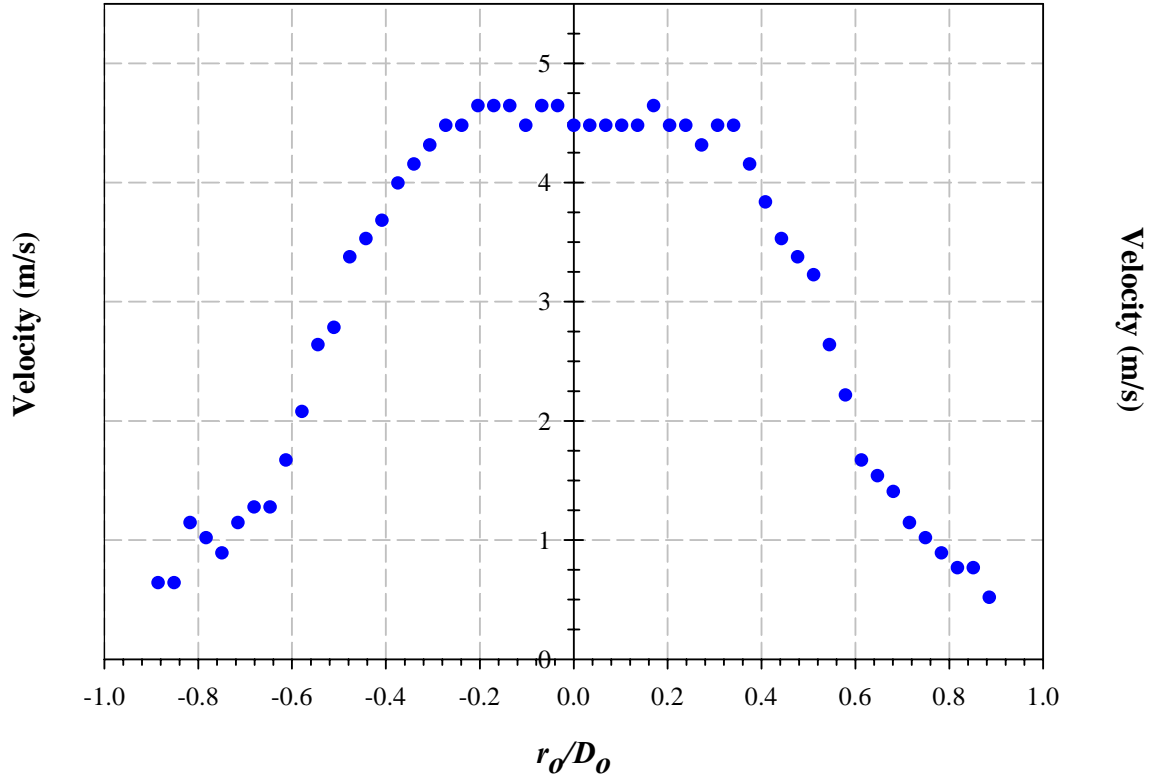
Figure 4.40 Velocity Profile with Cavity IV using a Sine Driving Signal for a RFD Diaphragm at 32 Hz and 800 Vpp

4.5 Discussion and Summary

While testing for relevance of changes in cavity volume on the jet velocity it was observed that orifice size had an effect on the results. From the results it was not certain which factor has a greater influence on the velocity. In order to derive a relation between the cavity volume, orifice diameter and the jet velocity the equation for the conservation of mass (Fox and McDonald 1992) is considered as shown in Equation 4.9.

$$0 = \frac{\partial}{\partial t} \int_{CV} \rho \, dV\!\!\!\!- + \int_{CS} \rho \vec{V} \cdot d\vec{A} \qquad\qquad \textbf{Equation 4.9}$$

The first term represents the rate of change of mass within the control volume in this case the active cavity of the synthetic jet actuator and the second term represents the net rate of mass flux out through the control surface. Conservation of mass requires that the sum of the rate of change of mass within the control volume, and the net rate of mass outflow through the control surface be zero. With respect to the current study a simplified version of the first term of Equation 4.9 in terms of the cavity geometry is shown in Equation 4.10.

$$\frac{\partial}{\partial t}\int_{CV}\rho dV = \rho\frac{\pi D_D{}^2}{4}\cdot\frac{\Delta C_H}{\Delta t}$$ **Equation 4.10**

D_D is the diameter of the diaphragm and the density is assumed to be constant. The right side of the equation represents the change in the volume of the synthetic jet cavity with respect to time.

Similarly the second term of Equation 4.9 can also be written in terms of the cavity dimensions, particularly in this case the dimensions of the exit or the orifice. The simplified equation is given in Equation 4.11.

$$\int_{CS}\rho\vec{V}\cdot d\vec{A} = \rho V_j\cdot\frac{\pi D_o{}^2}{4}$$ **Equation 4.11**

V_j is the velocity of the jet and density is assumed to be constant. Equating Equations 4.10 and 4.11 gives a relation between jet velocity and the two factors as shown by Equation 4.12.

$$V_j \propto \frac{C_H}{D_o{}^2}$$

Equation 4.12

This relationship shows that the jet velocity is directly proportional to the cavity height and inversely proportional to square of the orifice diameter. Thus the orifice diameter has a larger effect on the velocity than the cavity volume and any study on the cavity volume has to take into account the orifice diameter.

A summary of the statistical analysis showing the relevant factors by a tick mark and the factors, which were eliminated by a cross for each actuator, is given in Table 4.12.

Table 4.11 Summary of Relevant Factors

	F_Z	E	f	D_o	C_H	P_B
Bimorph	√	X	X	√	√	X
Thunder®	√	√	X	√	√	ND
Lipca	√	√	X	√	√	X

ND : Not Determined

Table 4.122 Summary of Peak Velocities

	Bimorph	**Thunder®**	**Lipca**	**RFD**
Velocity (m/s)	35 - 50	30 - 45	30 – 45	25 - 35
Frequency (Hz)	1 - 100	1 - 100	1 - 100	1 - 60

Considering the magnitudes of the jet velocities measured with each device the Bimorph was seen to produce the highest range of velocities and the RFD the lowest. All the actuators produced velocities in the range of 25 – 50 m/s as shown in Table 4.12.

Besides the factors considered in this project the study can be expanded to include a number of additional factors such as, the cavity design, the covering plate thickness, the orifice shape, the size of the diaphragm, etc. Although these factors have not been considered in this study they could have an effect of the synthetic jet performance.

CHAPTER 5

5. Conclusions

Four actuators, Bimorph, Thunder®, Lipca and RFD were studied to test the effects of specific factors on the performance of the synthetic jet actuator using velocity of the jet as the response variable. Using statistical analysis tools such as screening designs and fractional factorial models, an empirical equation was derived to predict the velocity of the jet for a set of conditions. Among the factors studied were the driving signal used to excite the diaphragms, the magnitude and frequency of the signal, the volume of the cavity described by the cavity height, the size of the exit or orifice and the pressure in the passive cavity of the jet.

Two driving signals, sine and sawtooth were tested for all actuators. An additional waveform, square was tested only in case of the RFD. Results show that driving signal has a significant effect on velocity for all actuators. The sawtooth signal produces higher velocities then the sine signal. This effect may be due to the additional impulse provided by the sawtooth signal. The sine signal produced two velocity peaks with all actuators, the larger peak is assumed to be during the expulsion part of the synthetic jet cycle and the

smaller peak the ingestion part. With the sawtooth signal a single peak was formed in all cases, but also oscillations are seen in the velocity signals that increase in frequency as the driving frequency is increased. As the actuators are clamped along the perimeter, they tend to oscillate when a voltage is applied. In case of the RFD, with a square signal, the synthetic jet produces velocities in the same range as the sawtooth signal. Due to the double impulse present in the square signal, two velocity peaks having different magnitudes are formed for the expulsion and ingestions parts of the cycle. Even though the square signal produces high velocities this type of waveform causes dielectric breakdown at low frequencies thus damaging the actuator.

The actuators were driven at two voltages, high and low according to their respective allowable driving fields to test the effects of the jet velocity. The velocities tended to increase at higher voltages regardless of the driving signal used. The maximum voltages the actuators were driven at were below the maximum allowed voltage for each device to avoid damage to the actuator.

To see the effects of frequency on synthetic jets the actuators were driven at various frequencies. For the range of frequencies tested for each actuator, the velocity increased as frequency was increased in case of a sine driving signal. But with a sawtooth signal the trend was very different with the velocity reaching a constant value at approximately 10 Hz for all actuators. The reason for such behavior with the sawtooth signal could be something called the choking condition seen in nozzle flows (John 1984). If the flow is fast enough, the pressure in the restriction drops to zero, so the flow is limited to this rate regardless of the pressure in the back of the restriction. The phenomenon of choking exists only in

compressible flow and can occur in several flow situations. It is possible that with a sawtooth signal saturation point is reached making the fluid in the cavity compressible and restricting the velocity through the cavity. Due to the additional force present in the sawtooth signal, this saturation point is reached at a low frequency. It is possible that a similar choking condition could occur with a sine signal at much higher frequencies above the ranges tested in the current study. With a square wave, the RFD behaves in a similar manner to a sawtooth signal, choking at a low frequency of approximately 10 Hz.

Next geometrical factors of the synthetic jet cavity such as cavity volume and orifice size are tested. Four cavity configurations are studied for Bimorph, Thunder® and Lipca with the sine and sawtooth driving signals. Changing the cavity height leads to changing the volume of the cavity, thus the effects of changing the volume of the cavity are studied. For all actuators, the cavity with the smaller volume produces higher velocities irrespective of the driving waveform used. But the differences were smaller with the sawtooth driven actuators than the sine driving actuators and in a few cases almost negligible.

To test the effects of orifice size, cavities having similar volumes or heights but different orifice diameters were tested. The differences in velocities due to orifice diameter seemed to be higher in case of jets formed using a sine wave. With sawtooth driving signal the differences were smaller again indicating that the driving signal is an important fact affecting the functioning of a synthetic jet.

The last factor studied was the effect of pressurizing the passive cavity in the form of a uniformly distributed load on the diaphragm. The passive cavity was pressurized to

various levels and the effects on the jet velocity were studied at various voltages and frequencies. In the case of the Thunder® and Lipca, it was observed that as the passive pressure was increased the velocity also increased to a maximum value after which it dropped back to the initial value. The peak was observed at approximately 20 kPa for the Thunder® and 18 kPa for the Lipca with both the driving signals. For the Bimorph, the passive cavity pressure had an adverse effect with the velocity falling with increasing passive pressure with both the signals.

In case of the RFD the active cavity pressure was studied at different driving frequencies and voltages of the actuator. The sawtooth and square signals produced higher active cavity pressures than the sine. With a sine signal the pressures were too small to be measured as they fell below the resolution of the pressure transducer. The active cavity pressure follows the same trend as the jet velocity for the sawtooth and the square signal at various frequencies and voltages indicating a coupling between pressure and velocity and cavity height/volume as well as actuator displacement.

Linear models for all actuators with the most relevant factors are developed. This models may be utilized both numerically and experimentally to optimize the performance of synthetic jet with a piezoelectric diaphragms.

CHAPTER 6

6. Future Work

   While a number of factors have been studied in the current project, several aspects of the synthetic jet need further investigation. The sawtooth waveform proved to produce high velocities but oscillations caused in the diaphragm affected the performance of the synthetic jet. Thus an arbitrary waveform could be designed that would reduce the oscillations. Although past research on piezoelectric actuators has shown that they have a low power consumption, it has not been tested in the synthetic jet. The power consumption for an optimized condition of the synthetic jet needs to be measured, to compare with other traditional flow control devices. The actuators used in the current study performed satisfactorily, but based on the knowledge gained, new actuators can be modeled using tools such as finite element analysis. These actuators can be application dependent and thus enhance the performance of the synthetic jet. The displacement of the actuator can be modeled to better understand the volumetric displacement in the synthetic jet cavity. Based on the displacement models the cavity design can be modified effecting an improvement in the synthetic jet velocities.

Similarly the synthetic jet cavity can be modeled numerically using flow analysis tools such as Fluent. Although experimental investigations provide a good insight into the behavior of a synthetic jet, most experimental studies do not provide a clear picture of the flow behavior inside the cavity. Using such numerical models it is easier to do a complete parametric study for each actuator which becomes a tedious and expensive proposition through experiments.

One of the major applications of synthetic jets is flow control devices on aircrafts. A single synthetic jet actuator may not be capable of effecting significant changes in the flow fields present around aircrafts during flight. The surface of the aircraft will have to be lined with a number of these devices. Thus experimental and numerical tests on the interaction of adjacent jets are necessary. Once the synthetic jet actuator has been optimized it has to be tested in a continuous flow and finally on an aircraft in flight.

List of References

Amitay, M., Honohan, A., Trautman, M., and Glezer, A., "Modification of the Aerodynamic Characteristics of Bluff Bodies using Fluidic Actuators", AIAA, 97–2004, 1997.

Amitay, M., Smith, B., and Glezer, A., "Aerodynamic flow control using synthetic jet technology", AIAA, 98–0208, 1998.

Bowen, L., J., and French, K., W., ''Fabrication of Piezoelectric Ceramic/Polymer Composites by Injection Molding'', Proceedings 1992 IEEE International Symposium on the Applications of Ferroelectrics, IEEE, pp. 160–163, 1992.

Bryant, R., G., ''LaRC-SI: A Soluble Aromatic Polyimide'', High Performance Polymers, Vol. **8**, No. 4, pp. 607–615, 1996.

Bryant, R., G., Fox, R., L., Lachowicz, J., T., and Chen, F., J., "Piezoelectric Synthetic Jets for Aircraft Control Surfaces", SPIE, 3674, pp. 220–227, 1999.

Bryant, R., G., Effinger, R., T., Aranda, I., Jr., Copeland, B., M., Jr., Covington, E., W., III and Hogge, J., M., "Radial Field Piezoelectric Diaphragms", Journal of Intelligent Material Systems and Structures, Vol. 15, 2004.

Cady, W., G., *Piezoelectricity*, McGraw-Hill, New York, pp. 25–47, 1964.

Cattafesta, L., N., Garg, S., and Shukla, D., "Development of Piezoelectric Actuators for Active Flow Control", AIAA, Vol. **39**, No. 8, 2001.

Coe, D., J., Allen, M., G., Trautman, M., A., and Glezer, A., "Micromachined Jets for Manipulation of Micro Flows", Solid-State Sensor and Actuator Wrokshop, pp. 243–247, 1994.

Collis, S., S., Joslin, R., D., Seifert, A., and Theofilis, V., "Issues in Active Flow Control: Theory, Control, Simulation, and Experiment", Progress in Aerospace Science, Vol. **40**, pp. 237–289, 2004.

Crook, A., Sadri, A.,M. and Wood, N.,J., "The Development and Implementation of Synthetic Jets for the Control of Separated Flow", AIAA, 99–3176, 1999.

Dausch, D., E., and Wise, S., A., "Composition Effects on Electromechanical Degradation of RAINBOW Actuators", NASA TM–1998–206282, pp. 2–3, January 1998.

Devore, J., L., *Probability and Statistics for Engineering and the Sciences*, Duxbury Thomson Learning, Pacific Grove, California, 2004.

Dogan, A., Tressler, J., and Newnham, R., E., "Solid-State Ceramic Actuator Designs", AIAA, Vol. **39**, No. 7, 2001.

Donovan, J., F., Kral, L., D., and Cary, A., W., "Active Flow Control Applied to an Airfoil", AIAA, 98–0210.

Fox, R., W., McDonald, A., T, *Introduction to Fluid Mechanics*, 4th Edition, John Wiley & Sons, New York, pp 104–105, 1992.

Gad-el-Hak, M., Pollard, A., Bonnet, J., *Flow Control: Fundamentals and Practices*, Springer-Verlag, Berlin, 1998.

Gad-el-Hak, M., *Flow Control: Passive, Active, and Reactive Flow Management*, Cambridge University Press, Cambridge United Kingdom, Chapter 1, 2000.

Haertling, G., H., "Chemically Reduced PLZT Ceramics for Ultra High Displacment Actuators", Ferroelectrics, Vol. **154**, pp. 110–106, 1994.

Hellbaum, F., R., Bryant, R., G., and Fox, R., L., "Thin Layer Composite Unimorph Ferroelectric Driver and Sensor", U.S. Patent, No. 5,632,841, 1997.

Hassan, A., A., "Numerical Simulations and Potential Applications of Zero-Mass Jets for Enhanced Rotorcraft Aerodynamic Performance", AIAA, 98–0211.

Ho, C., H., and Tai, Y., C., "Review: MEMS and Its Applications for Flow Control", Journal of Fluids Engineering, Vol. **118**, pp. 437–447, 1996.

Jaffe, B., Cook, W., R., Jr., and Jaffe, H., Piezoelectric Ceramics, Academic Press, New York, pp. 271–291, 1971.

John, J., E., A., *Gas Dynamics*, 2[ed] Edition, Allyn and Bacon, pp 180, 1984.

Kral, L., D., Donovan, J.,F., Cain, A.,B., and Cary, A.,W., "Numerical Simulation of Synthetic Jet Actuators", 28th AIAA Fluid Dynamics Conference, 97–1824, 1997.

Liew, K., M., Lim, H., K., Tan, M., J., and He, X., Q., "Analysis of Laminated Composite Beams and Plates with Piezoelectric Patches using the Element-Free Galerkin Method", Computational Mechanics, Vol. **29**, No. 6, pp. 486–497, 2002.

Mallinson, S., G., Reizes, J., A., Hong, G., and Buttini, M., "Synthetic Jet Actuators for Flow Control", SPIE Conference, 3891, pp. 146–156, 1999.

Mane, P., "Pressure Loading of Piezo Composite Unimorphs", MRS Fall Meeting, Hynes Convention Center, Boston, 28 November 2005.

McLean, J., D., Crouch, J., D., Stoner, R., C., Sakurai, S., Seidel, G., E., Feifel, W., M., and Rush, H., M., "Study of the application of separation control by unsteady excitation to civil transport aircraft", Technical report CR–1999–209338, NASA, 1999.

Montgomery, D., C., *Design and Analysis of Experiments*, John Wiley & Sons Inc., New Jersey, 2005.

Mossi, K., Selby, G., and Bryant, R., "Thin-Layer Composite Unimorph Ferroelectric Driver and Sensor Properties", Materials Letters, Vol. **35**, pp. 39–49, 1998.

Mossi, K., Bryant, R., "Pre-stressed Circular Actuators", American Ceramic Society, pp. 445–454, 2004a.

Mossi, K., Bryant, R., G., "Synthetic Jets for Piezoelectric Actuators", Materials Research Society, pp. 407–412, 2004b.

Mossi, K., Castro, N., D., Bryant, R., and Mane, P., "Boundary Condition Effects on Piezo-Synthetic Jets", Integrated Ferroelectrics, Vol. 71, pp. 257–266, 2005a.

Mossi, K., Mane, P., and Bryant, R., "Velocity Profiles for Synthetic Jets Using Piezoelectric Circular Actuators", AIAA, 2005-2341, 2005b.

Newnham, R., E., and Ruschau, G., R., "Smart Electroceramics", Journal of American Ceramics Society, Vol. **74**, No. 3, pp. 463–480, 1991.

Park, K., H., Kim, Y., B., Kim, Y., S., Park, H., C., Yoon, K., J., "Experimental Performance Evaluation of Lightweight Piezo-Composite Curved Actuators", SPIE Conference, 4699–41, 2001.

Rathnasingham, R., and Breuer, K.,S., "Coupled fluid-structural characteristics of actuators for flow control", AIAA, J 35, pp. 832–837, 1997a.

Rathnasingham, R., and Breuer, K.,S., *System Identification and Active Control of a Turbulent Boundary Layer*, PhD Thesis, MIT, 1997b.

Rizetta, D., P., Visbal, M., R., and Stanek, M., J., "Numerical Investigation of Synthetic Jet Flow Fields, AIAA Jounal, Vol, **9**, pp. 919–927, 1999.

Schaeffler, N.,W., Hepner, T.,E., Jones, G.S., and Kegerise, M.,A., "Overview of Active Flow Control Actuator Development at NASA Langley Research Center", AIAA, 2002–3159, 2002.

Schubauer, G., B., Skramstad, H., K., "Laminar Boundary Layer Oscillations and Transitions on a Flat Plate", Journal of Aerospace Science, Vol. **14**, pp. 69–79, 1947.

Schwartz, R., W., Laoratanakul, P., Nothwang, W., D., Ballato, J., Moon, Y., and Jackson, A., "Understanding Mechanics and Stress Effects in Rainbow and Thunder Stress-Biased Actuators", SPIE Smart Structures and Materials, Active Materials: Behavior and Mechanics, Vol. **392**, pp. 363–375, 2000.

Seifert, A., Bachar, T., Koss, D., Shepshelovich, M., and Wygnanski, I., "Oscillatory Blowing: A Tool to delay Boundary-Layer Separation", AIAA Journal, Vol. **31**, No. 11, 1993.

Seifert, A., Darabi, A., and Wygnanski, I., "Delay of Airfoil Stall by Periodic Excitation", Jornal of Aircraft, Vol. **33**, No. 4, 1996.

Seifert, A., and Pack, L., G., "Oscillatory Control of Separation at High Reynolds Numbers", AIAA Journal, Vol. **37**, pp. 1062–1071, 1999.

Smith, B., L., *Synthetic Jets and their Interaction with Adjacent Jets*, PhD Thesis, Georgia Institute of Engineering, 143 pp., June 1999.

Smith, B., L., and Glezer, A., "Vectoring and Small Scale Motions Effected in Free Shear Flows Using Synthetic Jet Actuators", AIAA, 97–0213, 1997.

Smith, B., L., and Glezer, A., "The formation and evolution of synthetic jets", Physics of Fluids, Vol. **10**, pp. 2281–2297, 1998.

Smits, J., G., Dalke, S., I., and Cooney, T., K., "The Constituent Equations of Piezoelectric Bimorphs", Sensors and Actuators A, Vol. **28**, pp. 41–61, 1991.

Uchino, K., *Ferroelectric Devices*, Marcel Dekker Inc., New York, pp. 57–66, 2000.

Wise, S., A., "Displacement Properties of RAINBOW and THUNDER piezoelectric actuators", Sensors and Actuators A, Vol. **69**, 1998.

Wlezien, R., W., Horner, G., C., McGowan, A., R., Padula, S., L., Scott, M., A., Silcox, R., J., and Simpson, J., O., "The Aircraft Morphing Program", AIAA, 98-1927, 1998.

Wood, N., J., Sadri, A., M., and Crook, A., "Control of Turbulent Separation by Synthetic Jets", AIAA, 2000–4331, 2000.

Yoon, K., J., Shin, S., Park, H., C., and Goo, N., S., "Design and Manufacture of Lightweight Piezoceramic Curved Actuator", Smart Materials and Structures, Vol. **11**, pp. 163–168, 2002.

Yoon, K., J., Park, K., H., Park, H., C., Lee, S., K., and Goo, N., S., "Analytical Design Model for a Piezo-Composite Unimorph Actuator and its verification using Lightweight Piezo-Composite Curved Actuators", Smart Materials and Structures, Vol. **13**, pp. 459–467, 2003a.

Yoon, K., J., Park, K., H., Park, H., C. and Perraux, D., "Thermal Deformation Analysis of Curved Actuator LIPCA with Piezoceramic Layer and Fiber Composite Layers", Composites Science and Technology, Vol. **63**, pp. 501–506, 2003b.

APPENDIX

Mathcad Program for Converting Hotwire Voltages to Velocities
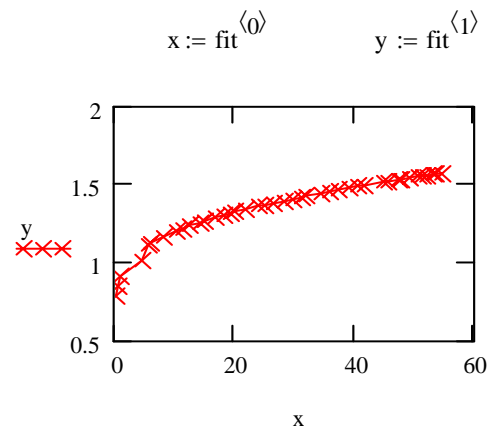
Hotwire Polynomial Fit Worksheet

$i := 0..2501$

Bridge=

	0
0	0.969
1	0.975
2	0.969
3	0.963
4	0.963
5	0.956
6	0.956
7	0.95

Enter Bridge Voltage Displayed:

Data Collected

10.22698071	1.1972
11.390362	1.2147
12.56376891	1.2342
14.06382435	1.253
15.02994005	1.266
16.79627886	1.2842
18.19159262	1.2971
19.25816471	1.3103
19.90040502	1.3214
21.78147118	1.3384
23.88705169	1.3583

Velocity   Voltage

$$x := fit^{\langle 0 \rangle} \qquad y := fit^{\langle 1 \rangle}$$

Plot of x and y

$$X := fit^{\langle 0 \rangle} \qquad Y := fit^{\langle 1 \rangle} \qquad n := rows\,(fit)$$

Enter degree of polynomial to fit:

$$k := 4$$

Number of data points:

$$n = 41$$

$$z := regress\,(X, Y, k)$$

Polynomial fitting function:

$$fit(x) := interp\,(z, X, Y, x)$$
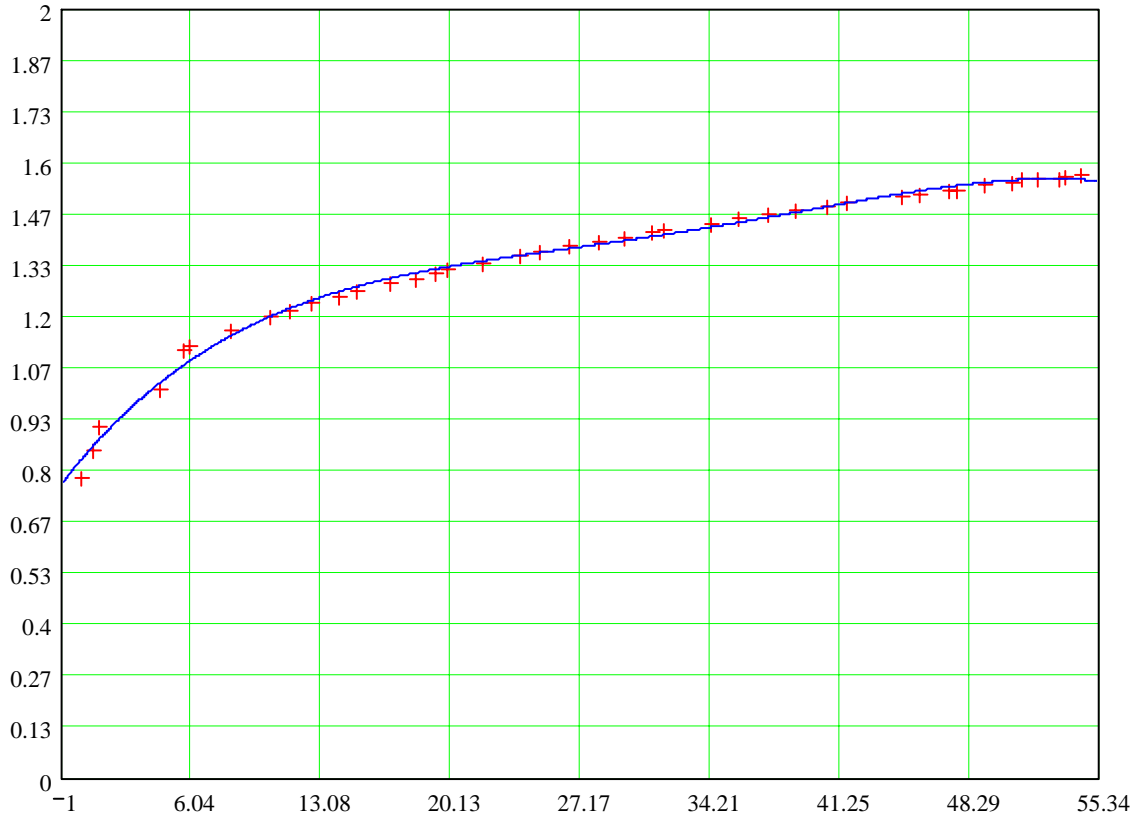
$$coeffs := submatrix\,(z, 3, length\,(z) - 1, 0, 0)$$

Coefficients:

$$coeffs^{T} = \left(0.827 \quad 0.056 \quad -2.409 \times 10^{-3} \quad 5.076 \times 10^{-5} \quad -3.842 \times 10^{-7}\right)$$

R^2:

$$\frac{\sum \overrightarrow{(fit(X) - mean\,(Y))^2}}{\sum \overrightarrow{(Y - mean\,(Y))^2}} = 0.994$$

Degrees of freedom:

$$n - k - 1 = 36$$

Polynomial Regression of Y on X

+++ X-Y data
— Least-squares fit

$$\underset{\sim\sim\sim\sim}{\text{scale}} := \max\left(\overrightarrow{\left|\text{fit}(X) - Y\right|}\right) \cdot 1.1$$

Residual Plot
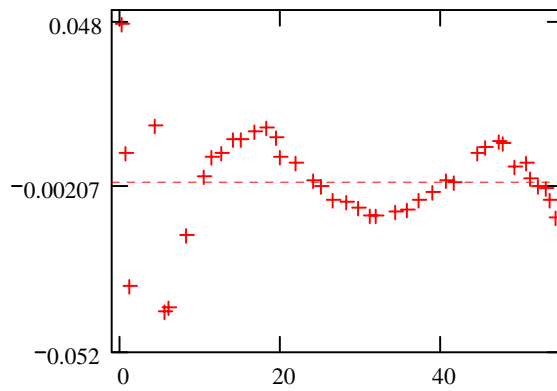
$$
\text{coeffs} = \begin{pmatrix} 0.827 \\ 0.056 \\ -2.409 \times 10^{-3} \\ 5.076 \times 10^{-5} \\ -3.842 \times 10^{-7} \end{pmatrix}
$$

$$
\text{velocity}_i := \text{root}\left(\text{coeffs}_{0,0} + \text{coeffs}_{1,0} \cdot g + \text{coeffs}_{2,0} \cdot g^2 + \text{coeffs}_{3,0} \cdot g^3 + \text{coeffs}_{4,0} \cdot g^4 - \text{Bridge}_i, g, -1, 54.4 \right)
$$

Velocity determined from the bridge voltage is:

velocity =

	0
0	2.862
1	3.001
2	2.862
3	2.725
4	2.725
5	2.567
6	2.567
7	2.433
8	2.301
9	2.301
10	2.301
11	2.021
12	2.171
13	2.021
14	2.021
15	2.021